

UNIVERSIDADE ESTADUAL PAULISTA
"JÚLIO DE MESQUITA FILHO"

Faculdade de Engenharia de Ilha Solteira (FEIS)

Departamento de Física e Química (DFQ)

Programa de Pós-Graduação em Ciência dos Materiais (PPGCM)

Colapso atômico em impurezas no grafeno multicamada

Antonio Marcos Dias Freitas

Mestrado

Ilha Solteira - SP

27-02-2024



UNIVERSIDADE ESTADUAL PAULISTA
"JÚLIO DE MESQUITA FILHO"

Faculdade de Engenharia de Ilha Solteira (FEIS)

Departamento de Física e Química (DFQ)

Programa de Pós-Graduação em Ciência dos Materiais (PPGCM)

Colapso atômico em impurezas no grafeno multicamada

Antonio Marcos Dias Freitas

Orientador: Prof. Dr. Antonio Carlos Ferreira Seridonio

Dissertação apresentada ao Programa de Pós-Graduação em Ciências dos Materiais, Departamento de Física e Química, Universidade Estadual Paulista - UNESP, Faculdade de Engenharia de Ilha Solteira - SP, como parte das exigências para obtenção do título de Mestre em Ciências dos Materiais, Área de concentração: Física da Matéria Condensada.

Ilha Solteira - SP

27-02-2024

FICHA CATALOGRÁFICA
Desenvolvido pelo Serviço Técnico de Biblioteca e Documentação

F866c

Freitas, Antonio Marcos Dias.
Colapso atômico em impurezas no grafeno multicamada / Antonio Marcos Dias Freitas. -- Ilha Solteira: [s.n.], 2023
68 f. : il.

Dissertação (mestrado) - Universidade Estadual Paulista. Faculdade de Engenharia de Ilha Solteira. Área de conhecimento: Física da Matéria Condensada, 2023

Orientador: Antonio Carlos Ferreira Seridonio

Inclui bibliografia

1. Grafeno multicamadas. 2. Colapso atômico. 3. Estados ligados virtuais.

Amanda Sertori dos Santos
Bibliotecária - CRB/8-9061
Seção Técnica de Referência, Atendimento ao Usuário e Documentação
Diretoria Técnica de Biblioteca e Documentação

UNIVERSIDADE ESTADUAL PAULISTA

Câmpus de Ilha Solteira

CERTIFICADO DE APROVAÇÃO

TÍTULO DA DISSERTAÇÃO: COLAPSO ATÔMICO EM IMPUREZAS NO GRAFENO MULTICAMADA

AUTOR: ANTONIO MARCOS DIAS FREITAS
ORIENTADOR: ANTONIO CARLOS FERREIRA SERIDONIO

Aprovado como parte das exigências para obtenção do Título de Mestre em Ciência dos Materiais, área: Física da Matéria Condensada pela Comissão Examinadora:

gov.br Documento assinado digitalmente
ANTONIO CARLOS FERREIRA SERIDONIO
Data: 05/03/2024 11:23:55-0300
Verifique em https://validar.iti.gov.br

Prof. Dr. ANTONIO CARLOS FERREIRA SERIDONIO (Participaçao Virtual)
Departamento de Fisica e Quimica / Faculdade de Engenharia de Ilha Solteira - UNESP

Prof. Dr. EDSON VERNEK (Participaçao Virtual)
Instituto de Física / Universidade Federal de Uberlândia - UFU

Dr. WENDELL SIMÕES E SILVA (Participaçao Virtual)
Laboratório Nacional Luz Síncrotron / Centro Nacional de Pesquisa em Energia e Materiais - CNPEM

Ilha Solteira, 27 de fevereiro de 2024

Impacto e Relevância Cientpífico-Social

Impacto e Relevância Científico-Social Os resultados aqui obtidos na exploração do Grafeno romboédrico multicamadas influenciam significativamente a física de materiais, a ciência em geral e além de deter um grande potencial para avanços significativos na física experimental e aplicações tecnológicas.

As propriedades eletrônicas aqui discutidas do grafeno multicamada nos trazem resultados relevantes no contexto do transporte eletrônico, logo diferenciando significativamente de materiais convencionais. As características eletrônicas aqui trabalhadas, tornam o grafeno multicamada romboédrico um material propício para o estudo do colapso atômico.

Não distante de outras áreas do saber humano, fazer ciência por meio da exploração do grafeno multicamadas mediada pela física de materiais proporcionam oportunidades para o desenvolvimento e aprimoramento do conhecimento científico. Os resultados advindos da pesquisa podem ser aplicados em diferentes campos da ciência e tecnologia. Já no âmbito social serão de grande valia esses saberes construídos no contexto da educação e formação científica, assim refletindo no desenvolvimento da sociedade como um todo.

Este dedico a familiares que contribuíram e acreditaram.

Agradecimentos

Agradeço à CAPES pelo auxílio financeiro, pois com este recurso foi possível a realização do Mestrado.

Agradeço aos familiares que contribuíram em apoio a esta etapa de minha vida, em especial a minha mãe Maria de Lourdes Dias Freitas que me fortaleceu em momentos difíceis.

Agradeço ao grupo de pesquisa por ter auxiliado e compartilhado dentro do possível a respeito dos saberes pertinente ao campo de pesquisa.

Agradeço ao Willian Carvalho da Silva por ter auxiliado no desenvolvimento dos modelos analíticos do problema proposto no desenvolvimento desta pesquisa, na instalação de softwares de acesso livre e por ter contribuído no desenvolvimento dos códigos para o levantamento dos gráficos a partir dos resultados analíticos.

Ao Prof. Dr. Antonio Carlos Ferreira Seridonio pela oportunidade concedida a realização e participação do grupo de pesquisa.

A todos os docentes que contribuíram direta e indiretamente ao aprimoramento de minha carreira acadêmica.

A todos fica a gratidão pela confiança e incentivo.

"Todo jardim começa com um sonho de amor. Antes que qualquer árvore seja plantada ou qualquer lago seja construído, é preciso que as árvores e os lagos tenham nascido dentro da alma.

Quem não tem jardins por dentro, não planta jardins por fora e nem passeia por eles..."

Rubens Alves

Resumo

Propusemos que o multi-grafeno de empilhamento do tipo ABC produz estados ligados virtuais situados dentro do *gap* isolante de Coulomb de uma impureza do tipo Anderson. Surpreendentemente, um estado virtual constitui o análogo do fenômeno do colapso atômico proposto na Física Atômica Relativística, enquanto que o segundo emerge decorrente da simetria partícula-buraco, análogo a um estado de pósitron. Assim, introduzimos o efeito do colapso atômico, que ocorre devido a uma banda chata sem dispersão e uma densidade de estados divergente $\sim |\varepsilon - \varepsilon_F|^{2/J-1}$ na energia de Fermi ε_F para $J \geq 3$, onde $J\pi$ é a fase de Berry. Concluímos esse cenário com base na transformação de Kramers-Kronig do alargamento de quasipartícula, de onde observamos que a citada singularidade de van Hove induz estados ligados virtuais. Contraintuitivamente, perto da singularidade, encontramos esses estados acima e abaixo da energia de Fermi correlacionados com a existência das bordas inferior e superior do *gap* isolante de Coulomb, respectivamente. À medida que tal comportamento surge sem torção, o sistema é conhecido como não de moiré e o fenômeno emerge também assistido pelas correlações de Coulomb da impureza. Assim, apontamos que o multi-grafeno é um sistema adequado para emular fenômenos relativísticos bem estabelecidos.

Palavras-chave: Grafeno Multicamadas, Colapso Atômico Estados Ligados Virtuais e Fenômenos Relativísticos.

Abstract

We propose that a multi-graphene of ABC-type stacking yields virtual bound states lying within the Coulomb insulating *gap* of an Anderson-like adatom. Wondrously, a virtual state constitutes the counterpart of the atomic collapse phenomenon proposed in relativistic atomic Physics, while the second emerges as its particle-hole symmetric, analogous to a positron state. Thus, we introduce the eect as the adatomic collapse, which occurs due to a at band with a dispersionless state and a divergent density of states $\sim |\varepsilon - \varepsilon_F|^{2/J-1}$ near the Fermi energy ε_F for $J \geq 3$, where J is the Berry phase. We conclude this scenario based on the Kramers-Kronig transformation of the quasiparticle broadening, from where we observe that the aforementioned van Hove singularity induces virtual bound states. Counterintuitively, near the singularity, we nd these states above and below the Fermi energy correlated to the existence of the bottom and top edges of the Coulomb insulating region, respectively. As such a behavior rises without a twist, the system is known as moireless and the phenomenon emerges also assisted by the adatom Coulomb correlations. Thus, we point out that multi-graphene is a proper playground for emulating well-established relativistic phenomena.

Keywords: Multilayer Graphene, Atomic Collapse, Virtual Bound States and Relativistic Phenomena.

Sumário

1 Introdução **12**

2 Modelo teórico **15**

3 Equação de Movimento **17**

3.1 Auto energias 30

3.2 Calculando a $\mathcal{G}_{dd}$ 35

3.3 Função de Green para quatro operadores 43

3.4 Aproximação de Hubbard I 45

3.5 Síntese de alguns resultados parciais 46

4 A DOS da impureza e LDOS do hospedeiro **48**

5 Resultados e discussões **51**

6 Conclusões **56**

7 Artigo publicado Phys. Rev. B 108, 205407 (2023) **57**

Lista de Figuras

1.1 (a) Vista lateral do multi-grafeno seguindo o empilhamento do tipo ABC e uma impureza no seu topo [painel a)-I]. (b)-(d) Os casos $J = 3, 4$ e 6, onde a estrutura de banda [Eq. 2.2] e o alargamento de quasipartículas [Eq.4.8] versus energia mostram um estado sem dispersão e uma singularidade de van Hove na energia de Fermi, respectivamente. Ao aumentar a fase de Berry $J\pi$, a extensão da banda no espaço recíproco também aumenta. Além disso, J representa o total de monocamadas [35]. 13

5.1 A simetria partícula-buraco (PHS) é considerada. (a) Grafeno único com uma impureza [a)-I], alargamento de quasipartícula linear na energia com um *pseudo-gap* no nível de Fermi [a)-II] e *gap* de Coulomb típico na DOS da impureza. (b) As bordas do *gap* aparecem como P1 e P2 na transformação de Kramers-Kronig de $-\mathrm{Im}\Sigma$, isto é, $\mathrm{Re}\Sigma$. (c) Para $J = 3, 4$ e 6 a DOS da impureza exibe estados ligados virtuais internos ao *gap*, marcados por P3 e P4 apenas para $J = 3$. (d) Para o empilhamento ABC, $\mathrm{Re}\Sigma$ diverge na energia de Fermi e as bordas inferior do *gap* de Coulomb P1 e P2 superior levam aos estados ligados virtuais P4 e P3, respectivamente. O pico ressonante P3 é devido à correlação U e emula o colapso atômico, uma vez que um estado eletronico se localiza-se em $\varepsilon < 0$. Em contraste, P4 é o simétrico partícula-buraco de P3 em $\varepsilon > 0$, analogamente a um estado de pósitron. 52

5.2 Mecanismo do colapso atômico no empilhamento ABC: (a) DOS da impureza do regime PHS para várias energias ε_d onde a extinção dos estados de ligação virtual ocorre ao enterrar a energia da impureza dentro do mar de Fermi do multigrafeno tipo ABC. (b) ReΣ revela quanto mais profundo é ε_d mais os estados virtuais caem na singularidade de van Hove e se desacoplam do átomo. (c) Esses estados aparecem na LDOS do sistema, onde a singularidade está ausente. (d) Esaa falta é devida à ΔLDOS induzida, em que uma singularidade de van Hove negativa cancela a positiva em $-\mathrm{Im}/\pi v^2$. 54

Capítulo 1

Introdução

O colapso atômico é um efeito previsto pela Física Atômica Relativística [1, 2], consistindo em um fenômeno em que a carga de um núcleo ultrapassa seu limite e torna-se capaz de capturar um elétron, seguido por uma emissão de pósitron. Para observar esse fenômeno são requeridos núcleos ultra-pesados, no entanto, tais átomos não existem na natureza espontaneamente. Infelizmente, apesar dos esforços para fabricar as condições certas para emular esses átomos, no cenário experimental próprio desse campo de investigação, a observação do colapso atômico permanece em aberto [3,4]. Entretanto, algumas plataformas da Física da Matéria Condensada surgem como potenciais emuladores para esse efeito, em que os sistemas baseados no grafeno assumem um caráter elevado para esse fim. Nesses materiais, as características mencionadas acima devem-se à sabida baixa supercriticalidade, que pode ser fabricada artificialmente. Como exemplos, citamos íons de cálcio [5], cargas de vacância e potenciais eletrotáticos [6, 7], uma vez adicionados aos sistemas dados pela monocamada de grafeno, desempenham o papel de átomos supercríticos efetivos. Como consequência, esses átomos dentro desse regime extremamente crítico exibem um estado ligado virtual localizado, aparecendo na densidade local de estados (LDOS) como um estado ressonante abaixo do nível de Fermi [5] sendo análogo ao estado do colapso atômico. Alternativamente à monocamada de grafeno, que já se provou confiável para emular o colapso atômico, somos livres para perguntar se as heteroestruturas de van der Waals também poderiam ser candidatas para esse fim, uma vez que são caracterizadas por bandas chatas [8, 9], ou seja, aquelas com singularidades de van Hove. Porém, para se alcançar essas características, é necessário um ajuste fino do "ângulo mágico de torção" e do potencial de Moiré. O grafeno bicamada torcido, os de bicamada dupla e tricamada [8–25], o grafeno tricamada ABC em nitreto de boro hexagonal alinhado [26–28] e os dichalcogenetos de metais

de transição [29–34], compõem um conjunto de exemplos mais comuns nesta área de pesquisa. Para superar tal desafio técnico, uma maneira é levar em consideração o grafeno romboédrico

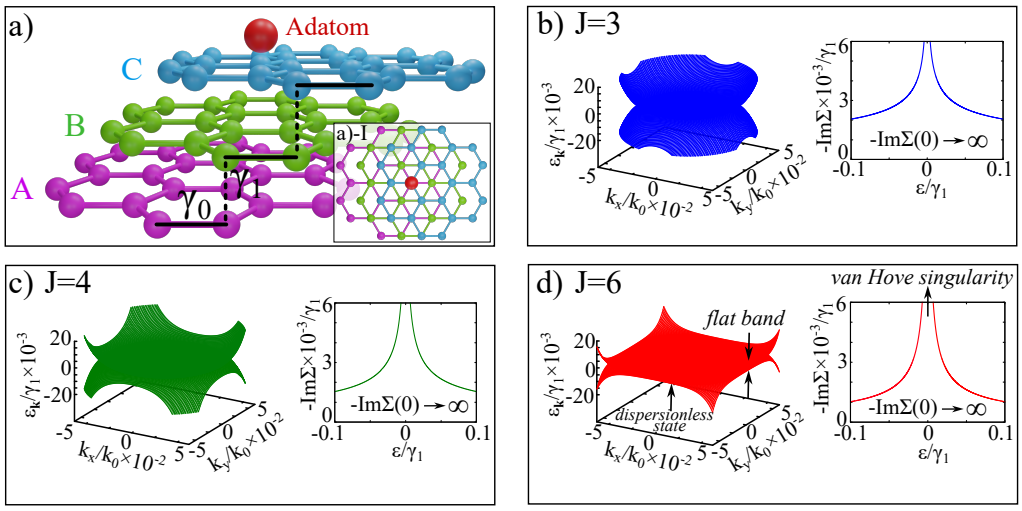


Figura 1.1: (a) Vista lateral do multi-grafeno seguindo o empilhamento do tipo ABC e uma impureza no seu topo [painel a)-I]. (b)-(d) Os casos $J = 3, 4$ e 6, onde a estrutura de banda [Eq. 2.2] e o alargamento de quasipartículas [Eq.4.8] versus energia mostram um estado sem dispersão e uma singularidade de van Hove na energia de Fermi, respectivamente. Ao aumentar a fase de Berry $J\pi$, a extensão da banda no espaço recíproco também aumenta. Além disso, J representa o total de monocamadas [35].

multicamadas (ABC) [35, 36], que naturalmente apresenta uma banda chata de baixa energia sem ter sido induzida por uma super-rede de moiré decorrente por uma torção. Curiosamente, isso é atribuído à densidade de estados (DOS) divergente no nível de Fermi [35], onde reside um estado sem dispersão. Assim, o sistema é conhecido como não de Moiré. Consequentemente, com base nesse importante aspecto experimental, nos beneficiamos dele em uma perspectiva teórica ao propor o efeito do colapso atômico. Aqui, descobrimos que o multi-grafeno com empilhamento do tipo ABC [35, 36] acaba tornando-se uma nova plataforma para concretizar o colapso atômico. Diferentemente dos resultados anteriores [5–7], o comportamento aqui relatado é o efeito líquido da interação entre as correlações de Coulomb e a singularidade de van Hove na energia de Fermi. Curiosamente, essa singularidade entra na DOS do hospedeiro pela lei de potência $|\varepsilon - \varepsilon_F|^{2/J-1}$, onde a energia de Fermi é ε_F e leva a uma divergência para $J \geq 3$, sendo $J\pi$ a fase de Berry. Fisicamente falando, uma impureza do tipo Anderson [37] no topo do sistema multi-grafeno ABC, conforme representado na Fig.1.1 (a), cumpre inteiramente as características anteriores. Simultaneamente, tal interação impõe um *gap* na DOS da impureza, onde encontramos estados ligados virtuais. Um deles encontra-se abaixo da energia de Fermi, devido à correlação e caracteriza um elétron aprisionado dentro da banda de valência, enquanto

o outro, corresponde ao seu simétrico partícula-buraco dentro da banda de condução, emulando assim um estado semelhante ao pósitron. Para a quantificação desse efeito de singularidade de van Hove, como veremos a seguir, é adotada a transformação de Kramers-Kronig do alargamento de quasipartícula, a partir da qual a emergência de estados ligados virtuais torna-se claramente evidente no sítio da impureza.

Nos capítulos seguintes serão trabalhados os seguintes tópicos, o modelo teórico, tratado no capítulo 2 onde será discutido sobre a construção do Hamiltoniano do sistema considerado. No terceiro capítulo, serão trabalhadas as equações de movimento visando determinar as autoenergias e a aproximação de Hubbard I pelo fato do sistema não ser exatamente solúvel. Já no Capítulo 4, determinaremos a DOS da impureza e a LDOS do hospedeiro. No Capítulo 5, com os resultados obtidos nos capítulos que antecedem a este, serão analisados e estudados visando compreender os fenômenos por meio dos perfis dos gráficos levantados e, por fim, buscar compreender e descrever os fenômenos obtidos pelo arranjo teórico antes descrito no capítulo 2. Finalizando com o capítulo 6, este tratará dos resultados obtidos nos capítulos anteriores. Ao final anexamos a versão do artigo científico gerado e disponível no repositório https://arxiv.org/abs/2304.02680v2 e pulicado no PRB 108, 205407 (2023), mas informamos que este texto de dissertação está baseado na versão anterior https://arxiv.org/abs/2304.02680v1, pois já tinha sido elaborado antes do término da avaliação por pares.

Capítulo 2

Modelo teórico

O Hamiltoniano do sistema [Fig.1.1 (a)] é dado por $\mathcal{H} = \mathcal{H}_{ABC} + \mathcal{H}_{Ada} + \mathcal{H}_{Hyb}$, sendo

$$\mathcal{H}_{ABC} = \sum_{\boldsymbol{ks}} \psi^{\dagger}_{\boldsymbol{ks}} s \left[D_J \left(\widetilde{k}^J_{-}\sigma_{+} + \widetilde{k}^J_{+}\sigma_{-} \right) \right] \psi_{\boldsymbol{ks}}, \tag{2.1}$$

o primeiro termo do Hamiltoniano em que descreve o multi-grafeno ABC por um conjunto de J monocamadas independentes [35, 36], sendo $J\pi$ a fase de Berry, $\psi^{\dagger}_{\boldsymbol{ks}} = \left(c^{\dagger}_{\boldsymbol{ks}}, c_{\boldsymbol{ks}} \right)$ representa o espinor, $c^{\dagger}_{\boldsymbol{ks}}(c_{\boldsymbol{ks}})$ descreve o operador de criação (aniquilação) de um elétron com momento k, spin $\sigma = \uparrow, \downarrow$ e índice de vale $s = \pm 1$ [35]. O termo em $k_{\pm} = \left(k_x \pm i k_y\right)/k_{D_J}$ não é relativístico, sendo $k_{D_J} = D_J/v_F$ ($D_{J=1} \approx \gamma_0$, $D_{J\geq 3} \approx \gamma_1 = 0,1\gamma_0$ com $\gamma_0 = 3\text{eV}$) o *cutoff* de momento (energia) *Debye-like* como no sistema de grafeno [38], v_F é a velocidade de Fermi e $\sigma_{\pm} = \frac{1}{2}(\sigma_x \pm i\sigma_y)$ as matrizes de Pauli. A estrutura de banda da Eq.(2.1) é dada diretamente pela relação de dispersão

$$\varepsilon^{\pm}_{\mathbf{k}s} = \pm v_F |\tilde{k}_{+}|^J k_{D_J}, \tag{2.2}$$

em que o sinal $+(-)$ corresponde a banda de condução (valência). Além disso, vale a pena citar que para J = 1 recuperamos uma única camada de grafeno com cones de Dirac bem definidos no espaço dos momentos, enquanto que para $J \geq 3$ temos o multi-grafeno, em que sua estrutura eletrônica exibe uma banda altamente chata com uma singularidade de van Hove extremamente aguda, devido a um estado sem dispersão na energia de Fermi. Tendo como base o modelo de Anderson [37], o Hamiltoniano que descreve o sistema de uma impureza.

$$\mathcal{H}_{\text{Ada.}} = -\frac{U}{2} + \sum_{\sigma} \left(\varepsilon_{d\sigma} + \frac{U}{2} \right) n_{d\sigma} + \frac{U}{2} \left(\sum_{\sigma} n_{d\sigma} - 1 \right)^2, \tag{2.3}$$

no qual os níveis da impureza são $\varepsilon_{d\sigma}$ e $\varepsilon_{d\sigma} + U$, também conhecidos como as bordas inferior e superior do *gap* isolante de Coulomb, respectivamente [39]. O termo U representa a repulsão de Coulomb entre dois elétrons de spin opostos ($\bar{\sigma} = -\sigma$), assim como o tamanho do *gap* e $n_{d\sigma} = (n_{d\sigma})^2 = d^\dagger_\sigma d_\sigma$ representa o operador número, sendo $d^\dagger_\sigma$ (d_σ) o correspondente operador de criação (aniquilação). O termo de hibridização, que acopla o hospedeiro ao átomo, é dado por

$$\mathcal{H}_{\text{Hyb.}} = v \left(\frac{1}{\sqrt{\mathcal{N}}} \sum_{\mathbf{k}s\sigma} c^\dagger_{\mathbf{k}s\sigma} d_\sigma + \text{H.c.} \right), \tag{2.4}$$

sendo v a amplitude de hibridização e $\mathcal{N}$ é o número de estados delimitados pelo raio de Debye k_D.

Capítulo 3

Equação de Movimento

Para obter as auto energias do sistema proposto no capítulo anterior, faremos uso da função de Green retardada,

$$\mathcal{G}^{R}_{c_{\boldsymbol{k}s\sigma},c_{\boldsymbol{k}'s'\sigma}}(t) = -\frac{i}{\hbar}\theta(t-t')\,Z^{-1}\sum_{n} e^{-\beta E_n}\left\langle n\left|\left[c_{\boldsymbol{k}s\sigma}, c^{\dagger}_{\boldsymbol{k}'s'\sigma}\right]_{+}\right|n\right\rangle, \tag{3.1}$$

e também, vamos recorrer ao método da equação de movimento (do Inglês Equation of Motion)

$$\begin{aligned}
\frac{\partial}{\partial t}\mathcal{G}_{c_{\boldsymbol{k}s\sigma},c_{\boldsymbol{k}'s'\sigma}}(t) &= -\frac{\partial}{\partial t}\frac{i}{\hbar}\theta(t)\,Z^{-1}\sum_{n} e^{-\beta E_n}\left\langle n\left|\left[c_{\boldsymbol{k}s\sigma}, c^{\dagger}_{\boldsymbol{k}'s'\sigma}\right]_{+}\right|n\right\rangle \\
&= -\frac{i}{\hbar}\delta(t)\,Z^{-1}\sum_{n} e^{-\beta E_n}\left\langle n\left|\left[c_{\boldsymbol{k}s\sigma}, c^{\dagger}_{\boldsymbol{k}'s'\sigma}\right]_{+}\right|n\right\rangle \\
&- \frac{i}{\hbar}\theta(t)\,Z^{-1}\sum_{n} e^{-\beta E_n}\left\langle n\left|\left[\frac{\partial}{\partial t}c_{\boldsymbol{k}s\sigma}, c^{\dagger}_{\boldsymbol{k}'s'\sigma}\right]_{+}\right|n\right\rangle,
\end{aligned} \tag{3.2}$$

mas pela equação de Heisenberg, temos que

$$\begin{aligned}
\frac{\partial}{\partial t}c_{\boldsymbol{k}s\sigma} &= -\frac{i}{\hbar}\left[c_{\boldsymbol{k}s\sigma},\mathcal{H}\right] \\
&= -\frac{i}{\hbar}\left[c_{\boldsymbol{k}s\sigma},\sum_{k's'\sigma'}\left(c^{\dagger}_{\boldsymbol{k'}s'\sigma'}sv_{\perp}\frac{k_{+}^{J}}{k_{D_J}^{J-1}}c_{\boldsymbol{k'}s'\bar{\sigma'}}\right)\right] \\
&- \frac{i}{\hbar}\left[c_{\boldsymbol{k}s\sigma},\sum_{\sigma'}\varepsilon_{d'\sigma'}d^{\dagger}_{\sigma'}d_{\sigma'}\right] \\
&- \frac{i}{\hbar}\left[c_{\boldsymbol{k}s\sigma},Ud^{\dagger}_{\uparrow}d_{\uparrow}d^{\dagger}_{\downarrow}d_{\downarrow}\right] \\
&- \frac{i}{\hbar}\left[c_{\boldsymbol{k}s\sigma},\frac{1}{\sqrt{\mathcal{N}}}\sum_{\sigma'\boldsymbol{k'}s'}vc^{\dagger}_{\boldsymbol{k'}s'\sigma'}d_{\sigma'}\right] \\
&- \frac{i}{\hbar}\left[c_{\boldsymbol{k}s\sigma},\frac{1}{\sqrt{\mathcal{N}}}\sum_{\sigma'\boldsymbol{k'}s'}v^{*}d^{\dagger}_{\sigma'}c_{\boldsymbol{k'}s'\sigma'}\right]. \qquad (3.3)
\end{aligned}$$

Resolvendo os comutadores do hamiltoniano apresentado em Eq.(3.3) separadamente, obtemos.

$$\begin{aligned}
-\frac{i}{\hbar}\left[c_{ks\sigma},\sum_{k's'\sigma'}\left(c^{\dagger}_{k's'\sigma'}sv_{\perp}\frac{k_{\bar{\sigma}}^{J}}{k_{D_J}^{J-1}}c_{k's'\bar{\sigma'}}\right)\right] &= -\frac{i}{\hbar}\sum_{k's'\sigma'}sv_{\perp}\frac{k_{\bar{\sigma}}^{J}}{k_{D_J}^{J-1}}\left[c_{\boldsymbol{k}s\sigma},c^{\dagger}_{\boldsymbol{k'}s'\sigma'}c_{\boldsymbol{k'}s'\bar{\sigma'}}\right] \\
&= -\frac{i}{\hbar}\sum_{k's'\sigma'}sv_{\perp}\frac{k_{\bar{\sigma}}^{J}}{k_{D_J}^{J-1}}\left[c_{\boldsymbol{k}s\sigma}c^{\dagger}_{\boldsymbol{k'}s'\sigma'}c_{\boldsymbol{k'}s'\bar{\sigma'}}-c^{\dagger}_{\boldsymbol{k'}s'\sigma'}c_{\boldsymbol{k'}s'\bar{\sigma'}}c_{\boldsymbol{k}s\sigma}\right] \\
&= -\frac{i}{\hbar}\sum_{k's'\sigma'}sv_{\perp}\frac{k_{\bar{\sigma}}^{J}}{k_{D_J}^{J-1}}\left[c_{\boldsymbol{k}s\sigma}c^{\dagger}_{\boldsymbol{k'}s'\sigma'}c_{\boldsymbol{k'}s'\bar{\sigma'}}+c^{\dagger}_{\boldsymbol{k'}s'\sigma'}c_{\boldsymbol{k}s\sigma}c_{\boldsymbol{k'}s'\bar{\sigma'}}\right] \\
&= -\frac{i}{\hbar}\sum_{k's'\sigma'}sv_{\perp}\frac{k_{\bar{\sigma}}^{J}}{k_{D_J}^{J-1}}\Big[c_{\boldsymbol{k}s\sigma}c^{\dagger}_{\boldsymbol{k'}s'\sigma'}c_{\boldsymbol{k'}s'\bar{\sigma'}} \\
&+ \left(\delta_{\boldsymbol{k'k}}\delta_{s's}\delta_{\sigma'\sigma}-c_{\boldsymbol{k}s\sigma}c^{\dagger}_{\boldsymbol{k'}s'\sigma'}\right)c_{\boldsymbol{k'}s'\bar{\sigma'}}\Big] \\
&= -\frac{i}{\hbar}\sum_{k's'\sigma'}sv_{\perp}\frac{k_{\bar{\sigma}}^{J}}{k_{D_J}^{J-1}}\Big[\cancel{c_{\boldsymbol{k}s\sigma}c^{\dagger}_{\boldsymbol{k'}s'\sigma'}c_{\boldsymbol{k'}s'\bar{\sigma'}}}+\delta_{\boldsymbol{k'k}}\delta_{s's}\delta_{\sigma'\sigma}c_{\boldsymbol{k'}s'\bar{\sigma'}} \\
&- \cancel{c_{\boldsymbol{k}s\sigma}c^{\dagger}_{\boldsymbol{k'}s'\sigma'}c_{\boldsymbol{k'}s'\bar{\sigma'}}}\Big] \\
&= -\frac{i}{\hbar}\sum_{k's'\sigma'}sv_{\perp}\frac{k_{\bar{\sigma}}^{J}}{k_{D_J}^{J-1}}\delta_{\boldsymbol{k'k}}\delta_{s's}\delta_{\sigma'\sigma}c_{\boldsymbol{k'}s'\bar{\sigma'}} \\
&= -\frac{i}{\hbar}sv_{\perp}\frac{k_{\bar{\sigma}}^{J}}{k_{D_J}^{J-1}}c_{\boldsymbol{k}s\bar{\sigma}}, \qquad (3.4)
\end{aligned}$$

$$
\begin{aligned}
-\frac{i}{\hbar}\left[c_{\boldsymbol{k}s\sigma}, \sum_{\sigma'} \varepsilon_{d'\sigma'} d^\dagger_{\sigma'} d_{\sigma'}\right] &= -\frac{i}{\hbar}\sum_{\sigma'} \varepsilon_{d'\sigma'}\left[c_{\boldsymbol{k}s\sigma}, d^\dagger_{\sigma'} d_{\sigma'}\right] \\
&= -\frac{i}{\hbar}\sum_{\sigma'} \varepsilon_{d'\sigma'}\left[c_{\boldsymbol{k}s\sigma} d^\dagger_{\sigma'} d_{\sigma'} - d^\dagger_{\sigma'} d_{\sigma'} c_{\boldsymbol{k}s\sigma}\right] \\
&= -\frac{i}{\hbar}\sum_{\sigma'} \varepsilon_{d'\sigma'}\left[c_{\boldsymbol{k}s\sigma} d^\dagger_{\sigma'} d_{\sigma'} + d^\dagger_{\sigma'} c_{\boldsymbol{k}s\sigma} d_{\sigma'}\right] \\
&= -\frac{i}{\hbar}\sum_{\sigma'} \varepsilon_{d'\sigma'}\left[\cancel{c_{\boldsymbol{k}s\sigma} d^\dagger_{\sigma'} d_{\sigma'}} - \cancel{c_{\boldsymbol{k}s\sigma} d^\dagger_{\sigma'} d_{\sigma'}}\right] \\
&= 0, \qquad (3.5)
\end{aligned}
$$

$$
\begin{aligned}
-\frac{i}{\hbar}\left[c_{\boldsymbol{k}s\sigma}, U d^\dagger_\uparrow d_\uparrow d^\dagger_\downarrow d_\downarrow\right] &= -\frac{i}{\hbar}U\left[c_{\boldsymbol{k}s\sigma}, d^\dagger_\uparrow d_\uparrow d^\dagger_\downarrow d_\downarrow\right] \\
&= -\frac{i}{\hbar}U\left[c_{\boldsymbol{k}s\sigma} d^\dagger_\uparrow d_\uparrow d^\dagger_\downarrow d_\downarrow - d^\dagger_\uparrow d_\uparrow d^\dagger_\downarrow d_\downarrow c_{\boldsymbol{k}s\sigma}\right] \\
&= -\frac{i}{\hbar}U\left[c_{\boldsymbol{k}s\sigma} d^\dagger_\uparrow d_\uparrow d^\dagger_\downarrow d_\downarrow + d^\dagger_\uparrow d_\uparrow d^\dagger_\downarrow c_{\boldsymbol{k}s\sigma} d_\downarrow\right] \\
&= -\frac{i}{\hbar}U\left[c_{\boldsymbol{k}s\sigma} d^\dagger_\uparrow d_\uparrow d^\dagger_\downarrow d_\downarrow - d^\dagger_\uparrow d_\uparrow c_{\boldsymbol{k}s\sigma} d^\dagger_\downarrow d_\downarrow\right] \\
&= -\frac{i}{\hbar}U\left[c_{\boldsymbol{k}s\sigma} d^\dagger_\uparrow d_\uparrow d^\dagger_\downarrow d_\downarrow + d^\dagger_\uparrow c_{\boldsymbol{k}s\sigma} d_\uparrow d^\dagger_\downarrow d_\downarrow\right] \\
&= -\frac{i}{\hbar}U\left[\cancel{c_{\boldsymbol{k}s\sigma} d^\dagger_\uparrow d_\uparrow d^\dagger_\downarrow d_\downarrow} - \cancel{c_{\boldsymbol{k}s\sigma} d^\dagger_\uparrow d_\uparrow d^\dagger_\downarrow d_\downarrow}\right] \\
&= 0, \qquad (3.6)
\end{aligned}
$$

$$
\begin{aligned}
-\frac{i}{\hbar}\left[c_{\boldsymbol{k}s\sigma}, \frac{1}{\sqrt{\mathcal{N}}}\sum_{\sigma'} v \sum_{\boldsymbol{k'}s'} c^{\dagger}_{\boldsymbol{k'}s'\sigma'} d_{\sigma'}\right] &= -\frac{i}{\hbar}\frac{1}{\sqrt{\mathcal{N}}}\sum_{\sigma'\boldsymbol{k'}s'} v\left[c_{\boldsymbol{k}s\sigma}, c^{\dagger}_{\boldsymbol{k'}s'\sigma'} d_{\sigma'}\right] \\
&= -\frac{i}{\hbar}\frac{1}{\sqrt{\mathcal{N}}}\sum_{\sigma'\boldsymbol{k'}s'} v\left[c_{\boldsymbol{k}s\sigma} c^{\dagger}_{\boldsymbol{k'}s'\sigma'} d_{\sigma'} - c^{\dagger}_{\boldsymbol{k'}s'\sigma'} d_{\sigma'} c_{\boldsymbol{k}s\sigma}\right] \\
&= -\frac{i}{\hbar}\frac{1}{\sqrt{\mathcal{N}}}\sum_{\sigma'\boldsymbol{k'}s'} v\left[c_{\boldsymbol{k}s\sigma} c^{\dagger}_{\boldsymbol{k'}s'\sigma'} d_{\sigma'} + c^{\dagger}_{\boldsymbol{k'}s'\sigma'} c_{\boldsymbol{k}s\sigma} d_{\sigma'}\right] \\
&= -\frac{i}{\hbar}\frac{1}{\sqrt{\mathcal{N}}}\sum_{\sigma'\boldsymbol{k'}s'} v\Big[c_{\boldsymbol{k}s\sigma} c^{\dagger}_{\boldsymbol{k'}s'\sigma'} d_{\sigma'} \\
&+ \left(\delta_{\boldsymbol{k'}\boldsymbol{k}}\delta_{s's}\delta_{s's} - c_{\boldsymbol{k}s\sigma} c^{\dagger}_{\boldsymbol{k'}s'\sigma'}\right) d_{\sigma'}\Big] \\
&= -\frac{i}{\hbar}\frac{1}{\sqrt{\mathcal{N}}}\sum_{\sigma'\boldsymbol{k'}s'} v\Big[\cancel{c_{\boldsymbol{k}s\sigma} c^{\dagger}_{\boldsymbol{k'}s'\sigma'} d_{\sigma'}} + \delta_{\boldsymbol{k'}\boldsymbol{k}}\delta_{s's}\delta_{s's} d_{\sigma'} \\
&- \cancel{c_{\boldsymbol{k}s\sigma} c^{\dagger}_{\boldsymbol{k'}s'\sigma'} d_{\sigma'}}\Big] \\
&= -\frac{i}{\hbar}\frac{1}{\sqrt{\mathcal{N}}}\sum_{\sigma'\boldsymbol{k'}s'} v\delta_{\boldsymbol{k'}\boldsymbol{k}}\delta_{s's}\delta_{s's} d_{\sigma'} \\
&= -\frac{i}{\hbar}\frac{1}{\sqrt{\mathcal{N}}}\sum_{\sigma'\boldsymbol{k'}s'} v d_{\sigma} \qquad (3.7)
\end{aligned}
$$

e

$$
\begin{aligned}
-\frac{i}{\hbar}\left[c_{\boldsymbol{k}s\sigma}, \frac{1}{\sqrt{\mathcal{N}}}\sum_{\sigma'\boldsymbol{k'}s'} v^{*} d^{\dagger}_{\sigma'} c_{\boldsymbol{k'}s'\sigma'}\right] &= -\frac{i}{\hbar}\frac{1}{\sqrt{\mathcal{N}}}\sum_{\sigma'\boldsymbol{k'}s'} v^{*}\left[c_{\boldsymbol{k}s\sigma}, d^{\dagger}_{\sigma'} c_{\boldsymbol{k'}s'\sigma'}\right] \\
&= -\frac{i}{\hbar}\frac{1}{\sqrt{\mathcal{N}}}\sum_{\sigma'\boldsymbol{k'}s'} v^{*}\left[c_{\boldsymbol{k}s\sigma} d^{\dagger}_{\sigma'} c_{\boldsymbol{k'}s'\sigma'} - d^{\dagger}_{\sigma'} c_{\boldsymbol{k'}s'\sigma'} c_{\boldsymbol{k}s\sigma}\right] \\
&= -\frac{i}{\hbar}\frac{1}{\sqrt{\mathcal{N}}}\sum_{\sigma'\boldsymbol{k'}s'} v^{*}\left[c_{\boldsymbol{k}s\sigma} d^{\dagger}_{\sigma'} c_{\boldsymbol{k'}s'\sigma'} + d^{\dagger}_{\sigma'} c_{\boldsymbol{k}s\sigma} c_{\boldsymbol{k'}s'\sigma'}\right] \\
&= -\frac{i}{\hbar}\frac{1}{\sqrt{\mathcal{N}}}\sum_{\sigma'\boldsymbol{k'}s'} v^{*}\left[\cancel{c_{\boldsymbol{k}s\sigma} d^{\dagger}_{\sigma'} c_{\boldsymbol{k'}s'\sigma'}} - \cancel{c_{\boldsymbol{k}s\sigma} d^{\dagger}_{\sigma'} c_{\boldsymbol{k'}s'\sigma'}}\right]. \qquad (3.8)
\end{aligned}
$$

Assim a Eq.(3.3) pode ser reescrita como

$$
\begin{aligned}
\frac{\partial}{\partial t} c_{\boldsymbol{k}s\sigma} &= -\frac{i}{\hbar} s v_{\perp} \frac{k^{J}_{\bar{\sigma}}}{k^{J-1}_{D_J}} c_{\boldsymbol{k}s\bar{\sigma}} \\
&- \frac{i}{\hbar}\frac{1}{\sqrt{\mathcal{N}}}\sum_{\sigma'\boldsymbol{k'}s'} v d_{\sigma}. \qquad (3.9)
\end{aligned}
$$

Então,

$$\begin{aligned}\frac{\partial}{\partial t}\mathcal{G}^{R}_{c_{\boldsymbol{k}s\sigma},c_{\boldsymbol{k}'s'\sigma}}(t) &= -\frac{i}{\hbar}\delta(t-t')\,Z^{-1}\sum_{n}e^{-\beta E_n}\left\langle n\left|\left[c_{\boldsymbol{k}s\sigma},c^{\dagger}_{\boldsymbol{k}'s'\sigma}\right]_{+}\right|n\right\rangle \\ &- \frac{i}{\hbar}sv_{\perp}\frac{k^{J}_{\bar{\sigma}}}{k^{J-1}_{D_J}}\left\{-\frac{i}{\hbar}\theta(t-t')\,Z^{-1}\sum_{n}e^{-\beta E_n}\left\langle n\left|\left[c_{\boldsymbol{k}s\bar{\sigma}},c^{\dagger}_{\boldsymbol{k}'s'\sigma}\right]_{+}\right|n\right\rangle\right\} \\ &- \frac{i}{\hbar}\frac{1}{\sqrt{N}}\sum_{\sigma'\boldsymbol{k}'s'}v\left\{-\frac{i}{\hbar}\theta(t-t')\,Z^{-1}\sum_{n}e^{-\beta E_n}\left\langle n\left|\left[d_{\sigma},c^{\dagger}_{\boldsymbol{k}'s'\sigma}\right]_{+}\right|n\right\rangle\right\} \quad (3.10)\end{aligned}$$

Ou seja,

$$\begin{aligned}\frac{\partial}{\partial t}\mathcal{G}^{R}_{c_{\boldsymbol{k}s\sigma},c_{\boldsymbol{k}'s'\sigma}}(t) &= -\frac{i}{\hbar}\delta(t-t')\,Z^{-1}\sum_{n}e^{-\beta E_n}\left\langle n\left|\left[c_{\boldsymbol{k}s\sigma},c^{\dagger}_{\boldsymbol{k}'s'\sigma}\right]_{+}\right|n\right\rangle \\ &- \frac{i}{\hbar}sv_{\perp}\frac{k^{J}_{\bar{\sigma}}}{k^{J-1}_{D_J}}\mathcal{G}^{R}_{c_{\boldsymbol{k}s\bar{\sigma}},c_{\boldsymbol{k}'s'\sigma}}(t) \\ &- \frac{i}{\hbar}\frac{1}{\sqrt{\mathcal{N}}}\sum_{\sigma'\boldsymbol{k}'s'}v\mathcal{G}^{R}_{d_{\sigma},c_{\boldsymbol{k}'s'\sigma}}(t)\,. \quad (3.11)\end{aligned}$$

Realizando a transformada de Fourier,

$$\begin{aligned}\varepsilon^{+}\widetilde{\mathcal{G}}^{R}_{c_{\boldsymbol{k}s\sigma},c_{\boldsymbol{k}'s'\sigma}}(\varepsilon^{+}) &= \delta_{\boldsymbol{k}'\boldsymbol{k}}\delta_{s's}\delta_{\sigma'\sigma} \\ &+ sv_{\perp}\frac{k^{J}_{\bar{\sigma}}}{k^{J-1}_{D_J}}\widetilde{\mathcal{G}}^{R}_{c_{\boldsymbol{k}s\bar{\sigma}},c_{\boldsymbol{k}'s'\sigma}}(\varepsilon^{+}) \\ &+ \frac{1}{\sqrt{\mathcal{N}}}\sum_{\sigma'\boldsymbol{k}'s'}v\widetilde{\mathcal{G}}^{R}_{d_{\sigma},c_{\boldsymbol{k}'s'\sigma}}(\varepsilon^{+})\,. \quad (3.12)\end{aligned}$$

Utilizando a Eq.(3.12), podemos escrever quatro funções de Green por $\sigma = \uparrow,\downarrow$ e $\sigma' = \uparrow,\downarrow$

$$\begin{aligned}\widetilde{\mathcal{G}}^{R}_{c_{\boldsymbol{k}s\uparrow}c_{\boldsymbol{k}'s'\uparrow}}(\varepsilon^{+}) &= \frac{\delta_{\boldsymbol{k}\boldsymbol{k}'}\delta_{ss'}}{\varepsilon^{+}} \\ &+ \frac{sv_{\perp}\frac{k^{J}_{-}}{k^{J-1}_{D_J}}}{\varepsilon^{+}}\widetilde{\mathcal{G}}^{R}_{c_{ks\downarrow}c_{\boldsymbol{k}'s'\uparrow}}(\varepsilon^{+}) \\ &+ \frac{1}{\varepsilon^{+}\sqrt{\mathcal{N}}}v\widetilde{\mathcal{G}}^{R}_{d_{\uparrow}c_{\boldsymbol{k}'s'\uparrow}}(\varepsilon^{+})\,, \quad (3.13)\end{aligned}$$

$$\widetilde{\mathcal{G}}^{R}_{c_{\boldsymbol{k}s\downarrow}c_{\boldsymbol{k'}s'\uparrow}}\left(\varepsilon^{+}\right) = \frac{sv_{\perp}\frac{k_{+}^{J}}{k_{D_J}^{J-1}}}{\varepsilon^{+}}\widetilde{\mathcal{G}}^{R}_{c_{ks\uparrow}c_{\boldsymbol{k'}s'\uparrow}}\left(\varepsilon^{+}\right) + \frac{1}{\varepsilon^{+}\sqrt{\mathcal{N}}}v\widetilde{\mathcal{G}}^{R}_{d_{\downarrow}c_{\boldsymbol{k'}s'\uparrow}}\left(\varepsilon^{+}\right), \tag{3.14}$$

$$\widetilde{\mathcal{G}}^{R}_{c_{\boldsymbol{k}s\uparrow}c_{\boldsymbol{k'}s'\downarrow}}\left(\varepsilon^{+}\right) = \frac{sv_{\perp}\frac{k_{-}^{J}}{k_{D_J}^{J-1}}}{\varepsilon^{+}}\widetilde{\mathcal{G}}^{R}_{c_{ks\downarrow}c_{\boldsymbol{k'}s'\downarrow}}\left(\varepsilon^{+}\right) + \frac{1}{\varepsilon^{+}\sqrt{\mathcal{N}}}v\widetilde{\mathcal{G}}^{R}_{d_{\uparrow}c_{\boldsymbol{k'}s'\downarrow}}\left(\varepsilon^{+}\right) \tag{3.15}$$

e

$$\begin{aligned}\widetilde{\mathcal{G}}^{R}_{c_{\boldsymbol{k}s\downarrow}c_{\boldsymbol{k'}s'\downarrow}}\left(\varepsilon^{+}\right) &= \frac{\delta_{\boldsymbol{kk'}}\delta_{ss'}}{\varepsilon^{+}} \\ &+ \frac{sv_{\perp}\frac{k_{+}^{J}}{k_{D_J}^{J-1}}}{\varepsilon^{+}}\widetilde{\mathcal{G}}^{R}_{c_{ks\uparrow}c_{\boldsymbol{k'}s'\downarrow}}\left(\varepsilon^{+}\right) \\ &+ \frac{1}{\varepsilon^{+}\sqrt{\mathcal{N}}}v\widetilde{\mathcal{G}}^{R}_{d_{\downarrow}c_{\boldsymbol{k'}s'\downarrow}}\left(\varepsilon^{+}\right).\end{aligned} \tag{3.16}$$

Substituindo a Eq.(3.14) na Eq.(3.13), obtemos.

$$\begin{aligned}\widetilde{\mathcal{G}}^{R}_{c_{\boldsymbol{k}s\uparrow}c_{\boldsymbol{k'}s'\uparrow}}\left(\varepsilon^{+}\right) &= \frac{\delta_{\boldsymbol{kk'}}\delta_{ss'}}{\varepsilon^{+}} \\ &+ \frac{sv_{\perp}\frac{k_{-}^{J}}{k_{D_J}^{J-1}}}{\varepsilon^{+}}\left(\frac{sv_{\perp}\frac{k_{+}^{J}}{k_{D_J}^{J-1}}}{\varepsilon^{+}}\widetilde{\mathcal{G}}^{R}_{c_{ks\uparrow}c_{\boldsymbol{k'}s'\uparrow}}\left(\varepsilon^{+}\right) + \frac{1}{\varepsilon^{+}\sqrt{\mathcal{N}}}v\widetilde{\mathcal{G}}^{R}_{d_{\downarrow}c_{\boldsymbol{k'}s'\uparrow}}\left(\varepsilon^{+}\right)\right) \\ &+ \frac{1}{\varepsilon^{+}\sqrt{\mathcal{N}}}v\widetilde{\mathcal{G}}^{R}_{d_{\uparrow}c_{\boldsymbol{k'}s'\uparrow}}\left(\varepsilon^{+}\right),\end{aligned} \tag{3.17}$$

$$
\begin{aligned}
\widetilde{\mathcal{G}}^{R}_{c_{ks\uparrow}c_{\boldsymbol{k'}s'\uparrow}} &= \left(\frac{(\varepsilon^{+})}{(\varepsilon^{+})^{2}-v_{\perp}^{2}\frac{k_{-}^{J}k_{+}^{J}}{k_{D_J}^{2J-2}}}\right)\delta_{\boldsymbol{kk'}}\delta_{ss'} \\
&+ \left(\frac{sv_{\perp}\frac{k_{-}^{J}}{k_{D_J}^{J-1}}v}{(\varepsilon^{+})^{2}-v_{\perp}^{2}\frac{k_{-}^{J}k_{+}^{J}}{k_{D_J}^{2J-2}}}\right)\frac{1}{\sqrt{\mathcal{N}}}\widetilde{G}^{R}_{d_{\downarrow}c_{\boldsymbol{k'}s'\uparrow}}\left(\varepsilon^{+}\right) \\
&+ \left(\frac{(\varepsilon^{+})\,v}{(\varepsilon^{+})^{2}-v_{\perp}^{2}\frac{k_{-}^{J}k_{+}^{J}}{k_{D_J}^{2J-2}}}\right)\frac{1}{\sqrt{\mathcal{N}}}\widetilde{\mathcal{G}}^{R}_{d_{\uparrow}c_{\boldsymbol{k'}s'\uparrow}}\left(\varepsilon^{+}\right). \qquad (3.18)
\end{aligned}
$$

De modo análogo, substituindo a Eq.(3.14) na Eq.(3.16) obtém-se,

$$
\begin{aligned}
\widetilde{\mathcal{G}}^{R}_{c_{\boldsymbol{k}s\downarrow}c_{\boldsymbol{k'}s'\downarrow}} &= \frac{\delta_{\boldsymbol{kk'}}\delta_{ss'}}{\varepsilon^{+}} \\
&+ \frac{sv_{\perp}\frac{k_{+}^{J}}{k_{D_J}^{J-1}}}{\varepsilon^{+}}\left(\frac{sv_{\perp}\frac{k_{-}^{J}}{k_{D_J}^{J-1}}}{\varepsilon^{+}}\widetilde{\mathcal{G}}^{R}_{c_{\boldsymbol{k}s\downarrow}c^{\dagger}_{\boldsymbol{k'}s'\downarrow}}\left(\varepsilon^{+}\right)+\frac{1}{\varepsilon^{+}\sqrt{\mathcal{N}}}v\widetilde{\mathcal{G}}^{R}_{d_{\uparrow}c^{\dagger}_{\boldsymbol{k'}s'\downarrow}}\left(\varepsilon^{+}\right)\right) \\
&+ \frac{1}{\varepsilon^{+}\sqrt{\mathcal{N}}}v\widetilde{\mathcal{G}}^{R}_{d_{\downarrow}c^{\dagger}_{\boldsymbol{k'}s'\downarrow}}\left(\varepsilon^{+}\right), \qquad (3.19)
\end{aligned}
$$

$$
\begin{aligned}
\widetilde{\mathcal{G}}^{R}_{c_{ks\downarrow}c^{\dagger}_{\boldsymbol{k'}s'\downarrow}}\left(\varepsilon^{+}\right) &= \left(\frac{(\varepsilon^{+})}{(\varepsilon^{+})^{2}-v_{\perp}^{2}\frac{k_{+}^{J}k_{-}^{J}}{k_{D_J}^{2J-2}}}\right)\delta_{\boldsymbol{kk'}}\delta_{ss'} \\
&+ \left(\frac{sv_{\perp}\frac{k_{+}^{J}}{k_{D_J}^{J-1}}v}{(\varepsilon^{+})^{2}-v_{\perp}^{2}\frac{k_{+}^{J}k_{-}^{J}}{k_{D_J}^{2J-2}}}\right)\frac{1}{\sqrt{\mathcal{N}}}\widetilde{\mathcal{G}}^{R}_{d_{\uparrow},c_{\boldsymbol{k'}s'\downarrow}}\left(\varepsilon^{+}\right) \\
&+ \left(\frac{(\varepsilon^{+})\,v}{(\varepsilon^{+})^{2}-v_{\perp}^{2}\frac{k_{+}^{J}k_{-}^{J}}{k_{D_J}^{2J-2}}}\right)\frac{1}{\sqrt{\mathcal{N}}}\widetilde{\mathcal{G}}^{R}_{d_{\downarrow},c_{\boldsymbol{k'}s'\downarrow}}\left(\varepsilon^{+}\right). \qquad (3.20)
\end{aligned}
$$

Agora precisamos calcular $\mathcal{G}^{R}_{dc}\left(\varepsilon^{+}\right)$. Pare este caso, utilizaremos a função de Green avançada

$$
\mathcal{G}^{A}_{d_{\sigma}c_{\boldsymbol{a'}s'\sigma'}}(t)=\frac{i}{\hbar}\theta(-t)Z^{-1}\sum_{n}e^{-\beta E_{n}}\left\langle n\left|\left[d^{\dagger}_{\sigma}(0),c_{\boldsymbol{a'}s'\sigma'}(t)\right]_{+}\right|n\right\rangle. \qquad (3.21)
$$

Então

$$\begin{aligned}\frac{\partial}{\partial t}\mathcal{G}^{A}_{d_\sigma c_{\boldsymbol{a}'s'\sigma'}}(t) &= -\frac{i}{\hbar}\delta(-t)Z^{-1}\sum_n e^{-\beta E_n}\left\langle n\left|\left[d^\dagger_\sigma(0), c_{\boldsymbol{a}'s'\sigma'}(t)\right]_+\right|n\right\rangle \\ &- \frac{i}{\hbar}\theta(-t)Z^{-1}\sum_n e^{-\beta E_n}\left\langle n\left|\left[d^\dagger_\sigma(0), \frac{\partial}{\partial t}c_{\boldsymbol{a}'s'\sigma'}(t)\right]_+\right|n\right\rangle \end{aligned} \tag{3.22}$$

e

$$\begin{aligned}\frac{\partial}{\partial t}c_{\boldsymbol{a}'s'\sigma'} &= -\frac{i}{\hbar}\left[c_{\boldsymbol{a}'s'\sigma'}, \mathcal{H}\right] \\ &= -\frac{i}{\hbar}\sum_{\boldsymbol{a}s\sigma} s v_\perp \frac{k^J_{\bar\sigma}}{k^{J-1}_{D_J}}\left[c_{\boldsymbol{a}'s'\sigma'}, c^\dagger_{\boldsymbol{a}s\sigma}c_{\boldsymbol{a}s\bar\sigma}\right] \\ &- \frac{i}{\hbar}\sum_\sigma \varepsilon_{d\sigma}\left[c_{\boldsymbol{a}'s'\sigma'}, d^\dagger_\sigma d_\sigma\right] \\ &- \frac{i}{\hbar}U\left[c_{\boldsymbol{a}'s'\sigma'}, d^\dagger_\uparrow d_\uparrow d^\dagger_\downarrow d_\downarrow\right] \\ &- \frac{i}{\hbar}\frac{1}{\sqrt{N}}\sum_{\boldsymbol{a}s\sigma} v\left[c_{\boldsymbol{a}'s'\sigma'}, c^\dagger_{\boldsymbol{a}s\sigma}d_\sigma\right] \\ &- \frac{i}{\hbar}\frac{1}{\sqrt{N}}\sum_{\boldsymbol{a}s\sigma} v^*\left[c_{\boldsymbol{a}'s'\sigma'}, d^\dagger_\sigma c_{\boldsymbol{a}s\sigma}\right]. \end{aligned} \tag{3.23}$$

Resolvendo os comutadores da Eq.(3.23) separadamente

$$\begin{aligned}-\frac{i}{\hbar}\sum_{\boldsymbol{a}s\sigma} s v_\perp \frac{k^J_{\bar\sigma}}{k^{J-1}_{D_J}}\left[c_{\boldsymbol{a}'s'\sigma'}, c^\dagger_{\boldsymbol{a}s\sigma}c_{\boldsymbol{a}s\bar\sigma}\right] &= -\frac{i}{\hbar}\sum_{\boldsymbol{a}s\sigma} s v_\perp \frac{k^J_{\bar\sigma}}{k^{J-1}_{D_J}}\left[c_{\boldsymbol{a}'s'\sigma'}c^\dagger_{\boldsymbol{a}s\sigma}c_{\boldsymbol{a}s\bar\sigma} - c^\dagger_{\boldsymbol{a}s\sigma}c_{\boldsymbol{a}s\bar\sigma}c_{\boldsymbol{a}'s'\sigma'}\right] \\ &= -\frac{i}{\hbar}\sum_{\boldsymbol{a}s\sigma} s v_\perp \frac{k^J_{\bar\sigma}}{k^{J-1}_{D_J}}\left[c_{\boldsymbol{a}'s'\sigma'}c^\dagger_{\boldsymbol{a}s\sigma}c_{\boldsymbol{a}s\bar\sigma} + c^\dagger_{\boldsymbol{a}s\sigma}c_{\boldsymbol{a}'s'\sigma'}c_{\boldsymbol{a}s\bar\sigma}\right] \\ &= -\frac{i}{\hbar}\sum_{\boldsymbol{a}s\sigma} s v_\perp \frac{k^J_{\bar\sigma}}{k^{J-1}_{D_J}}\left[c_{\boldsymbol{a}'s'\sigma'}c^\dagger_{\boldsymbol{a}s\sigma}c_{\boldsymbol{a}s\bar\sigma}\right. \\ &+ \left.\left(\delta_{\boldsymbol{k}'\boldsymbol{k}}\delta_{s's}\delta_{\sigma'\sigma} - c_{\boldsymbol{a}'s'\sigma'}c^\dagger_{\boldsymbol{a}s\sigma}\right)c_{\boldsymbol{a}s\bar\sigma}\right] \\ &= -\frac{i}{\hbar}\sum_{\boldsymbol{a}s\sigma} s v_\perp \frac{k^J_{\bar\sigma}}{k^{J-1}_{D_J}}\left[\cancel{c_{\boldsymbol{a}'s'\sigma'}c^\dagger_{\boldsymbol{a}s\sigma}c_{\boldsymbol{a}s\bar\sigma}} + \delta_{\boldsymbol{k}'\boldsymbol{k}}\delta_{s's}\delta_{\sigma'\sigma}c_{\boldsymbol{a}s\bar\sigma}\right. \\ &- \left.\cancel{c_{\boldsymbol{a}'s'\sigma'}c^\dagger_{\boldsymbol{a}s\sigma}c_{\boldsymbol{a}s\bar\sigma}}\right] \\ &= -\frac{i}{\hbar}\sum_{\boldsymbol{a}s\sigma} s v_\perp \frac{k^J_{\bar\sigma}}{k^{J-1}_{D_J}}\left[\delta_{\boldsymbol{k}'\boldsymbol{k}}\delta_{s's}\delta_{\sigma'\sigma}c_{\boldsymbol{a}s\bar\sigma}\right] \\ &= -\frac{i}{\hbar}s v_\perp \frac{k^J_{\bar\sigma}}{k^{J-1}_{D_J}}c_{\boldsymbol{a}s\bar\sigma}, \end{aligned} \tag{3.24}$$

$$
\begin{aligned}
-\frac{i}{\hbar}\sum_{\sigma}\varepsilon\left[c_{\boldsymbol{a}'s'\sigma'},d_{\sigma}^{\dagger}d_{\sigma}\right] &= -\frac{i}{\hbar}\sum_{\sigma}\varepsilon\left[c_{\boldsymbol{a}'s'\sigma'}d_{\sigma}^{\dagger}d_{\sigma}-d_{\sigma}^{\dagger}d_{\sigma}c_{\boldsymbol{a}'s'\sigma'}\right]\\
&= -\frac{i}{\hbar}\sum_{\sigma}\varepsilon\left[c_{\boldsymbol{a}'s'\sigma'}d_{\sigma}^{\dagger}d_{\sigma}+d_{\sigma}^{\dagger}c_{\boldsymbol{a}'s'\sigma'}d_{\sigma}\right]\\
&= -\frac{i}{\hbar}\sum_{\sigma}\varepsilon\left[\cancel{c_{\boldsymbol{a}'s'\sigma'}d_{\sigma}^{\dagger}d_{\sigma}}-\cancel{c_{\boldsymbol{a}'s'\sigma'}d_{\sigma}^{\dagger}d_{\sigma}}\right]\\
&= 0, \qquad (3.25)
\end{aligned}
$$

$$
\begin{aligned}
-\frac{i}{\hbar}U\left[c_{\boldsymbol{a}'s'\sigma'},d_{\uparrow}^{\dagger}d_{\uparrow}d_{\downarrow}^{\dagger}d_{\downarrow}\right] &= -\frac{i}{\hbar}U\left[c_{\boldsymbol{a}'s'\sigma'}d_{\uparrow}^{\dagger}d_{\uparrow}d_{\downarrow}^{\dagger}d_{\downarrow}-d_{\uparrow}^{\dagger}d_{\uparrow}d_{\downarrow}^{\dagger}d_{\downarrow}c_{\boldsymbol{a}'s'\sigma'}\right]\\
&= -\frac{i}{\hbar}U\left[c_{\boldsymbol{a}'s'\sigma'}d_{\uparrow}^{\dagger}d_{\uparrow}d_{\downarrow}^{\dagger}d_{\downarrow}+d_{\uparrow}^{\dagger}d_{\uparrow}d_{\downarrow}^{\dagger}c_{\boldsymbol{a}'s'\sigma'}d_{\downarrow}\right]\\
&= -\frac{i}{\hbar}U\left[c_{\boldsymbol{a}'s'\sigma'}d_{\uparrow}^{\dagger}d_{\uparrow}d_{\downarrow}^{\dagger}d_{\downarrow}-d_{\uparrow}^{\dagger}d_{\uparrow}c_{\boldsymbol{a}'s'\sigma'}d_{\downarrow}^{\dagger}d_{\downarrow}\right]\\
&= -\frac{i}{\hbar}U\left[c_{\boldsymbol{a}'s'\sigma'}d_{\uparrow}^{\dagger}d_{\uparrow}d_{\downarrow}^{\dagger}d_{\downarrow}+d_{\uparrow}^{\dagger}c_{\boldsymbol{a}'s'\sigma'}d_{\uparrow}d_{\downarrow}^{\dagger}d_{\downarrow}\right]\\
&= -\frac{i}{\hbar}U\left[\cancel{c_{\boldsymbol{a}'s'\sigma'}d_{\uparrow}^{\dagger}d_{\uparrow}d_{\downarrow}^{\dagger}d_{\downarrow}}-\cancel{c_{\boldsymbol{a}'s'\sigma'}d_{\uparrow}^{\dagger}d_{\uparrow}d_{\downarrow}^{\dagger}d_{\downarrow}}\right]\\
&= 0, \qquad (3.26)
\end{aligned}
$$

$$
\begin{aligned}
-\frac{i}{\hbar}\frac{1}{\sqrt{N}}\sum_{\boldsymbol{a}s\sigma}v\left[c_{\boldsymbol{a}'s'\sigma'},c_{\boldsymbol{a}s\sigma}^{\dagger}d_{\sigma}\right] &= -\frac{i}{\hbar}\frac{1}{\sqrt{N}}\sum_{\boldsymbol{a}s\sigma}v\left[c_{\boldsymbol{a}'s'\sigma'}c_{\boldsymbol{a}s\sigma}^{\dagger}d_{\sigma}-c_{\boldsymbol{a}s\sigma}^{\dagger}d_{\sigma}c_{\boldsymbol{a}'s'\sigma'}\right]\\
&= -\frac{i}{\hbar}\frac{1}{\sqrt{N}}\sum_{\boldsymbol{a}s\sigma}v\left[c_{\boldsymbol{a}'s'\sigma'}c_{\boldsymbol{a}s\sigma}^{\dagger}d_{\sigma}+c_{\boldsymbol{a}s\sigma}^{\dagger}c_{\boldsymbol{a}'s'\sigma'}d_{\sigma}\right]\\
&= -\frac{i}{\hbar}\frac{1}{\sqrt{N}}\sum_{\boldsymbol{a}s\sigma}v\left[\cancel{c_{\boldsymbol{a}'s'\sigma'}c_{\boldsymbol{a}s\sigma}^{\dagger}d_{\sigma}}+\delta_{\boldsymbol{a}'\boldsymbol{a}}\delta_{s's}\delta_{\sigma'\sigma}d_{\sigma}\right.\\
&- \left.\cancel{c_{\boldsymbol{a}'s'\sigma'}c_{\boldsymbol{a}s\sigma}^{\dagger}d_{\sigma}}\right]\\
&= -\frac{i}{\hbar}\frac{1}{\sqrt{N}}\sum_{\boldsymbol{a}s\sigma}v\delta_{\boldsymbol{a}'\boldsymbol{a}}\delta_{s's}\delta_{\sigma'\sigma}d_{\sigma}\\
&= -\frac{i}{\hbar}\frac{1}{\sqrt{N}}vd_{\sigma} \qquad (3.27)
\end{aligned}
$$

e

$$
\begin{aligned}
-\frac{i}{\hbar}\frac{1}{\sqrt{N}}\sum_{\boldsymbol{a}s\sigma} v^{*}\left[c_{\boldsymbol{a}'s'\sigma'}, d_{\sigma}^{\dagger}c_{\boldsymbol{a}s\sigma}\right] &= -\frac{i}{\hbar}\frac{1}{\sqrt{N}}\sum_{\boldsymbol{a}s\sigma} v^{*}\left[c_{\boldsymbol{a}'s'\sigma'}d_{\sigma}^{\dagger}c_{\boldsymbol{a}s\sigma} - d_{\sigma}^{\dagger}c_{\boldsymbol{a}s\sigma}c_{\boldsymbol{a}'s'\sigma'}\right] \\
&= -\frac{i}{\hbar}\frac{1}{\sqrt{N}}\sum_{\boldsymbol{a}s\sigma} v^{*}\left[c_{\boldsymbol{a}'s'\sigma'}d_{\sigma}^{\dagger}c_{\boldsymbol{a}s\sigma} + d_{\sigma}^{\dagger}c_{\boldsymbol{a}'s'\sigma'}c_{\boldsymbol{a}s\sigma}\right] \\
&= -\frac{i}{\hbar}\frac{1}{\sqrt{N}}\sum_{\boldsymbol{a}s\sigma} v^{*}\left[\cancel{c_{\boldsymbol{a}'s'\sigma'}d_{\sigma}^{\dagger}c_{\boldsymbol{a}s\sigma}} - \cancel{c_{\boldsymbol{a}'s'\sigma'}d_{\sigma}^{\dagger}c_{\boldsymbol{a}s\sigma}}\right] \\
&= -\frac{i}{\hbar}\frac{1}{\sqrt{N}}\sum_{\boldsymbol{a}s\sigma} v^{*}\cdot 0 \\
&= 0. \qquad (3.28)
\end{aligned}
$$

Assim,

$$
\frac{\partial}{\partial t}c_{\boldsymbol{a}s\sigma}(t) = -\frac{i}{\hbar}sv_{\perp}\frac{a_{\bar{\sigma}}^{J}}{a_{0}^{J-1}}c_{\boldsymbol{a}s\bar{\sigma}} - \frac{i}{\hbar}\frac{1}{\sqrt{N}}vd_{\sigma} \qquad (3.29)
$$

e deste modo podemos escrever:

$$
\begin{aligned}
\frac{\partial}{\partial t}\mathcal{G}^{A}_{d_{\sigma}c_{\boldsymbol{a}'s'\sigma'}}(t) = &- \frac{i}{\hbar}\delta(-t)Z^{-1}\sum_{n} e^{-\beta E_{n}}\left\langle n\left|\left[d_{\sigma}^{\dagger}(0), c_{\boldsymbol{a}s\sigma}(t)\right]_{+}\right|n\right\rangle \\
&+ \left(-\frac{i}{\hbar}\right)sv_{\perp}\frac{a_{\bar{\sigma}'}^{J}}{a_{0}^{J-1}}\mathcal{G}^{A}_{d_{\sigma}c_{\boldsymbol{a}s\sigma}}(t) \\
&+ \left(-\frac{i}{\hbar}\right)\frac{1}{\sqrt{N}}v\mathcal{G}^{A}_{d_{\sigma}d_{\sigma}}(t). \qquad (3.30)
\end{aligned}
$$

Realizando a transformada de Fourier

$$
\begin{aligned}
\varepsilon^{-}\widetilde{\mathcal{G}}^{A}_{d_{\sigma}c_{\boldsymbol{a}s\sigma}}(\varepsilon^{-}) &= \cancelto{0}{\left[d_{\sigma}^{\dagger}(0), e_{\boldsymbol{a}s\sigma}(t)\right]_{+}} \\
&+ sv_{\perp}\frac{a_{\bar{\sigma}'}^{J}}{a_{0}^{J-1}}\widetilde{\mathcal{G}}^{A}_{d_{\sigma}c_{\boldsymbol{a}s\bar{\sigma}}}(\varepsilon^{-}) \\
&+ \frac{1}{\sqrt{N}}v\widetilde{\mathcal{G}}^{A}_{d_{\sigma}d_{\sigma}}(\varepsilon^{-}), \qquad (3.31)
\end{aligned}
$$

ou seja,

$$
\begin{aligned}
\varepsilon^{-}\widetilde{\mathcal{G}}^{A}_{d_{\sigma}c_{\boldsymbol{a}s\sigma}}(\varepsilon^{-}) &= sv_{\perp}\frac{a_{\bar{\sigma}'}^{J}}{a_{0}^{J-1}}\widetilde{\mathcal{G}}^{A}_{d_{\sigma}c_{\boldsymbol{a}s\bar{\sigma}}}(\varepsilon^{-}) \\
&+ \frac{1}{\sqrt{N}}v\widetilde{\mathcal{G}}^{A}_{d_{\sigma}d_{\sigma}}(\varepsilon^{-}), \qquad (3.32)
\end{aligned}
$$

sendo que $\varepsilon^{-} = \varepsilon - i\eta$.

Aplicando a propriedade $\widetilde{\mathcal{G}}^{R}_{d_\sigma c_{\boldsymbol{a}s\sigma}}\left(\varepsilon^{+}\right)=\left[\widetilde{\mathcal{G}}^{A}_{d_\sigma c_{\boldsymbol{a}s\sigma}}\left(\varepsilon^{-}\right)\right]^{\dagger}$, temos a função de Green Retardada

$$\begin{aligned}\widetilde{\mathcal{G}}^{R}_{d_\sigma c_{\boldsymbol{a}'s'\sigma'}}\left(\varepsilon^{+}\right) &= \left[\widetilde{\mathcal{G}}^{A}_{d_\sigma c_{\boldsymbol{a}'s'\sigma'}}\left(\varepsilon^{-}\right)\right]^{\dagger} \\ &= \frac{sv_{\perp}\frac{a_\sigma^J}{a_0^{J-1}}}{\varepsilon^{+}}\widetilde{\mathcal{G}}^{R}_{d_\sigma c_{\boldsymbol{a}'s'\bar{\sigma}'}}\left(\varepsilon^{+}\right)+\frac{\frac{1}{\sqrt{N}}v^{*}}{\varepsilon^{+}}\widetilde{\mathcal{G}}^{R}_{d_\sigma d_{\sigma'}}\left(\varepsilon^{+}\right), \qquad (3.33)\end{aligned}$$

$$\widetilde{\mathcal{G}}^{R}_{d_\sigma c_{\boldsymbol{a}'s'\uparrow}}\left(\varepsilon^{+}\right)=\frac{sv_{\perp}\frac{a_+^J}{a_0^{J-1}}}{\varepsilon^{+}}\widetilde{\mathcal{G}}^{R}_{d_\sigma c_{\boldsymbol{a}'s\downarrow}}\left(\varepsilon^{+}\right)+\frac{\frac{1}{\sqrt{N}}v^{*}}{\varepsilon^{+}}\widetilde{\mathcal{G}}^{R}_{d_\sigma d_{\uparrow}}\left(\varepsilon^{+}\right) \qquad (3.34)$$

e

$$\widetilde{\mathcal{G}}^{R}_{d_\sigma c_{\boldsymbol{a}'s'\downarrow}}\left(\varepsilon^{+}\right)=\frac{sv_{\perp}\frac{a_{-'}^J}{a_0^{J-1}}}{\varepsilon^{+}}\widetilde{\mathcal{G}}^{R}_{d_\sigma c_{\boldsymbol{a}'s\uparrow}}\left(\varepsilon^{+}\right)+\frac{\frac{1}{\sqrt{N}}v^{*}}{\varepsilon^{+}}\widetilde{\mathcal{G}}^{R}_{d_\sigma d_{\downarrow}}\left(\varepsilon^{+}\right). \qquad (3.35)$$

Combinando as Eq.(3.35) e Eq.(3.34), temos

$$\begin{aligned}\widetilde{\mathcal{G}}^{R}_{d_\sigma c_{\boldsymbol{a}'s\uparrow}}\left(\varepsilon^{+}\right) &= \frac{\frac{a_+^J}{a_0^{J-1}}\frac{sv_{\perp}}{\sqrt{N}}v^{*}}{\left(\varepsilon^{+}\right)^{2}-v_{\perp}^{2}\frac{a_+^J a_-^J}{a_0^{2J-2}}}\widetilde{\mathcal{G}}^{R}_{d_\sigma d_{\downarrow}}\left(\varepsilon^{+}\right) \\ &+ \frac{\varepsilon^{+}\frac{1}{\sqrt{N}}v^{*}}{\left(\varepsilon^{+}\right)^{2}-v_{\perp}^{2}\frac{a_+^J a_-^J}{a_0^{2J-2}}}\widetilde{\mathcal{G}}^{R}_{d_\sigma d_{\uparrow}}\left(\varepsilon^{+}\right) \qquad (3.36)\end{aligned}$$

$$\begin{aligned}\widetilde{\mathcal{G}}^{R}_{d_\sigma c_{\boldsymbol{a}'s\downarrow}}\left(\varepsilon^{+}\right) &= \frac{\frac{a_-^J}{a_0^{J-1}}\frac{sv_{\perp}}{\sqrt{N}}v^{*}}{\left(\varepsilon^{+}\right)^{2}-v_{\perp}^{2}\frac{a_-^J a_+^J}{a_0^{2J-2}}}\widetilde{\mathcal{G}}^{R}_{d_\sigma d_{\uparrow}}\left(\varepsilon^{+}\right) \\ &+ \frac{\varepsilon^{+}\frac{1}{\sqrt{N}}v^{*}}{\left(\varepsilon^{+}\right)^{2}-v_{\perp}^{2}\frac{a_-^J a_+^J}{a_0^{2J-2}}}\widetilde{\mathcal{G}}^{R}_{d_\sigma d_{\downarrow}}\left(\varepsilon^{+}\right). \qquad (3.37)\end{aligned}$$

Substituindo $\sigma=\uparrow,\downarrow$, obtemos as quatro funções de Green.

$$\begin{aligned}\widetilde{\mathcal{G}}^{R}_{d_\uparrow c_{\boldsymbol{a}'s'\uparrow}}\left(\varepsilon^{+}\right) &= \frac{\frac{a_+^J}{a_0^{J-1}}\frac{sv_{\perp}}{\sqrt{N}}v^{*}}{\left(\varepsilon^{+}\right)^{2}-v_{\perp}^{2}\frac{a_+^J a_-^J}{a_0^{2J-2}}}\widetilde{\mathcal{G}}^{R}_{d_\uparrow d_{\downarrow}}\left(\varepsilon^{+}\right) \\ &+ \frac{\varepsilon^{+}\frac{1}{\sqrt{N}}v^{*}}{\left(\varepsilon^{+}\right)^{2}-v_{\perp}^{2}\frac{a_+^J a_-^J}{a_0^{2J-2}}}\widetilde{\mathcal{G}}^{R}_{d_\uparrow d_{\uparrow}}\left(\varepsilon^{+}\right), \qquad (3.38)\end{aligned}$$

$$\widetilde{\mathcal{G}}^{R}_{d_{\uparrow}c_{\boldsymbol{a}'s'\downarrow}}\left(\varepsilon^{+}\right) = \frac{\frac{a_{-}^{J}}{a_{0}^{J-1}}\frac{sv_{\perp}}{\sqrt{N}}v^{*}}{\left(\varepsilon^{+}\right)^{2}-v_{\perp}^{2}\frac{a_{-}^{J}a_{+}^{J}}{a_{0}^{2J-2}}}\widetilde{\mathcal{G}}^{R}_{d_{\uparrow}d_{\uparrow}}\left(\varepsilon^{+}\right) + \frac{\varepsilon^{+}\frac{1}{\sqrt{N}}v^{*}}{\left(\varepsilon^{+}\right)^{2}-v_{\perp}^{2}\frac{a_{-}^{J}a_{+}^{J}}{a_{0}^{2J-2}}}\widetilde{\mathcal{G}}^{R}_{d_{\uparrow}d_{\downarrow}}\left(\varepsilon^{+}\right), \tag{3.39}$$

$$\widetilde{\mathcal{G}}^{R}_{d_{\downarrow}c_{\boldsymbol{a}'s'\downarrow}}\left(\varepsilon^{+}\right) = \frac{\frac{a_{-}^{J}}{a_{0}^{J-1}}\frac{sv_{\perp}}{\sqrt{N}}v^{*}}{\left(\varepsilon^{+}\right)^{2}-v_{\perp}^{2}\frac{a_{-}^{J}a_{+}^{J}}{a_{0}^{2J-2}}}\widetilde{\mathcal{G}}^{R}_{d_{\downarrow}d_{\uparrow}}\left(\varepsilon^{+}\right) + \frac{\varepsilon^{+}\frac{1}{\sqrt{N}}v^{*}}{\left(\varepsilon^{+}\right)^{2}-v_{\perp}^{2}\frac{a_{-}^{J}a_{+}^{J}}{a_{0}^{2J-2}}}\widetilde{\mathcal{G}}^{R}_{d_{\downarrow}d_{\downarrow}}\left(\varepsilon^{+}\right) \tag{3.40}$$

e

$$\widetilde{\mathcal{G}}^{R}_{d_{\uparrow}c_{\boldsymbol{a}'s'\downarrow}}\left(\varepsilon^{+}\right) = \frac{\frac{a_{-}^{J}}{a_{0}^{J-1}}\frac{sv_{\perp}}{\sqrt{N}}v^{*}}{\left(\varepsilon^{+}\right)^{2}-v_{\perp}^{2}\frac{a_{-}^{J}a_{+}^{J}}{a_{0}^{2J-2}}}\widetilde{\mathcal{G}}^{R}_{d_{\uparrow}d_{\uparrow}}\left(\varepsilon^{+}\right) + \frac{\varepsilon^{+}\frac{1}{\sqrt{N}}v^{*}}{\left(\varepsilon^{+}\right)^{2}-v_{\perp}^{2}\frac{a_{-}^{J}a_{+}^{J}}{a_{0}^{2J-2}}}\widetilde{\mathcal{G}}^{R}_{d_{\uparrow}d_{\downarrow}}\left(\varepsilon^{+}\right). \tag{3.41}$$

Substituindo os resultados da Eq.(3.38) e Eq.(3.39) na Eq.(3.18), obtemos

$$\widetilde{\mathcal{G}}_{d_{\uparrow}c_{\mathbf{a}s'\uparrow}}\left(\varepsilon^{+}\right) = \frac{s'\frac{v_{\perp}}{a_{0}^{J-1}}a_{+}^{J}v^{*}}{\sqrt{\mathcal{N}}\left(\left(\varepsilon^{+}\right)^{2}-\frac{v_{\perp}^{2}}{a_{0}^{2J-2}}a_{+}^{J}a_{-}^{J}\right)}\widetilde{\mathcal{G}}_{d_{\uparrow}d_{\downarrow}}\left(\varepsilon^{+}\right) + \frac{v^{*}\varepsilon^{+}}{\sqrt{\mathcal{N}}\left(\left(\varepsilon^{+}\right)^{2}-\frac{v_{\perp}^{2}}{a_{0}^{2J-2}}a_{+}^{J}a_{-}^{J}\right)}\widetilde{\mathcal{G}}_{d_{\uparrow}d_{\uparrow}}\left(\varepsilon^{+}\right) \tag{3.42}$$

$$
\begin{aligned}
\widetilde{\mathcal{G}}_{c_{\mathbf{k}s\uparrow}c_{\mathbf{a}s'\uparrow}}\left(\varepsilon^{+}\right) &= \frac{\varepsilon^{+}\delta_{\mathbf{ka}}\delta_{ss'}}{\left(\varepsilon^{+}\right)^{2}-\frac{v_{\perp}^{2}}{k_{D_J}^{2J-2}}k_{-}^{J}k_{+}^{J}}+\frac{s\frac{v_{\perp}}{k_{D_J}^{J-1}}k_{-}^{J}v}{\sqrt{\mathcal{N}}\left(\left(\varepsilon^{+}\right)^{2}-\frac{v_{\perp}^{2}}{k_{D_J}^{2J-2}}k_{-}^{J}k_{+}^{J}\right)}\widetilde{\mathcal{G}}_{d_{\downarrow}c_{\mathbf{a}s'\uparrow}}\left(\varepsilon^{+}\right)+\\
&+\frac{\varepsilon^{+}v}{\sqrt{\mathcal{N}}\left(\left(\varepsilon^{+}\right)^{2}-\frac{v_{\perp}^{2}}{k_{D_J}^{2J-2}}k_{-}^{J}k_{+}^{J}\right)}\mathcal{G}_{d_{\uparrow}c_{\mathbf{a}s'\uparrow'}}\left(\varepsilon^{+}\right)\\
&= \frac{\varepsilon^{+}\delta_{\mathbf{ka}}\delta_{ss'}}{\left(\varepsilon^{+}\right)^{2}-\frac{v_{\perp}^{2}}{k_{D_J}^{2J-2}}k_{-}^{J}k_{+}^{J}}+\\
&+\frac{1}{\mathcal{N}}\left[\frac{s\frac{v_{\perp}}{k_{D_J}^{J-1}}k_{-}^{J}v}{\left(\varepsilon^{+}\right)^{2}-\frac{v_{\perp}^{2}}{k_{D_J}^{2J-2}}k_{-}^{J}k_{+}^{J}}\right]\left[\frac{s'\frac{v_{\perp}}{a_{0}^{J-1}}a_{+}^{J}v^{*}}{\left(\varepsilon^{+}\right)^{2}-\frac{v_{\perp}^{2}}{a_{0}^{2J-2}}a_{+}^{J}a_{-}^{J}}\right]\widetilde{\mathcal{G}}_{d_{\downarrow}d_{\downarrow}}\left(\varepsilon^{+}\right)\\
&+\frac{1}{\mathcal{N}}\left[\frac{s\frac{v_{\perp}}{k_{D_J}^{J-1}}k_{-}^{J}v}{\left(\varepsilon^{+}\right)^{2}-\frac{v_{\perp}^{2}}{k_{D_J}^{2J-2}}k_{-}^{J}k_{+}^{J}}\right]\left[\frac{v^{*}\varepsilon^{+}}{\left(\varepsilon^{+}\right)^{2}-\frac{v_{\perp}^{2}}{a_{0}^{2J-2}}a_{+}^{J}a_{-}^{J}}\right]\widetilde{\mathcal{G}}_{d_{\downarrow}d_{\uparrow}}\left(\varepsilon^{+}\right)\\
&+\frac{1}{\mathcal{N}}\left[\frac{\varepsilon^{+}v}{\left(\varepsilon^{+}\right)^{2}-\frac{v_{\perp}^{2}}{k_{D_J}^{2J-2}}k_{-}^{J}k_{+}^{J}}\right]\left[\frac{s'\frac{v_{\perp}}{a_{0}^{J-1}}a_{+}^{J}v^{*}}{\left(\varepsilon^{+}\right)^{2}-\frac{v_{\perp}^{2}}{a_{0}^{2J-2}}a_{+}^{J}a_{-}^{J}}\right]\widetilde{\mathcal{G}}_{d_{\uparrow}d_{\downarrow}}\left(\varepsilon^{+}\right)\\
&+\frac{1}{\mathcal{N}}\left[\frac{\varepsilon^{+}v}{\left(\varepsilon^{+}\right)^{2}-\frac{v_{\perp}^{2}}{k_{D_J}^{2J-2}}k_{-}^{J}k_{+}^{J}}\right]\left[\frac{v^{*}\varepsilon^{+}}{\left(\varepsilon^{+}\right)^{2}-\frac{v_{\perp}^{2}}{a_{0}^{2J-2}}a_{+}^{J}a_{-}^{J}}\right]\widetilde{\mathcal{G}}_{d_{\uparrow}d_{\uparrow}}\left(\varepsilon^{+}\right) \qquad (3.43)
\end{aligned}
$$

Substituindo os resultados das Eq.(3.40) e Eq.(3.41) na Eq.(3.20), obtemos

$$
\begin{aligned}
\widetilde{\mathcal{G}}_{c_{\mathbf{k}s\downarrow}c_{\mathbf{a}s'\downarrow}}\left(\varepsilon^{+}\right) &= \frac{\varepsilon^{+}\delta_{\mathbf{ka}}\delta_{ss'}}{\left(\varepsilon^{+}\right)^{2}-\frac{v_{\perp}^{2}}{k_{D_J}^{2J-2}}k_{+}^{J}k_{-}^{J}}+\\
&+\frac{1}{\mathcal{N}}\left[\frac{vs\frac{v_{\perp}}{k_{D_J}^{J-1}}k_{+}^{J}}{\left(\varepsilon^{+}\right)^{2}-\frac{v_{\perp}^{2}}{k_{D_J}^{2J-2}}k_{-}^{J}k_{+}^{J}}\right]\left[\frac{s'\frac{v_{\perp}}{a_{0}^{J-1}}a_{-}^{J}v^{*}}{\left(\varepsilon^{+}\right)^{2}-\frac{v_{\perp}^{2}}{a_{0}^{2J-2}}a_{-}^{J}a_{+}^{J}}\right]\widetilde{\mathcal{G}}_{d_{\uparrow}d_{\uparrow}}\left(\varepsilon^{+}\right)\\
&+\frac{1}{\mathcal{N}}\left[\frac{vs\frac{v_{\perp}}{k_{D_J}^{J-1}}k_{+}^{J}}{\left(\varepsilon^{+}\right)^{2}-\frac{v_{\perp}^{2}}{k_{D_J}^{2J-2}}k_{+}^{J}k_{-}^{J}}\right]\left[\frac{\varepsilon^{+}v^{*}}{\left(\varepsilon^{+}\right)^{2}-\frac{v_{\perp}^{2}}{a_{0}^{2J-2}}a_{-}^{J}a_{+}^{J}}\right]\widetilde{\mathcal{G}}_{d_{\uparrow}d_{\downarrow}}\left(\varepsilon^{+}\right)\\
&+\frac{1}{\mathcal{N}}\left[\frac{v\varepsilon^{+}}{\left(\varepsilon^{+}\right)^{2}-\frac{v_{\perp}^{2}}{k_{D_J}^{2J-2}}k_{+}^{J}k_{-}^{J}}\right]\left[\frac{s'\frac{v_{\perp}}{a_{0}^{J-1}}a_{-}^{J}v^{*}}{\left(\varepsilon^{+}\right)^{2}-\frac{v_{\perp}^{2}}{a_{0}^{2J-2}}a_{-}^{J}a_{+}^{J}}\right]\widetilde{\mathcal{G}}_{d_{\downarrow}d_{\uparrow}}\left(\varepsilon^{+}\right)\\
&+\frac{1}{\mathcal{N}}\left[\frac{v\varepsilon^{+}}{\left(\varepsilon^{+}\right)^{2}-\frac{v_{\perp}^{2}}{k_{D_J}^{2J-2}}k_{+}^{J}k_{-}^{J}}\right]\left[\frac{\varepsilon^{+}v^{*}}{\left(\varepsilon^{+}\right)^{2}-\frac{v_{\perp}^{2}}{a_{0}^{2J-2}}a_{-}^{J}a_{+}^{J}}\right]\widetilde{\mathcal{G}}_{d_{\downarrow}d_{\downarrow}}\left(\varepsilon^{+}\right) \qquad (3.44)
\end{aligned}
$$

3.1 Auto energias

A quiralidade s será retomada somente ao final, logo omitida para fins de calculo.

$$\Sigma_{\boldsymbol{k}s} = \frac{|v|^2}{\mathcal{N}} \sum_{\mathbf{k}} \frac{\varepsilon^+}{(\varepsilon^+)^2 - \frac{v_\perp^2}{k_{D_J}^{2J-2}} k_-^J k_+^J} \tag{3.45}$$

de modo que

$$\begin{aligned}
\Sigma_{\boldsymbol{k}s} &= \frac{|v|^2}{\mathcal{N}} \sum_{\mathbf{k}} \frac{\varepsilon^+}{(\varepsilon^+)^2 - \frac{v_\perp^2}{k_{D_J}^{2J-2}} k_-^J k_+^J} \\
&= \frac{|v|^2}{\mathcal{N}} \sum_{\mathbf{k}} \left[\frac{\varepsilon + i\eta}{(\varepsilon + i\eta)^2 - \left(\frac{v_\perp}{k_{D_J}^{J-1}} \right)^2 k_-^J k_+^J} \right] \\
&= \frac{|v|^2}{\mathcal{N}} \sum_{\mathbf{k}} \left[\frac{\varepsilon + i\eta}{(\varepsilon + i\eta)^2 - \left(\frac{v_\perp}{k_{D_J}^{J-1}} \right)^2 k_-^J k_+^J} \right] \\
&= \frac{|v|^2}{\mathcal{N}} \sum_{\mathbf{k}} \left[\frac{\varepsilon + i\eta}{(\varepsilon + i\eta)^2 - v_\perp^2 \left(\frac{k_\perp^{2J}}{k_{D_J}^{2J-2}} \right)} \right] \\
&= \frac{|v|^2}{\mathcal{N}} \sum_{\mathbf{k}} \left[\frac{\varepsilon + i\eta}{(\varepsilon + i\eta)^2 - \varepsilon_{\mathbf{k}}^2} \right],
\end{aligned} \tag{3.46}$$

no qual $\varepsilon_{\mathbf{k}} = v_\perp \sqrt{\frac{k_\perp^{2J}}{k_{D_J}^{2J-2}}}$ e $k_\perp^2 = k_x^2 + k_y^2$. Então,

$$
\begin{aligned}
\Sigma_{\boldsymbol{k}s} &= \frac{|v|^2}{\mathcal{N}}\sum_{\mathbf{k}}\left[\frac{\varepsilon+i\eta}{(\varepsilon+i\eta)^2-\varepsilon_{\mathbf{k}}^2}\right] \\
&= \frac{|v|^2}{\mathcal{N}}\sum_{\mathbf{k}}\left[\frac{\varepsilon+i\eta}{\varepsilon^2-\varepsilon_{\mathbf{k}}^2+i\eta}\right] \\
&= \frac{|v|^2}{\mathcal{N}}\sum_{\mathbf{k}}\left[\frac{\varepsilon+i\eta}{\varepsilon^2-\varepsilon_{\mathbf{k}}^2+i\eta}\left(\frac{\varepsilon^2-\varepsilon_{\mathbf{k}}^2-i\eta}{\varepsilon^2-\varepsilon_{\mathbf{k}}^2-i\eta}\right)\right] \\
&= \frac{|v|^2}{\mathcal{N}}\sum_{\mathbf{k}}\left[\frac{(\varepsilon+i\eta)\left(\varepsilon^2-\varepsilon_{\mathbf{k}}^2-i\eta\right)}{\left(\varepsilon^2-\varepsilon_{\mathbf{k}}^2\right)^2+\eta^2}\right] \\
&= \frac{|v|^2}{\mathcal{N}}\sum_{\mathbf{k}}\left[\frac{\varepsilon\left(\varepsilon^2-\varepsilon_{\mathbf{k}}^2-i\eta\right)}{\left(\varepsilon^2-\varepsilon_{\mathbf{k}}^2\right)^2+\eta^2}\right] \\
&= \frac{|v|^2}{\mathcal{N}}\sum_{\mathbf{k}}\left[\left(\frac{\varepsilon}{\varepsilon^2-\varepsilon_{\mathbf{k}}^2}-i\frac{\eta}{\left(\varepsilon^2-\varepsilon_{\mathbf{k}}^2\right)^2+\eta^2}|\varepsilon|\right)\right] \\
&= \frac{|v|^2}{\mathcal{N}}\sum_{\mathbf{k}}\left[\frac{\varepsilon}{\varepsilon^2-\varepsilon_{\mathbf{k}}^2}\right] \\
&- i\frac{|v|^2}{\mathcal{N}}\sum_{\mathbf{k}}\left[\frac{\eta}{\left(\varepsilon^2-\varepsilon_{\mathbf{k}}^2\right)^2+\eta^2}|\varepsilon|\right] \\
&= \frac{|v|^2}{\mathcal{N}}\sum_{\mathbf{k}}\left[\frac{\varepsilon}{\varepsilon^2-\varepsilon_{\mathbf{k}}^2}\right] \\
&- i\frac{|v|^2}{\mathcal{N}}\sum_{\mathbf{k}}\left[\pi\delta\left(\varepsilon^2-\varepsilon_{\mathbf{k}}^2\right)|\varepsilon|\right] \\
&= \frac{|v|^2}{\mathcal{N}}\sum_{\mathbf{k}}\left[\frac{\varepsilon}{\varepsilon^2-\varepsilon_{\mathbf{k}}^2}\right] \\
&- i\frac{v}{\mathcal{N}}\sum_{\mathbf{k}}\left[\frac{\pi}{2|\varepsilon|}\left(\delta\left(\varepsilon-\varepsilon_{\mathbf{k}}\right)+\delta\left(\varepsilon+\varepsilon_{\mathbf{k}}\right)\right)|\varepsilon|\right] \\
&= \frac{|v|^2}{\mathcal{N}}\sum_{\mathbf{k}}\left[\frac{\varepsilon}{\varepsilon^2-\varepsilon_{\mathbf{k}}^2}\right] \\
&- i\frac{|v|^2}{\mathcal{N}}\sum_{\mathbf{k}}\left[\frac{\pi}{2}\left(\delta\left(\varepsilon-\varepsilon_{\mathbf{k}}\right)+\delta\left(\varepsilon+\varepsilon_{\mathbf{k}}\right)\right)\right] \\
&= \mathrm{Re}\left(\Sigma_{\boldsymbol{k}s}\right)+i\mathrm{Im}\left(\Sigma_{\boldsymbol{k}s}\right), \qquad (3.47)
\end{aligned}
$$

De modo que, $\mathrm{Re}\left(\Sigma^s_{k\sigma z}\right)=\frac{|v|^2}{\mathcal{N}}\sum_{\mathbf{k}}\left[\frac{\varepsilon}{\varepsilon^2-\varepsilon_{\mathbf{k}}^2}\right]$ e $\mathrm{Im}\left(\Sigma^s_{k\sigma z}\right)=-\frac{|v|^2}{\mathcal{N}}\sum_{\mathbf{k}}\left[\frac{\pi}{2}\left(\delta\left(\varepsilon-\varepsilon_{\mathbf{k}}\right)+\delta\left(\varepsilon+\varepsilon_{\mathbf{k}}\right)\right)\right]$. Calculando a parte real com:

$$
\sum_{\mathbf{k}}\rightarrow\frac{\Omega}{(2\pi)^2}\int_{-\infty}^{\infty}\int_{-\infty}^{\infty}dk_xdk_y, \qquad (3.48)
$$

então

$$\mathrm{Re}\left(\Sigma_{\boldsymbol{k}s}\right) = \frac{|v|^2\,\Omega}{\mathcal{N}\left(2\pi\right)^2}\int_{-\infty}^{\infty}\int_{-\infty}^{\infty}\left[\frac{\varepsilon}{\varepsilon^2-\varepsilon_{\mathbf{k}}^2}\right]dk_x dk_y. \tag{3.49}$$

Realizando a seguinte mudança de variável:

$$\begin{cases} k_x = k_{D_J}p_x \\ k_y = k_{D_J}p_y \end{cases}, \tag{3.50}$$

então,

$$\begin{aligned} \mathrm{Re}\left(\Sigma_{\boldsymbol{k}s}\right) &= \frac{|v|^2\,\Omega}{\mathcal{N}\left(2\pi\right)^2}k_{D_J}^2\int_{-\infty}^{\infty}\int_{-\infty}^{\infty}\left[\frac{\varepsilon}{\varepsilon^2-\varepsilon_{\mathbf{k}}^2}\right]dp_x dp_y \\ &= \frac{|v|^2\,\Omega}{\mathcal{N}\left(2\pi\right)^2}k_{D_J}^2\int_{-\infty}^{\infty}\int_{-\infty}^{\infty}\left[\frac{\varepsilon}{\varepsilon^2-v_\perp^2k_{D_J}^2\left(p_x^2+p_y^2\right)^J}\right]dp_x dp_y, \end{aligned} \tag{3.51}$$

de modo que

$$\begin{aligned} \varepsilon_{\mathbf{k}} &= v_\perp\sqrt{\frac{k_\perp^{2J}}{k_{D_J}^{2J-2}}} = v_\perp\frac{k_\perp^J}{k_{D_J}^{J-1}} \\ &= \sqrt{v_\perp^2k_{D_J}^2\left(\frac{k_x^2}{k_{D_J}^2}+\frac{k_y^2}{k_{D_J}^2}\right)^J} \\ &= \sqrt{v_\perp^2k_{D_J}^2\left(p_x^2+p_y^2\right)^J}, \end{aligned} \tag{3.52}$$

logo,

$$\begin{aligned} \mathrm{Re}\left(\Sigma_{\boldsymbol{k}s}\right) &= \frac{|v|^2\,\Omega}{\mathcal{N}\left(2\pi\right)^2}k_{D_J}^2\int_{-\infty}^{\infty}\int_{-\infty}^{\infty}\left[\frac{\varepsilon}{\varepsilon^2-\varepsilon_{\mathbf{k}}^2}\right]dp_x dp_y \\ &= \frac{|v|^2\,\Omega}{\mathcal{N}\left(2\pi\right)^2}k_{D_J}^2\int_{-\infty}^{\infty}\int_{-\infty}^{\infty}\left[\frac{\varepsilon}{\varepsilon^2-\varepsilon_{\mathbf{k}}^2}\right]dp_x dp_y. \end{aligned} \tag{3.53}$$

Realizando a mudança de variável:

$$\begin{cases} p_x = \left(\frac{\varepsilon_{\mathbf{k}}}{v_\perp k_{D_J}}\right)^{\frac{1}{J}}\cos\theta \\ p_y = \left(\frac{\varepsilon_{\mathbf{k}}}{v_\perp k_{D_J}}\right)^{\frac{1}{J}}\sin\theta \end{cases}, \tag{3.54}$$

tem-se

$$\begin{aligned}
\varepsilon_{\mathbf{k}} &= \sqrt{v_\perp^2 k_{D_J}^2 \left(p_x^2+p_y^2\right)^J} \\
&= \sqrt{v_\perp^2 k_{D_J}^2 \left(\left(\frac{\varepsilon_{\mathbf{k}}}{v_\perp k_{D_J}}\right)^{\frac{2}{J}} \cos^2\theta + \left(\frac{\varepsilon_{\mathbf{k}}}{v_\perp k_{D_J}}\right)^{\frac{2}{J}} \sin^2\theta\right)^J} \\
&= \sqrt{v_\perp^2 k_{D_J}^2 \left(\frac{\varepsilon_{\mathbf{k}}}{v_\perp k_{D_J}}\right)^{\frac{2}{J}\,J}} \\
&= \sqrt{v_\perp^2 k_{D_J}^2 \left(\frac{\varepsilon_{\mathbf{k}}}{v_\perp k_{D_J}}\right)^2} \\
&= \varepsilon_{\mathbf{k}}
\end{aligned} \tag{3.55}$$

de modo que $0 \leq \theta \leq \pi$. Calcular o Jacobiano afim de realizar a última mudança de variável:

$$\begin{cases} p_x &= \left(\frac{\varepsilon_k}{v_\perp k_{D_J}}\right)^{\frac{1}{J}} cos\theta \\ p_y &= \left(\frac{\varepsilon_k}{v_\perp k_{D_J}}\right)^{\frac{1}{J}} sen\theta \end{cases} \tag{3.56}$$

logo,

$$\begin{aligned}
J\left(\varepsilon_k,\theta\right) &= \begin{vmatrix} \frac{\partial p_x}{\partial \varepsilon_k} & \frac{\partial p_x}{\partial \theta} \\ \frac{\partial p_y}{\partial \varepsilon_k} & \frac{\partial p_y}{\partial \theta} \end{vmatrix} \\
&= \frac{1}{J}\frac{\varepsilon_k^{\frac{2}{J}-1}}{\left(v_\perp k_{D_J}\right)^{\frac{2}{J}}}
\end{aligned} \tag{3.57}$$

$$\begin{aligned}
\mathrm{Re}\left(\Sigma_{\boldsymbol{ks}}\right) &= \frac{\Omega\left|v\right|^2}{\mathcal{N}\left(2\pi\right)^2}\int_{-\infty}^{\infty}\int_{-\infty}^{\infty}\frac{\varepsilon}{\varepsilon^2-\varepsilon_k^2}k_{D_J}^2 dp_x dp_y \\
&= \frac{\Omega\left|v\right|^2}{\mathcal{N}\left(2\pi\right)^2}k_{D_J}^2\frac{2\pi}{J\left(v_\perp k_{D_J}\right)^{\frac{2}{J}}}\int_0^{\infty}\frac{\varepsilon\varepsilon_k^{\frac{2}{J}-1}}{\varepsilon^2-\varepsilon_k^2}d\varepsilon_k
\end{aligned} \tag{3.58}$$

Enfim, para $J=1$

$$\mathrm{Re}\left(\Sigma_{\boldsymbol{ks}}\right) = \frac{\Omega\left|v\right|^2}{\mathcal{N}\left(2\pi\right)^2}k_{D_J}^2\frac{2\pi}{\left(v_\perp k_{D_J}\right)^2}\int_0^{\infty}\frac{\varepsilon\varepsilon_k}{\varepsilon^2-\varepsilon_k^2}d\varepsilon_k \tag{3.59}$$

Por substituição simples

$$u = \frac{\varepsilon^2 - \varepsilon_k^2}{D^2} \rightarrow d\varepsilon_{\mathbf{k}} = -\frac{D^2}{2\varepsilon_k} du \tag{3.60}$$

Resolvendo

$$\begin{aligned} \mathrm{Re}\left(\Sigma_{\boldsymbol{k}\sigma}\right) &= -\frac{\Omega\left|v\right|^2}{\mathcal{N}\left(2\pi\right)^2} k_{D_J}^2 \frac{2\pi}{\left(v_\perp k_{D_J}\right)^2} \int \frac{\varepsilon\varepsilon_k}{uD^2} \frac{D^2}{2\varepsilon_k} du \\ &= \frac{\left|v\right|^2 \varepsilon k_{D_J}^2}{2k_D^2 \left(v_\perp k_{D_J}\right)^2} \left[ln \left| \frac{\varepsilon^2}{\varepsilon^2 - D^2} \right| \right] \end{aligned} \tag{3.61}$$

Como visto na literatura, é conhecido que o modelo não é válido para duas camadas, logo será realizado para $J \geq 3$, como segue.

$$\begin{aligned} \mathrm{Re}\left(\Sigma_{\boldsymbol{k}\sigma}\right) &= \frac{\Omega\left|v\right|^2}{\mathcal{N}\left(2\pi\right)^2} k_{D_J}^2 \frac{2\pi}{J\left(v_\perp k_{D_J}\right)^{\frac{2}{J}}} \int_0^\infty \frac{\varepsilon \varepsilon_k^{\frac{2}{J}-1}}{\varepsilon^2 - \varepsilon_k^2} d\varepsilon_k \\ &= \frac{\Omega\left|v\right|^2}{\mathcal{N}\left(2\pi\right)^2} k_{D_J}^2 \frac{2\pi}{J\left(v_\perp k_{D_J}\right)^{\frac{2}{J}}} \left[\int_0^\infty \frac{\frac{1}{2}}{\varepsilon + \varepsilon_k} \varepsilon_k^{\frac{2-J}{J}} d\varepsilon_k + \int_0^\infty \frac{\frac{1}{2}}{\varepsilon - \varepsilon_k} \varepsilon_k^{\frac{2-J}{J}} d\varepsilon_k \right] \end{aligned} \tag{3.62}$$

Separando os regimes energéticos e fazendo escolha em primeiro instante do regime positivo, isto é, para $\varepsilon > 0$. Assim, para $\varepsilon_{\boldsymbol{k}} = \varepsilon\varepsilon'_{\boldsymbol{k}}$

$$\begin{aligned} \mathrm{Re}\left(\Sigma_{\boldsymbol{k}s}\right) &= \frac{\left|v\right|^2 \Omega k_{D_J}^2}{J\mathcal{N}\left(2\pi\right)\left(v_\perp k_{D_J}\right)^{2/J}} \int_0^\infty \left[\frac{\varepsilon}{\varepsilon^2 - \varepsilon_{\mathbf{k}}^2}\right] \varepsilon_{\mathbf{k}}^{2/J-1} d\varepsilon_{\mathbf{k}} \\ &= \frac{\left|v\right|^2 \Omega k_{D_J}^2}{J\mathcal{N}\left(2\pi\right)\left(v_\perp k_{D_J}\right)^{2/J}} \int_0^\infty \left[\frac{\varepsilon}{\varepsilon^2 - \varepsilon_{\mathbf{k}}^2}\right] \varepsilon_{\mathbf{k}}^{(2-J)/J} d\varepsilon_{\mathbf{k}} \\ &= \frac{\left|v\right|^2 \Omega k_{D_J}^2}{J\mathcal{N}\left(2\pi\right)\left(v_\perp k_{D_J}\right)^{2/J}} \left[\int_0^\infty \left[\frac{1/2}{\varepsilon + \varepsilon_{\mathbf{k}}}\right] \varepsilon_{\mathbf{k}}^{(2-J)/J} d\varepsilon_{\mathbf{k}} + \int_0^\infty \left[\frac{1/2}{\varepsilon - \varepsilon_{\mathbf{k}}}\right] \varepsilon_{\mathbf{k}}^{(2-J)/J} d\varepsilon_{\mathbf{k}} \right] \end{aligned} \tag{3.63}$$

Logo, temos que analisar para o caso em que $\varepsilon > 0$ e $\varepsilon < 0$. No caso em que $\varepsilon > 0$ fazemos

$\varepsilon_{\mathbf{k}} = \varepsilon\varepsilon'_{\mathbf{k}}$:

$$\begin{aligned}
\mathrm{Re}\left(\Sigma^{s}_{k\sigma z}\right) &= \frac{|v|^2 \Omega k_{D_J}^2}{2J\mathcal{N}\left(2\pi\right)\left(v_\perp k_{D_J}\right)^{2/J}}\left[\int_0^\infty \left[\frac{\varepsilon'^{(2-J)/J}\omega^{(2-J)/J}}{-\omega+\omega\varepsilon'_{\mathbf{k}}}\right]\omega d\varepsilon'_{\boldsymbol{k}} + \int_0^\infty \left[\frac{\varepsilon'^{(2-J)/J}_{\mathbf{k}}\omega^{(2-J)/J}}{-\omega-\omega\varepsilon'_{\mathbf{k}}}\right]\omega d\varepsilon'_{\mathbf{k}}\right] \\
&= \frac{|v|^2 \Omega k_{D_J}^2}{2J\mathcal{N}\left(2\pi\right)\left(v_\perp k_{D_J}\right)^{2/J}}\left[\int_0^\infty \left[\frac{\varepsilon'^{(2-J)/J}_{\mathbf{k}}}{-1+\varepsilon'_{\mathbf{k}}}\right] d\varepsilon'_{\mathbf{k}} + \int_0^\infty \left[\frac{\varepsilon'^{(2-J)/J}_{\mathbf{k}}}{-1-\varepsilon'_{\mathbf{k}}}\right] d\varepsilon'_{\mathbf{k}}\right]\omega^{(2-J)/J} \\
&= \frac{\cancel{2\pi}\,|v|^2 \cancel{\Omega k_{D_J}^2}}{2J\cancel{\Omega k_D^2}\,\cancel{(2\pi)}\left(v_\perp k_{D_J}\right)^{2/J}}\left[\int_0^\infty \left[\frac{\varepsilon'^{(2-J)/J}_{\mathbf{k}}}{-1+\varepsilon'_{\mathbf{k}}}\right] d\varepsilon'_{\mathbf{k}} - \int_0^\infty \left[\frac{\varepsilon'^{(2-J)/J}_{\mathbf{k}}}{1+\varepsilon'_{\mathbf{k}}}\right] d\varepsilon'_{\boldsymbol{k}}\right]\omega^{(2-J)/J} \\
&= \frac{|v|^2}{2J\left(v_\perp k_{D_J}\right)^{2/J}}\left[\int_0^\infty \left[\frac{\varepsilon'^{(2-J)/J}_{\mathbf{k}}}{-1+\varepsilon'_{\mathbf{k}}}\right] d\varepsilon'_{\mathbf{k}} - \int_0^\infty \left[\frac{\varepsilon'^{(2-J)/J}_{\mathbf{k}}}{1+\varepsilon'_{\mathbf{k}}}\right] d\varepsilon'_{\mathbf{k}}\right]\omega^{(2-J)/J} \qquad (3.64)
\end{aligned}$$

Agora para $\varepsilon < 0$ primeiro escrevemos $-\varepsilon\varepsilon'_{\mathbf{k}} = \varepsilon_{\mathbf{k}}$.

$$\begin{aligned}
\mathrm{Re}\left(\Sigma_{\boldsymbol{k}\sigma}\right) &= \frac{\Omega\,|v|^2}{\mathcal{N}\left(2\pi\right)^2}k_{D_J}^2\frac{2\pi}{J\left(v_\perp k_{D_J}\right)^{\frac{2}{J}}}\left[\int_0^\infty \frac{\frac{1}{2}}{\varepsilon-\varepsilon\varepsilon'_{\boldsymbol{k}}}\left(-\varepsilon\varepsilon'_{\boldsymbol{k}}\right)^{\frac{2-J}{J}}\left(-\varepsilon\right)d\varepsilon'_{\boldsymbol{k}}\right. \\
&+ \left.\int_0^\infty \frac{\frac{1}{2}}{\varepsilon+\varepsilon\varepsilon'_{\boldsymbol{k}}}\left(-\varepsilon\varepsilon'_{\boldsymbol{k}}\right)^{\frac{2-J}{J}}\left(-\varepsilon\right)d\varepsilon'_{\boldsymbol{k}}\right] \\
&= \frac{\Omega\,|v|^2}{\mathcal{N}\left(2\pi\right)^2}k_{D_J}^2\frac{2\pi}{J\left(v_\perp k_{D_J}\right)^{\frac{2}{J}}}\left(-\varepsilon\right)^{\frac{2-J}{J}}\left[-\int_0^\infty \frac{\frac{1}{2}}{1-\varepsilon'_{\boldsymbol{k}}}\left(\varepsilon'_{\boldsymbol{k}}\right)^{\frac{2-J}{J}}d\varepsilon'_{\boldsymbol{k}}\right. \\
&- \left.\int_0^\infty \frac{\frac{1}{2}}{1+\varepsilon'_{\boldsymbol{k}}}\left(\varepsilon'_{\boldsymbol{k}}\right)^{\frac{2-J}{J}}d\varepsilon'_{\boldsymbol{k}}\right] \\
&= -\frac{\Omega\,|v|^2}{\mathcal{N}\left(2\pi\right)^2}k_{D_J}^2\frac{2\pi}{J\left(v_\perp k_{D_J}\right)^{\frac{2}{J}}}\left(-\varepsilon\right)^{\frac{2-J}{J}}\left[\int_0^\infty \frac{\frac{1}{2}}{1-\varepsilon'_{\boldsymbol{k}}}\varepsilon'^{\frac{2-J}{J}}_{\boldsymbol{k}}d\varepsilon'_{\boldsymbol{k}}\right. \\
&+ \left.\int_0^\infty \frac{\frac{1}{2}}{1+\varepsilon'_{\boldsymbol{k}}}\varepsilon'^{\frac{2-J}{J}}_{\boldsymbol{k}}d\varepsilon'_{\boldsymbol{k}}\right] \\
&= -\frac{\Omega\,|v|^2}{\mathcal{N}\left(2\pi\right)^2}k_{D_J}^2\frac{\pi}{J\left(v_\perp k_{D_J}\right)^{\frac{2}{J}}}\left(-\varepsilon\right)^{\frac{2-J}{J}}\left[\pi cot\frac{2\pi}{J}+\pi cossec\frac{2\pi}{J}\right] \\
&= -\frac{\Omega\,|v|^2}{\mathcal{N}\left(2\pi\right)^2}k_{D_J}^2\frac{\pi}{J\left(v_\perp k_{D_J}\right)^{\frac{2}{J}}}\left(-\varepsilon\right)^{\frac{2-J}{J}}\pi cot\frac{\pi}{J} \qquad (3.65)
\end{aligned}$$

3.2 Calculando a $\mathcal{G}_{dd}$

Agora é necessário calcular as funções de Green da impureza.

$$\mathcal{G}^{R}_{d_\sigma d_{\sigma'}}\left(t\right) = -\frac{i}{\hbar}\theta(t)Z^{-1}\sum_n e^{-\beta E_n}\left\langle n\left|\left[d_\sigma\left(t\right), d^\dagger_{\sigma'}\left(0\right)\right]_+\right|n\right\rangle \qquad (3.66)$$

Então,

$$\begin{aligned}\frac{\partial}{\partial t}\mathcal{G}^{R}_{d_\sigma d_{\sigma'}}(t) = &- \frac{i}{\hbar}\delta(t)Z^{-1}e^{-\beta E_n}\left\langle n\left|\left[d_\sigma(t), d^{\dagger}_{\sigma'}(0)\right]_+\right|n\right\rangle \\ &- \frac{i}{\hbar}\theta(t)Z^{-1}e^{-\beta E_n}\left\langle n\left|\left[\frac{\partial}{\partial t}d_\sigma(t), d^{\dagger}_{\sigma'}(0)\right]_+\right|n\right\rangle \end{aligned} \tag{3.67}$$

Com $\frac{\partial}{\partial t}d_\sigma(t) = \left[-\frac{i}{\hbar}d_\sigma(t), \mathcal{H}\right]$, logo

$$\begin{aligned}\frac{\partial}{\partial t}\mathcal{G}^{R}_{d_\sigma d_{\sigma'}}(t) = &- \frac{i}{\hbar}\delta(t)Z^{-1}e^{-\beta E_n}\left\langle n\left|\left[d_\sigma, d^{\dagger}_{\sigma'}\right]_+\right|n\right\rangle \\ &- \frac{i}{\hbar}\theta(t)Z^{-1}e^{-\beta E_n}\left\langle n\left|\left[\left[-\frac{i}{\hbar}d_\sigma, \mathcal{H}\right], d^{\dagger}_{\sigma'}\right]_+\right|n\right\rangle \end{aligned} \tag{3.68}$$

Após aplicação da definição de Heisenberg, obtemos.

$$\begin{aligned}\frac{\partial}{\partial t}d_\sigma(t) &= -\frac{i}{\hbar}\left[d_\sigma, \mathcal{H}\right] \\ &= -\frac{i}{\hbar}\left[d_\sigma, \sum_{\boldsymbol{k's'\sigma'}}\left(c^{\dagger}_{k's'\sigma'}sv_\perp\frac{k^J_{\bar\sigma}}{k^{J-1}_{D_J}}c_{\boldsymbol{k's'}\bar\sigma}\right)\right] \\ &= -\frac{i}{\hbar}\left[d_\sigma, \sum_{\sigma'}\left(\varepsilon_{d'\sigma'}d^{\dagger}_{\sigma'}d_{\sigma'}\right)\right] \\ &= -\frac{i}{\hbar}\left[Ud^{\dagger}_{\uparrow}d_{\uparrow}d^{\dagger}_{\downarrow}d_{\downarrow}\right] \\ &= -\frac{i}{\hbar}\frac{1}{\sqrt{\mathcal{N}}}\sum_{\boldsymbol{k's'\sigma'}}\left[d_\sigma, vc^{\dagger}_{\boldsymbol{k's'\sigma'}}d_{\sigma'}\right] \\ &= -\frac{i}{\hbar}\frac{1}{\sqrt{\mathcal{N}}}\sum_{\boldsymbol{k's'\sigma'}}\left[d_\sigma, v^*d^{\dagger}_{\sigma'}c_{\boldsymbol{k's'\sigma'}}\right]. \end{aligned} \tag{3.69}$$

Resolvendo os comutadores

$$\begin{aligned}\left[d_\sigma, \sum_{k's'\sigma'}\left(c^{\dagger}_{k's'\sigma'}sv_\perp\frac{k^J_{\bar\sigma}}{k^{J-1}_{D_J}}c_{k's'\bar{\sigma'}}\right)\right] &= \sum_{k's'\sigma'}sv_\perp\frac{k^J_{\bar\sigma}}{k^{J-1}_{D_J}}\left[d_\sigma, c^{\dagger}_{k's'\sigma'}c_{k's'\bar{\sigma'}}\right] \\ &= \sum_{k's'\sigma'}sv_\perp\frac{k^J_{\bar\sigma}}{k^{J-1}_{D_J}}\left[d_\sigma c^{\dagger}_{k's'\sigma'}c_{k's'\bar{\sigma'}} - c^{\dagger}_{k's'\sigma'}c_{k's'\bar{\sigma'}}d_\sigma\right] \\ &= \sum_{k's'\sigma'}sv_\perp\frac{k^J_{\bar\sigma}}{k^{J-1}_{D_J}}\left[d_\sigma c^{\dagger}_{k's'\sigma'}c_{k's'\bar{\sigma'}} + c^{\dagger}_{k's'\sigma'}d_\sigma c_{k's'\bar{\sigma'}}\right] \\ &= \sum_{k's'\sigma'}sv_\perp\frac{k^J_{\bar\sigma}}{k^{J-1}_{D_J}}\left[d_\sigma c^{\dagger}_{k's'\sigma'}c_{k's'\bar{\sigma'}} - d_\sigma c^{\dagger}_{k's'\sigma'}c_{k's'\bar{\sigma'}}\right] \\ &= 0, \end{aligned} \tag{3.70}$$

$$
\begin{aligned}
\left[d_\sigma, \sum_{\sigma'} \left(\varepsilon_{d'\sigma'} d^\dagger_{\sigma'} d_{\sigma'}\right)\right] &= \sum_{\sigma'} \varepsilon_{d'\sigma'} \left[d_\sigma, d^\dagger_{\sigma'} d_{\sigma'}\right] \\
&= \sum_{\sigma'} \varepsilon_{d'\sigma'} \left[d_\sigma d^\dagger_{\sigma'} d_{\sigma'} - d^\dagger_{\sigma'} d_{\sigma'} d_\sigma\right] \\
&= \sum_{\sigma'} \varepsilon_{d'\sigma'} \left[\left(\delta_{\sigma\sigma'} - d^\dagger_{\sigma'} d_\sigma\right) d_{\sigma'} - d^\dagger_{\sigma'} d_{\sigma'} d_\sigma\right] \\
&= \sum_{\sigma'} \varepsilon_{d'\sigma'} \left[\delta_{\sigma\sigma'} d_{\sigma'} - d^\dagger_{\sigma'} d_\sigma d_{\sigma'} - d^\dagger_{\sigma'} d_{\sigma'} d_\sigma\right] \\
&= \sum_{\sigma'} \varepsilon_{d'\sigma'} \left[\delta_{\sigma\sigma'} d_{\sigma'} + d^\dagger_{\sigma'} d_{\sigma'} d_\sigma - d^\dagger_{\sigma'} d_{\sigma'} d_\sigma\right] \\
&= \sum_{\sigma'} \varepsilon_{d'\sigma'} \delta_{\sigma\sigma'} d_{\sigma'} \\
&= \varepsilon_{d'\sigma'} d_\sigma, \qquad (3.71)
\end{aligned}
$$

$$
\begin{aligned}
\left[d_\sigma, U \sum_{\sigma} d^\dagger_\uparrow d_\uparrow d^\dagger_\downarrow d_\downarrow\right] &= U \left[d_\sigma d^\dagger_\uparrow d_\uparrow d^\dagger_\downarrow d_\downarrow - d^\dagger_\uparrow d_\uparrow d^\dagger_\downarrow d_\downarrow d_\sigma\right] \\
&= U \left[\left(\delta_{\sigma\uparrow} - d^\dagger_\uparrow d_\sigma\right) d_\uparrow d^\dagger_\downarrow d_\downarrow - d^\dagger_\uparrow d_\uparrow d^\dagger_\downarrow d_\downarrow d_\sigma\right] \\
&= U \left[\delta_{\sigma\uparrow} d_\uparrow d^\dagger_\downarrow d_\downarrow - d^\dagger_\uparrow d_\sigma d_\uparrow d^\dagger_\downarrow d_\downarrow - d^\dagger_\uparrow d_\uparrow d^\dagger_\downarrow d_\downarrow d_\sigma\right] \\
&= U \left[\delta_{\sigma\uparrow} d_\uparrow d^\dagger_\downarrow d_\downarrow + d^\dagger_\uparrow d_\uparrow d_\sigma d^\dagger_\downarrow d_\downarrow - d^\dagger_\uparrow d_\uparrow d^\dagger_\downarrow d_\downarrow d_\sigma\right] \\
&= U \left[\delta_{\sigma\uparrow} d_\uparrow d^\dagger_\downarrow d_\downarrow + d^\dagger_\uparrow d_\uparrow \left(\delta_{\sigma\downarrow} - d^\dagger_\downarrow d_\sigma\right) d_\downarrow - d^\dagger_\uparrow d_\uparrow d^\dagger_\downarrow d_\downarrow d_\sigma\right] \\
&= U \left[\delta_{\sigma\uparrow} d_\uparrow d^\dagger_\downarrow d_\downarrow + d^\dagger_\uparrow d_\uparrow \delta_{\sigma\downarrow} d_\downarrow - d^\dagger_\uparrow d_\uparrow d^\dagger_\downarrow d_\sigma d_\downarrow - d^\dagger_\uparrow d_\uparrow d^\dagger_\downarrow d_\downarrow d_\sigma\right] \\
&= U \left[\delta_{\sigma\uparrow} d_\uparrow d^\dagger_\downarrow d_\downarrow + d^\dagger_\uparrow d_\uparrow \delta_{\sigma\downarrow} d_\downarrow + d^\dagger_\uparrow d_\uparrow d^\dagger_\downarrow d_\downarrow d_\sigma - d^\dagger_\uparrow d_\uparrow d^\dagger_\downarrow d_\downarrow d_\sigma\right] \\
&= U \left[\delta_{\sigma\uparrow} d_\uparrow d^\dagger_\downarrow d_\downarrow + d^\dagger_\uparrow d_\uparrow \delta_{\sigma\downarrow} d_\downarrow\right] \\
&= U \left[d^\dagger_\uparrow d_\uparrow \delta_{\downarrow\sigma} d_\downarrow + \delta_{\uparrow\sigma} d_\uparrow d^\dagger_\downarrow d_\downarrow\right] \\
&= U \left[n_\uparrow \delta_{\downarrow\sigma} d_\downarrow + \delta_{\uparrow\sigma} d_\uparrow n_\downarrow\right] \\
&= U d_\sigma n_{\bar{\sigma}}, \qquad (3.72)
\end{aligned}
$$

$$\begin{aligned}
\sum_{\boldsymbol{k}'s'\sigma'}\left[d_\sigma, vc^\dagger_{k's'\sigma'}d_{\sigma'}\right] &= \sum_{\boldsymbol{k}'s'\sigma'} v\left[d_\sigma, c^\dagger_{k's'\sigma'}d_{\sigma'}\right] \\
&= \sum_{\boldsymbol{k}'s'\sigma'} v\left[d_\sigma c^\dagger_{k's'\sigma'}d_{\sigma'} - c^\dagger_{k's'\sigma'}d_{\sigma'}d_\sigma\right] \\
&= \sum_{\boldsymbol{k}'s'\sigma'} v\left[d_\sigma c^\dagger_{k's'\sigma'}d_{\sigma'} + c^\dagger_{k's'\sigma'}d_\sigma d_{\sigma'}\right] \\
&= \sum_{\boldsymbol{k}'s'\sigma'} v\left[d_\sigma c^\dagger_{k's'\sigma'}d_{\sigma'} - d_\sigma c^\dagger_{k's'\sigma'}d_{\sigma'}\right] \\
&= 0
\end{aligned} \tag{3.73}$$

e

$$\begin{aligned}
\sum_{\boldsymbol{k}'s'\sigma'}\left[d_\sigma, v^* d^\dagger_{\sigma'}c_{k's'\sigma'}\right] &= \sum_{\boldsymbol{k}'s'\sigma'} v^*\left[d_\sigma d^\dagger_{\sigma'}c_{k's'\sigma'} - d^\dagger_{\sigma'}c_{k's'\sigma'}d_\sigma\right] \\
&= \sum_{\boldsymbol{k}'s'\sigma'} v^*\left[\left(\delta_{\sigma\sigma'} - d^\dagger_{\sigma'}d_\sigma\right)c_{k's'\sigma'} - d^\dagger_{\sigma'}c_{k's'\sigma'}d_\sigma\right] \\
&= \sum_{\boldsymbol{k}'s'\sigma'} v^*\left[\delta_{\sigma\sigma'}c_{k's'\sigma'} - d^\dagger_{\sigma'}d_\sigma c_{k's'\sigma'} - d^\dagger_{\sigma'}c_{k's'\sigma'}d_\sigma\right] \\
&= \sum_{\boldsymbol{k}'s'\sigma'} v^*\left[\delta_{\sigma\sigma'}c_{k's'\sigma'} - d^\dagger_{\sigma'}d_\sigma c_{k's'\sigma'} + d^\dagger_{\sigma'}d_\sigma c_{k's'\sigma'}\right] \\
&= \sum_{\boldsymbol{k}'s'\sigma'} v^*\delta_{\sigma\sigma'}c_{k's'\sigma'} \\
&= \sum_{\boldsymbol{k}s} v^* c_{ks\sigma}
\end{aligned} \tag{3.74}$$

Dos resultados obtidos em Eq.(3.70) à Eq.(3.74) aplicados em Eq.(3.69), temos.

$$\begin{aligned}
\frac{\partial}{\partial t}d_{\boldsymbol{k}s\sigma} = &- \frac{i}{\hbar}\left[d_\sigma, \mathcal{H}\right] \\
= &- \frac{i}{\hbar}\varepsilon_{d\sigma}d_\sigma \\
&- \frac{i}{\hbar}Un_\sigma d_{\overline{\sigma}} \\
&- \frac{i}{\hbar}\frac{1}{\sqrt{\mathcal{N}}}\sum_{\boldsymbol{k}s} v^* c_{ks\sigma}
\end{aligned} \tag{3.75}$$

Agora, da Eq.(3.75) em Eq.(3.68), obtém

$$\begin{aligned}\frac{\partial}{\partial t}\mathcal{G}^{R}_{d_\sigma d_{\sigma'}}(t) = &- \frac{i}{\hbar}\delta(t)Z^{-1}e^{-\beta E_n}\left\langle n\left|\left[d_\sigma(t), d^{\dagger}_{\sigma'}(0)\right]_+\right|n\right\rangle \\ &- \frac{i}{\hbar}\varepsilon_{d\sigma}\mathcal{G}^{R}_{d_\sigma d_{\sigma'}}(t) \\ &- \frac{i}{\hbar}U\mathcal{G}^{R}_{d_\sigma n_{\bar\sigma} d^{\dagger}_{\sigma'}}(t) \\ &- \frac{i}{\hbar}\frac{1}{\sqrt{\mathcal{N}}}\sum_{\boldsymbol{k}s} v^{*}\mathcal{G}^{R}_{c_{ks\sigma} d_{\sigma'}}(t) \end{aligned} \tag{3.76}$$

Aplicando a transformada de Fourier, temos que

$$\left(\varepsilon^{+} - \varepsilon_{d\sigma}\right)\widetilde{\mathcal{G}}^{R}_{d_\sigma d_{\sigma'}}(\varepsilon) = \delta_{\sigma\sigma'} + U\widetilde{\mathcal{G}}^{R}_{d_\sigma n_{d\bar\sigma} d^{\dagger}_{\sigma'}}(\varepsilon) + \frac{1}{\sqrt{\mathcal{N}}}\sum_{\boldsymbol{k}s} v^{*}\widetilde{\mathcal{G}}^{R}_{c_{ks\sigma} d_{\sigma'}}(\varepsilon)$$

sendo que

$$\mathcal{G}^{R}_{c_{\mathbf{k}s\sigma} d_{\sigma'}}(t) = -\frac{i}{\hbar}\theta(t)Z^{-1}\sum_{n} e^{-\beta E_n}\left\langle n\left|\left[c_{\mathbf{k}s\sigma}(t), d^{\dagger}_{\sigma'}(0)\right]_+\right|n\right\rangle \tag{3.77}$$

Então

$$\begin{aligned}\frac{\partial}{\partial t}\mathcal{G}^{R}_{c_{\mathbf{k}s\sigma} d_{\sigma'}}(t) &= -\frac{i}{\hbar}\delta(t)Z^{-1}\sum_{n} e^{-\beta E_n}\left\langle n\left|\left[c_{\mathbf{k}s\sigma}(t), d^{\dagger}_{\sigma'}(0)\right]_+\right|n\right\rangle \\ &+ -\frac{i}{\hbar}\theta(t)Z^{-1}\sum_{n} e^{-\beta E_n}\left\langle n\left|\left[\frac{\partial}{\partial t}c_{\mathbf{k}s\sigma}(t), d^{\dagger}_{\sigma'}(0)\right]_+\right|n\right\rangle \end{aligned} \tag{3.78}$$

com,

$$\begin{aligned}\frac{\partial}{\partial t}c_{\boldsymbol{k}s\sigma} &= \left[-\frac{i}{\hbar}c_{\boldsymbol{k}s\sigma}, \mathcal{H}\right] \\ &= \left[-\frac{i}{\hbar}c_{\mathbf{k}s\sigma}, \sum_{k's'\sigma'}\left(c^{\dagger}_{k's'\sigma'} s v_{\perp}\frac{k^{J}_{\bar\sigma}}{k^{J-1}_{D_J}}c_{k's'\bar\sigma'}\right)\right] \\ &+ \left[-\frac{i}{\hbar}c_{\mathbf{k}s\sigma}\sum_{\sigma}\left(\varepsilon_{d'\sigma'}d^{\dagger}_{\sigma'}d_{\sigma'}\right)\right] \\ &+ \left[-\frac{i}{\hbar}c_{\mathbf{k}s\sigma}, U d^{\dagger}_{\uparrow}d_{\uparrow}d^{\dagger}_{\downarrow}d_{\downarrow}\right] \\ &+ \left[-\frac{i}{\hbar}c_{\mathbf{k}s\sigma}, \frac{1}{\sqrt{\mathcal{N}}}\sum_{\boldsymbol{k}s\sigma} v c^{\dagger}_{k's'\sigma'}d_{\sigma}\right] \\ &+ \left[-\frac{i}{\hbar}c_{\mathbf{k}s\sigma}, \frac{1}{\sqrt{\mathcal{N}}}\sum_{\boldsymbol{k}s\sigma} v^{*}d^{\dagger}_{\sigma'}c_{k's'\sigma'}\right], \end{aligned} \tag{3.79}$$

$$\begin{aligned}
\left[-\frac{i}{\hbar}c_{\mathbf{k}s\sigma}, \sum_{ks\sigma}\left(c^{\dagger}_{k's'\sigma'} s v_{\perp} \frac{k^J_{\bar{\sigma}}}{k^{J-1}_{D_J}} c_{k's'\bar{\sigma}'}\right)\right] &= -\frac{i}{\hbar}\sum_{ks\sigma} s v_{\perp} \frac{k^J_{\bar{\sigma}}}{k^{J-1}_{D_J}} \left[c_{\mathbf{k}s\sigma}, c^{\dagger}_{k's'\sigma'} c_{k's'\bar{\sigma}'}\right] \\
&= -\frac{i}{\hbar}\sum_{ks\sigma} s v_{\perp} \frac{k^J_{\bar{\sigma}}}{k^{J-1}_{D_J}} \left[c_{\mathbf{k}s\sigma} c^{\dagger}_{k's'\sigma'} c_{k's'\bar{\sigma}'} - c^{\dagger}_{k's'\sigma'} c_{k's'\bar{\sigma}'} c_{\mathbf{k}s\sigma}\right] \\
&= -\frac{i}{\hbar}\sum_{ks\sigma} s v_{\perp} \frac{k^J_{\bar{\sigma}}}{k^{J-1}_{D_J}} \left[\left(\delta_{kk'}\delta_{ss'}\delta_{\sigma\sigma'} - c^{\dagger}_{k's'\sigma'} c_{\mathbf{k}s\sigma}\right) c_{k's'\bar{\sigma}'}\right. \\
&+ \left. c^{\dagger}_{k's'\sigma'} c_{\mathbf{k}s\sigma} c_{k's'\bar{\sigma}'}\right] \\
&= -\frac{i}{\hbar}\sum_{ks\sigma} s v_{\perp} \frac{k^J_{\bar{\sigma}}}{k^{J-1}_{D_J}} \left[\delta_{kk'}\delta_{ss'}\delta_{\sigma\sigma'} c_{k's'\bar{\sigma}'}\right] \\
&= -\frac{i}{\hbar} s v_{\perp} \frac{k^J_{\bar{\sigma}}}{k^{J-1}_{D_J}} c_{ks\bar{\sigma}}, \qquad (3.80)
\end{aligned}$$

$$\begin{aligned}
\left[-\frac{i}{\hbar}c_{\mathbf{k}s\sigma}, \sum_{\sigma}\left(\varepsilon_{d'\sigma'} d^{\dagger}_{\sigma'} d_{\sigma'}\right)\right] &= -\frac{i}{\hbar}\sum_{\sigma} \varepsilon_{d'\sigma'} \left[c_{\mathbf{k}s\sigma}, d^{\dagger}_{\sigma'} d_{\sigma'}\right] \\
&= -\frac{i}{\hbar}\sum_{\sigma} \varepsilon_{d'\sigma'} \left[c_{\mathbf{k}s\sigma} d^{\dagger}_{\sigma'} d_{\sigma'} + d^{\dagger}_{\sigma'} c_{\mathbf{k}s\sigma} d_{\sigma'}\right] \\
&= -\frac{i}{\hbar}\sum_{\sigma} \varepsilon_{d'\sigma'} \left[c_{\mathbf{k}s\sigma} d^{\dagger}_{\sigma'} d_{\sigma'} - d^{\dagger}_{\sigma'} d_{\sigma'} c_{\mathbf{k}s\sigma}\right] \\
&= 0, \qquad (3.81)
\end{aligned}$$

$$\begin{aligned}
\left[-\frac{i}{\hbar}c_{\mathbf{k}s\sigma}, U d^{\dagger}_{\uparrow} d_{\uparrow} d^{\dagger}_{\downarrow} d_{\downarrow}\right] &= -\frac{i}{\hbar} U \left[c_{\mathbf{k}s\sigma}, d^{\dagger}_{\uparrow} d_{\uparrow} d^{\dagger}_{\downarrow} d_{\downarrow}\right] \\
&= -\frac{i}{\hbar} U \left[c_{\mathbf{k}s\sigma} d^{\dagger}_{\uparrow} d_{\uparrow} d^{\dagger}_{\downarrow} d_{\downarrow} - d^{\dagger}_{\uparrow} d_{\uparrow} d^{\dagger}_{\downarrow} d_{\downarrow} c_{\mathbf{k}s\sigma}\right] \\
&= -\frac{i}{\hbar} U \left[c_{\mathbf{k}s\sigma} d^{\dagger}_{\uparrow} d_{\uparrow} d^{\dagger}_{\downarrow} d_{\downarrow} + d^{\dagger}_{\uparrow} d_{\uparrow} d^{\dagger}_{\downarrow} c_{\mathbf{k}s\sigma} d_{\downarrow}\right] \\
&= -\frac{i}{\hbar} U \left[c_{\mathbf{k}s\sigma} d^{\dagger}_{\uparrow} d_{\uparrow} d^{\dagger}_{\downarrow} d_{\downarrow} - d^{\dagger}_{\uparrow} d_{\uparrow} c_{\mathbf{k}s\sigma} d^{\dagger}_{\downarrow} d_{\downarrow}\right] \\
&= -\frac{i}{\hbar} U \left[c_{\mathbf{k}s\sigma} d^{\dagger}_{\uparrow} d_{\uparrow} d^{\dagger}_{\downarrow} d_{\downarrow} + d^{\dagger}_{\uparrow} c_{\mathbf{k}s\sigma} d_{\uparrow} d^{\dagger}_{\downarrow} d_{\downarrow}\right] \\
&= -\frac{i}{\hbar} U \left[c_{\mathbf{k}s\sigma} d^{\dagger}_{\uparrow} d_{\uparrow} d^{\dagger}_{\downarrow} d_{\downarrow} - c_{\mathbf{k}s\sigma} d^{\dagger}_{\uparrow} d_{\uparrow} d^{\dagger}_{\downarrow} d_{\downarrow}\right] \\
&= 0, \qquad (3.82)
\end{aligned}$$

$$
\begin{aligned}
\left[-\frac{i}{\hbar}c_{\mathbf{k}s\sigma},\frac{1}{\sqrt{\mathcal{N}}}\sum_{\boldsymbol{k}s\sigma}vc^{\dagger}_{k's'\sigma'}d_{\sigma}\right] &= -\frac{i}{\hbar}\frac{1}{\sqrt{\mathcal{N}}}\sum_{\boldsymbol{k}s\sigma}v\left[c_{\mathbf{k}s\sigma},c^{\dagger}_{k's'\sigma'}d_{\sigma'}\right]\\
&= -\frac{i}{\hbar}\frac{1}{\sqrt{\mathcal{N}}}\sum_{\boldsymbol{k}s\sigma}v\left[c_{\mathbf{k}s\sigma}c^{\dagger}_{k's'\sigma'}d_{\sigma}-c^{\dagger}_{k's'\sigma'}d_{\sigma}c_{\mathbf{k}s\sigma}\right]\\
&= -\frac{i}{\hbar}\frac{1}{\sqrt{\mathcal{N}}}\sum_{\boldsymbol{k}s\sigma}v\left[\left(\delta_{\boldsymbol{k}\boldsymbol{k'}}\delta_{ss'}\delta_{\sigma\sigma'}-c^{\dagger}_{k's'\sigma'}c_{\mathbf{k}s\sigma}\right)d_{\sigma}\right.\\
&+ \left.c^{\dagger}_{k's'\sigma'}c_{\mathbf{k}s\sigma}d_{\sigma}\right]\\
&= -\frac{i}{\hbar}\frac{1}{\sqrt{\mathcal{N}}}\sum_{\boldsymbol{k}s\sigma}v\left[\delta_{\boldsymbol{k}\boldsymbol{k'}}\delta_{ss'}\delta_{\sigma\sigma'}d_{\sigma}-c^{\dagger}_{k's'\sigma'}c_{\mathbf{k}s\sigma}d_{\sigma}\right]\\
&+ \left.c^{\dagger}_{k's'\sigma'}c_{\mathbf{k}s\sigma}d_{\sigma}\right]\\
&= -\frac{i}{\hbar}\frac{1}{\sqrt{\mathcal{N}}}\sum_{\boldsymbol{k}s\sigma}v\left[\delta_{\boldsymbol{k}\boldsymbol{k'}}\delta_{ss'}\delta_{\sigma\sigma'}d_{\sigma}\right]\\
&= -\frac{i}{\hbar}\frac{1}{\sqrt{\mathcal{N}}}vd_{\sigma}, \qquad (3.83)
\end{aligned}
$$

e

$$
\begin{aligned}
\left[-\frac{i}{\hbar}c_{\mathbf{k}s\sigma},\frac{1}{\sqrt{N}}\sum_{\boldsymbol{k}s\sigma}v^{*}d^{\dagger}_{\sigma'}c_{k's'\sigma'}\right] &= -\frac{i}{\hbar}\frac{1}{\sqrt{\mathcal{N}}}\sum_{\boldsymbol{k}s\sigma}v^{*}\left[c_{\mathbf{k}s\sigma},d^{\dagger}_{\sigma'}c_{k's'\sigma'}\right]\\
&= -\frac{i}{\hbar}\frac{1}{\sqrt{\mathcal{N}}}\sum_{\boldsymbol{k}s\sigma}v^{*}\left[c_{\mathbf{k}s\sigma}d^{\dagger}_{\sigma'}c_{k's'\sigma'}-d^{\dagger}_{\sigma'}c_{k's'\sigma'}c_{\mathbf{k}s\sigma}\right]\\
&= -\frac{i}{\hbar}\frac{1}{\sqrt{\mathcal{N}}}\sum_{\boldsymbol{k}s\sigma}v^{*}\left[c_{\mathbf{k}s\sigma}d^{\dagger}_{\sigma'}c_{k's'\sigma'}+d^{\dagger}_{\sigma'}c_{\mathbf{k}s\sigma}c_{k's'\sigma'}\right]\\
&= -\frac{i}{\hbar}\frac{1}{\sqrt{\mathcal{N}}}v^{*}\left[c_{\mathbf{k}s\sigma}d^{\dagger}_{\sigma'}c_{k's'\sigma'}-c_{\mathbf{k}s\sigma}d^{\dagger}_{\sigma'}c_{k's'\sigma'}\right].
\end{aligned}
$$

Então, temos que:

$$
\begin{aligned}
\frac{\partial}{\partial t}\mathcal{G}^{R}_{c_{\mathbf{k}s\sigma}d_{\sigma'}}(t) &= -\frac{i}{\hbar}(\tau)Z^{-1}\sum_{n}e^{-\beta E_n}\left\langle n\left|\left[c_{\mathbf{k}s\sigma}(t),d^{\dagger}_{\sigma'}(0)\right]_{+}\right|n\right\rangle\\
&- \frac{i}{\hbar}sv_{\perp}\frac{k^{J}_{\bar{\sigma}}}{k^{J-1}_{D_J}}\mathcal{G}^{R}_{c_{\mathbf{k}s\bar{\sigma}}d^{\dagger}_{\sigma}}(t)\\
&- \frac{i}{\hbar}\frac{1}{\sqrt{\mathcal{N}}}v\mathcal{G}^{R}_{d_{\sigma},d^{\dagger}_{\sigma'}}(t) \qquad (3.84)
\end{aligned}
$$

Realizando a transformada de Fourier, obtemos.

$$\begin{aligned}\widetilde{\mathcal{G}}^{R}_{c_{\mathbf{k}s\sigma}d_{\sigma'}}\left(\varepsilon^{+}\right) &= \frac{sv_{\perp}}{\varepsilon^{+}}\frac{k_{\bar{\sigma}}^{J}}{k_{D_J}^{J-1}}\widetilde{\mathcal{G}}^{R}_{c_{ks\bar{\sigma}},d^{\dagger}_{\sigma'}}\left(\varepsilon^{+}\right)\\ &+ \frac{1}{\varepsilon^{+}\sqrt{\mathcal{N}}}v\widetilde{\mathcal{G}}^{R}_{d_{\sigma},d^{\dagger}_{\sigma}}\left(\varepsilon^{+}\right)\end{aligned} \tag{3.85}$$

$$\begin{aligned}\widetilde{\mathcal{G}}^{R}_{c_{\mathbf{k}s\bar{\sigma}}d_{\sigma'}}\left(\varepsilon^{+}\right) &= \frac{sv_{\perp}}{\varepsilon^{+}}\frac{k_{\sigma}^{J}}{k_{D_J}^{J-1}}\widetilde{\mathcal{G}}^{R}_{c_{ks\sigma},d^{\dagger}_{\sigma'}}\left(\varepsilon^{+}\right)\\ &+ \frac{1}{\varepsilon^{+}\sqrt{\mathcal{N}}}v\widetilde{\mathcal{G}}^{R}_{d_{\bar{\sigma}},d^{\dagger}_{\sigma'}}\left(\varepsilon^{+}\right)\end{aligned} \tag{3.86}$$

Aplicando Eq.(3.86) em Eq.(3.85), temos que.

$$\begin{aligned}\widetilde{\mathcal{G}}^{R}_{c_{\mathbf{k}s\sigma}d_{\sigma'}}\left(\varepsilon^{+}\right) &= \left(\frac{sv_{\perp}}{\varepsilon^{+}k_{D_J}^{J-1}}\right)^{2}k_{\bar{\sigma}}^{J}k_{\sigma}^{J}\widetilde{\mathcal{G}}^{R}_{c_{ks\sigma},d^{\dagger}_{\sigma'}}\left(\varepsilon^{+}\right)\\ &+ \frac{sv_{\perp}}{\left(\varepsilon^{+}\right)^{2}}\frac{k_{\bar{\sigma}}^{J}}{k_{D_J}^{J-1}}\frac{v}{\sqrt{\mathcal{N}}}\widetilde{\mathcal{G}}^{R}_{d_{\bar{\sigma}},d^{\dagger}_{\sigma'}}\left(\varepsilon^{+}\right)\\ &+ \frac{v}{\varepsilon^{+}\sqrt{N}}\widetilde{\mathcal{G}}^{R}_{d_{\sigma},d^{\dagger}_{\sigma}}\left(\varepsilon^{+}\right)\end{aligned} \tag{3.87}$$

Assim, temos

$$\begin{aligned}\widetilde{\mathcal{G}}^{R}_{c_{\mathbf{k}s\sigma}d_{\sigma'}}\left(\varepsilon^{+}\right) - \frac{v_{\perp}^{2}\left(\frac{1}{k_{D_J}^{J-1}}\right)k_{\bar{\sigma}}^{J}k_{\sigma}^{J2}}{\left(\varepsilon^{+}\right)^{2}}\widetilde{\mathcal{G}}^{R}_{c_{ks\sigma},d^{\dagger}_{\sigma'}}\left(\varepsilon^{+}\right) &= \frac{sv_{\perp}}{\sqrt{N}\left(\varepsilon^{+}\right)^{2}}\frac{k_{\bar{\sigma}}^{J}v}{k_{D_J}^{J-1}}\widetilde{\mathcal{G}}^{R}_{d_{\bar{\sigma}},d^{\dagger}_{\sigma'}}\left(\varepsilon^{+}\right)\\ &+ \frac{1}{\varepsilon^{+}\sqrt{N}}v\widetilde{\mathcal{G}}^{R}_{d_{\sigma},d^{\dagger}_{\sigma}}\left(\varepsilon^{+}\right)\end{aligned} \tag{3.88}$$

Logo,

$$\begin{aligned}\widetilde{\mathcal{G}}^{R}_{c_{\mathbf{k}s\sigma}d_{\sigma'}}\left(\varepsilon^{+}\right) &= \frac{sv_{\perp}}{\left[\left(\varepsilon^{+}\right)^{2}-v_{\perp}^{2}\left(\frac{1}{k_{D_J}^{J-1}}\right)^{2}k_{\bar{\sigma}}^{J}k_{\sigma}^{J}\right]}\frac{k_{\bar{\sigma}}^{J}v}{k_{D_J}^{J-1}\sqrt{\mathcal{N}}}\widetilde{\mathcal{G}}^{R}_{d_{\bar{\sigma}},d^{\dagger}_{\sigma'}}\left(\varepsilon^{+}\right)\\ &+ \frac{\varepsilon^{+}}{\left[\left(\varepsilon^{+}\right)^{2}-v_{\perp}^{2}\left(\frac{1}{k_{D_J}^{J-1}}\right)^{2}k_{\bar{\sigma}}^{J}k_{\sigma}^{J}\right]\sqrt{\mathcal{N}}}v\widetilde{\mathcal{G}}^{R}_{d_{\sigma},d^{\dagger}_{\sigma}}\left(\varepsilon^{+}\right)\end{aligned} \tag{3.89}$$

Substituindo a Eq.(3.89) na Eq.(3.77), obtemos.

$$\begin{aligned}\left(\varepsilon^{+}-\varepsilon_{d\sigma}\right)\widetilde{\mathcal{G}}^{R}_{d_\sigma d_{\sigma'}}\left(\varepsilon\right) &= \delta_{\sigma\sigma'} \\ &+ U\widetilde{\mathcal{G}}^{R}_{d_\sigma n_{d\bar{\sigma}} d^{\dagger}_{\sigma'}}\left(\varepsilon\right) \\ &+ \frac{1}{\sqrt{\mathcal{N}}}\sum_{\boldsymbol{ks}} v^{*}\frac{sv_{\perp}}{\left(\left(\varepsilon^{+}\right)^{2}-v_{\perp}^{2}\left(\frac{1}{k_{D_J}^{J-1}}\right)^{2}k_{\bar{\sigma}}^{J}k_{\sigma}^{J}\right)}\frac{k_{\bar{\sigma}}^{J}v}{k_{D_J}^{J-1}\sqrt{\mathcal{N}}}\widetilde{\mathcal{G}}^{R}_{d_{\bar{\sigma}},d^{\dagger}_{\sigma'}}\left(\varepsilon^{+}\right) \\ &+ \frac{1}{\sqrt{\mathcal{N}}}\sum_{\boldsymbol{ks}} v^{*}\varepsilon^{+}\frac{1}{\left(\left(\varepsilon^{+}\right)^{2}-v_{\perp}^{2}\left(\frac{1}{k_{D_J}^{J-1}}\right)^{2}k_{\bar{\sigma}}^{J}k_{\sigma}^{J}\right)\sqrt{\mathcal{N}}}v\widetilde{\mathcal{G}}^{R}_{d_\sigma,d^{\dagger}_{\sigma}}\left(\varepsilon^{+}\right)\end{aligned} \tag{3.90}$$

Podemos reescrever a Eq.(3.90)

$$\left(\varepsilon-\tilde{\varepsilon}_{d\sigma}+i\mathrm{Im}(\Sigma_{k\sigma})\right)\tilde{\mathcal{G}}_{d_\sigma d_\sigma}\left(\varepsilon^{+}\right)=1+U\widetilde{\mathcal{G}}_{d_\sigma n_{d\bar{\sigma}} d_\sigma}\left(\varepsilon^{+}\right) \tag{3.91}$$

com $\widetilde{\varepsilon}_{d\sigma}=\varepsilon_{d}+\mathrm{Re}\left(\Sigma_{\boldsymbol{k}\sigma}\right)$

3.3 Função de Green para quatro operadores

Agora vamos determinar a função de Green para quatro operadores.

$$\mathcal{G}_{d_\sigma n_{d\bar{\sigma}},d_{\sigma'}}\left(t\right)=-\frac{i}{\hbar}\theta\left(\tau\right)\sum_{n}e^{-\beta E_n}\left\langle n\left|d_\sigma\left(t\right)n_{d\bar{\sigma}},d_{\sigma'}\right|n\right\rangle \tag{3.92}$$

Então

$$\begin{aligned}\frac{\partial}{\partial\tau}\mathcal{G}_{d_\sigma n_{d\bar{\sigma}},d_{\sigma'}}\left(t\right) &= -\frac{i}{\hbar}\delta\left(t\right)\sum_{n}e^{-\beta E_n}\left\langle n\left|d_\sigma\left(t\right)n_{d\bar{\sigma}},d_{\sigma'}\right|n\right\rangle \\ &- \frac{i}{\hbar}\delta\left(t\right)\sum_{n}e^{-\beta E_n}\left\langle n\left|\frac{\partial}{\partial\tau}d_\sigma\left(t\right)n_{d\bar{\sigma}},d_{\sigma'}\right|n\right\rangle\end{aligned} \tag{3.93}$$

com

$$\begin{aligned}
\frac{\partial}{\partial t} d_\sigma(t)\, n_{d\bar{\sigma}}(t) &= -\frac{i}{\hbar}\varepsilon_{d\sigma} d_\sigma n_{d\bar{\sigma}} \\
&+ \left(-\frac{i}{\hbar}\right) U d_\sigma n_{d\bar{\sigma}} \\
&+ \left(-\frac{i}{\hbar}\right)\left(-\frac{1}{\sqrt{\mathcal{N}}}\sum_{\mathbf{k}s} v c^\dagger_{\mathbf{k}s\bar{\sigma}} d_{\bar{\sigma}} d_\sigma\right) \\
&+ \left(-\frac{i}{\hbar}\right)\left(\frac{1}{\sqrt{\mathcal{N}}}\sum_{\mathbf{k}s} v^* c_{\mathbf{k}s\sigma} d^\dagger_{\bar{\sigma}} d_{\bar{\sigma}}\right) \\
&+ \left(-\frac{i}{\hbar}\right)\left(\frac{1}{\sqrt{\mathcal{N}}}\sum_{\mathbf{k}s} v^* d^\dagger_{\bar{\sigma}} c_{\mathbf{k}s\bar{\sigma}} d_\sigma\right). \qquad (3.94)
\end{aligned}$$

Então, substituindo a Eq.(3.94) na equação Eq.(3.93), obtemos.

$$\begin{aligned}
\frac{\partial}{\partial \tau}\mathcal{G}_{d_\sigma n_{d\bar{\sigma}}, d_{\sigma'}}(t) &= -\frac{i}{\hbar}\delta(t)\sum_n e^{-\beta E_n}\left\langle n\left|d_\sigma(t)\, n_{d\bar{\sigma}}, d_{\sigma'}\right|n\right\rangle \\
&+ \left(-\frac{i}{\hbar}\right)\varepsilon_{d\sigma}\left\{-\frac{i}{\hbar}\delta(t)\sum_n e^{-\beta E_n}\left\langle n\left|d_\sigma n_{d\bar{\sigma}}, d_{\sigma'}\right|n\right\rangle\right\} \\
&+ \left(-\frac{i}{\hbar}\right) U\left\{-\frac{i}{\hbar}\delta(t)\sum_n e^{-\beta E_n}\left\langle n\left|d_\sigma n_{d\bar{\sigma}}, d_{\sigma'}\right|n\right\rangle\right\} \\
&+ \left(-\frac{i}{\hbar}\right)\left(-\frac{1}{\sqrt{\mathcal{N}}}\sum_{\mathbf{k}s} v\right)\left\{-\frac{i}{\hbar}\delta(t)\sum_n e^{-\beta E_n}\left\langle n\left|c^\dagger_{\mathbf{k}s\bar{\sigma}} d_{\bar{\sigma}} d_\sigma, d_{\sigma'}\right|n\right\rangle\right\} \\
&+ \left(-\frac{i}{\hbar}\right)\frac{1}{\sqrt{\mathcal{N}}}\sum_{\mathbf{k}s} v^*\left\{-\frac{i}{\hbar}\delta(t)\sum_n e^{-\beta E_n}\left\langle n\left|c_{\mathbf{k}s\sigma} d^\dagger_{\bar{\sigma}} d_{\bar{\sigma}}, d_{\sigma'}\right|n\right\rangle\right\} \\
&+ \left(-\frac{i}{\hbar}\right)\frac{1}{\sqrt{\mathcal{N}}}\sum_{\mathbf{k}s} v^*\left\{-\frac{i}{\hbar}\delta(t)\sum_n e^{-\beta E_n}\left\langle n\left|d^\dagger_{\bar{\sigma}} c_{\mathbf{k}s\bar{\sigma}} d_\sigma, d_{\sigma'}\right|n\right\rangle\right\}.
\end{aligned}$$

Ou seja,

$$\begin{aligned}
\frac{\partial}{\partial\tau}\mathcal{G}_{d_\sigma n_{d\bar{\sigma}},d_{\sigma'}}(t) &= -\frac{i}{\hbar}\delta(t)\sum_n e^{-\beta E_n}\left\langle n\left|d_\sigma(t)\, n_{d\bar{\sigma}}, d_{\sigma'}\right|n\right\rangle \\
&+ \left(-\frac{i}{\hbar}\right)\varepsilon_{d\sigma}\mathcal{G}^R_{d_\sigma n_{d\bar{\sigma}},d_{\sigma'}}(t) \\
&+ \left(-\frac{i}{\hbar}\right)U\mathcal{G}^R_{d_\sigma n_{d\bar{\sigma}},d_{\sigma'}}(t) \\
&+ \left(-\frac{i}{\hbar}\right)\left(-\frac{1}{\sqrt{\mathcal{N}}}\sum_{\mathbf{k}s}v\right)\mathcal{G}^R_{c^\dagger_{\mathbf{k}s\bar{\sigma}}d_{\bar{\sigma}}d_\sigma,d_{\sigma'}}(t) \\
&+ \left(-\frac{i}{\hbar}\right)\frac{1}{\sqrt{\mathcal{N}}}\sum_{\mathbf{k}s}v^*\mathcal{G}^R_{c_{\mathbf{k}s\sigma}d^\dagger_{\bar{\sigma}}d_{\bar{\sigma}},d_{\sigma'}}(t) \\
&+ \left(-\frac{i}{\hbar}\right)\frac{1}{\sqrt{\mathcal{N}}}\sum_{\mathbf{k}s}v^*\mathcal{G}^R_{d^\dagger_{\bar{\sigma}}c_{\mathbf{k}s\bar{\sigma}}d_\sigma,d_{\sigma'}}(t) \qquad (3.95)
\end{aligned}$$

Realizando a transformada de Fourier, tem-se

$$\begin{aligned}
\left(\varepsilon^+-\varepsilon_{d\sigma}-U\right)\tilde{\mathcal{G}}_{d_\sigma n_{d\bar{\sigma}}d_{\sigma'}}\left(\varepsilon^+\right) &= \langle n_{d\bar{\sigma}}\rangle \\
&+ \varepsilon_{d\sigma}\widetilde{\mathcal{G}}^R_{d_\sigma n_{d\bar{\sigma}},d_{\sigma'}}\left(\varepsilon^+\right) \\
&- \frac{1}{\sqrt{\mathcal{N}}}\sum_{\mathbf{k}s}v\widetilde{\mathcal{G}}^R_{c^\dagger_{\mathbf{k}s\bar{\sigma}}d_{\bar{\sigma}}d_\sigma,d_{\sigma'}}\left(\varepsilon^+\right) \\
&+ \frac{1}{\sqrt{\mathcal{N}}}\sum_{\mathbf{k}s}v^*\widetilde{\mathcal{G}}^R_{c_{\mathbf{k}s\sigma}d^\dagger_{\bar{\sigma}}d_{\bar{\sigma}},d_{\sigma'}}\left(\varepsilon^+\right) \\
&+ \frac{1}{\sqrt{\mathcal{N}}}\sum_{\mathbf{k}s}v^*\widetilde{\mathcal{G}}^R_{d^\dagger_{\bar{\sigma}}c_{\mathbf{k}s\bar{\sigma}}d_\sigma,d_{\sigma'}}\left(\varepsilon^+\right) \qquad (3.96)
\end{aligned}$$

3.4 Aproximação de Hubbard I

Na Eq.(3.96) utilizamos a aproximação de Hubbard I [39],

$$\tilde{\mathcal{G}}_{c^\dagger_{\mathbf{k}s\bar{\sigma}}d_{\bar{\sigma}}d_\sigma d_{\sigma'}}(\varepsilon) \simeq \left\langle c^\dagger_{\mathbf{k}s\bar{\sigma}}d_{\bar{\sigma}}\right\rangle\tilde{\mathcal{G}}_{d_\sigma d_{\sigma'}}(\varepsilon) \qquad (3.97)$$

e

$$\tilde{\mathcal{G}}_{d^\dagger_{\bar{\sigma}}c_{\mathbf{k}s\bar{\sigma}}d_\sigma d_{\sigma'}}(\varepsilon) \simeq \left\langle d^\dagger_{\bar{\sigma}}c_{\mathbf{k}s\bar{\sigma}}\right\rangle\tilde{\mathcal{G}}_{d_\sigma d_{\sigma'}}(\varepsilon) = \left\langle c^\dagger_{\mathbf{k}s\bar{\sigma}}d_{\bar{\sigma}}\right\rangle\tilde{\mathcal{G}}_{d_\sigma d_{\sigma'}}(\varepsilon) \qquad (3.98)$$

Logo, a Eq(3.96), pode ser reescrita como

$$\left(\varepsilon^+-\varepsilon_{d\sigma}-U\right)\tilde{\mathcal{G}}_{d_\sigma n_{d\bar{\sigma}}d_{\sigma'}}\left(\varepsilon^+\right) = \langle n_{d\bar{\sigma}}\rangle + \left(\frac{1}{\sqrt{\mathcal{N}}}\sum_{\mathbf{k}s}v^*\right)\tilde{\mathcal{G}}_{c_{\mathbf{k}s\sigma}d^\dagger_{\bar{\sigma}}d_{\bar{\sigma}},d_{\sigma'}}(\varepsilon) \qquad (3.99)$$

Aplicando a EOM e a transformada de Fourier, resulta em

$$\tilde{\mathcal{G}}_{c_{\mathbf{k}s\sigma}n_{d\bar{\sigma}}d_\sigma}(\varepsilon)=\frac{s\frac{v_\perp}{k_{D_J}^{J-1}}k_{\bar{\sigma}}^J\frac{1}{\sqrt{\mathcal{N}}}v}{\left((\varepsilon^+)^2-\left(\frac{v_\perp}{k_{D_J}^{J-1}}\right)^2k_+^Jk_-^J\right)}\tilde{\mathcal{G}}_{d_{\bar{\sigma}}n_{d\bar{\sigma}}d_\sigma}(\varepsilon)+\frac{\frac{1}{\sqrt{\mathcal{N}}}v\varepsilon^+}{\left((\varepsilon^+)^2-\left(\frac{v_\perp}{k_{D_J}^{J-1}}\right)^2k_+^Jk_-^J\right)}\tilde{\mathcal{G}}_{d_\sigma n_{d\bar{\sigma}}d_\sigma}(\varepsilon) \tag{3.100}$$

Considerando as aproximações: $\tilde{\mathcal{G}}_{d_{\bar{\sigma}}n_{d\bar{\sigma}}d_\sigma}(\varepsilon)\simeq\langle n_{d\bar{\sigma}}\rangle\,\tilde{\mathcal{G}}_{d_{\bar{\sigma}}d_\sigma}(\varepsilon)$ e $\tilde{\mathcal{G}}_{d_\sigma n_{d\bar{\sigma}}d_\sigma}(\varepsilon)\simeq\langle n_{d\bar{\sigma}}\rangle\,\tilde{\mathcal{G}}_{d_\sigma d_\sigma}(\varepsilon)$, obtemos.

$$\tilde{\mathcal{G}}_{c_{\mathbf{k}s\sigma}n_{d\bar{\sigma}}d_\sigma}(\varepsilon)=\frac{s\frac{v_\perp}{k_{D_J}^{J-1}}k_{\bar{\sigma}}^J\frac{1}{\sqrt{\mathcal{N}}}v}{\left((\varepsilon^+)^2-\left(\frac{v_\perp}{k_{D_J}^{J-1}}\right)^2k_+^Jk_-^J\right)}\langle n_{d\bar{\sigma}}\rangle\,\tilde{\mathcal{G}}_{d_{\bar{\sigma}}d_\sigma}(\varepsilon)+\frac{\frac{1}{\sqrt{\mathcal{N}}}v\varepsilon^+}{\left((\varepsilon^+)^2-\left(\frac{v_\perp}{k_{D_J}^{J-1}}\right)^2k_+^Jk_-^J\right)}\langle n_{d\bar{\sigma}}\rangle\,\tilde{\mathcal{G}}_{d_\sigma d_\sigma}(\varepsilon) \tag{3.101}$$

3.5 Síntese de alguns resultados parciais

Trabalhando com as equações Eq.(3.99) e Eq.(3.101), tem-se

$$\begin{aligned}\left(\varepsilon^+-\varepsilon_{d\sigma}-U\right)\tilde{\mathcal{G}}_{d_\sigma n_{d\bar{\sigma}}d_{\sigma'}}(\varepsilon^+) &= \langle n_{d\bar{\sigma}}\rangle+\left(\frac{1}{\sqrt{\mathcal{N}}}\sum_{\mathbf{k}s}v^*\right)\frac{s\frac{v_\perp}{k_{D_J}^{J-1}}k_{\bar{\sigma}}^J\frac{1}{\sqrt{\mathcal{N}}}v}{\left((\varepsilon_s^+)^2-\left(\frac{v_\perp}{k_{D_J}^{J-1}}\right)^2k_+^Jk_-^J\right)}\tilde{\mathcal{G}}_{d_{\bar{\sigma}}n_{d\bar{\sigma}}d_\sigma}(\varepsilon)\\ &+ \left(\frac{1}{\sqrt{\mathcal{N}}}\sum_{\mathbf{k}s}v^*\right)\frac{\frac{1}{\sqrt{\mathcal{N}}}v\varepsilon^+}{\left((\varepsilon^+)^2-\left(\frac{v_\perp}{k_{D_J}^{J-1}}\right)^2k_+^Jk_-^J\right)}\tilde{\mathcal{G}}_{d_\sigma n_{d\bar{\sigma}}d_\sigma}(\varepsilon)\\ &= \langle n_{d\bar{\sigma}}\rangle+\Sigma_{k\bar{\sigma}}^s\tilde{\mathcal{G}}_{d_{\bar{\sigma}}n_{d\bar{\sigma}}d_\sigma}(\varepsilon)+\Sigma_{k\sigma z}^s\tilde{\mathcal{G}}_{d_\sigma n_{d\bar{\sigma}}d_\sigma}(\varepsilon)\end{aligned} \tag{3.102}$$

onde

$$\Sigma_{k\sigma}^s=\sum_{s\mathbf{k}}\frac{s\frac{v_\perp}{k_{D_J}^{J-1}}k_\sigma^J}{(\varepsilon^+)^2-\frac{v_\perp^2}{k_{D_J}^{2J-2}}k_+^Jk_-^J} \tag{3.103}$$

e

$$\Sigma_{k\sigma}^s=\sum_{s\mathbf{k}}\frac{\varepsilon^+}{(\varepsilon^+)^2-\frac{v_\perp^2}{k_{D_J}^{2J-2}}k_-^Jk_+^J} \tag{3.104}$$

Lembrando que, $\Sigma^s_{k\bar{\sigma}} = 0$ e $\Sigma^s_{k\sigma z} = \frac{1}{\mathcal{N}}\sum_{s\mathbf{k}} |v|^2 \frac{\varepsilon^+}{\left(\varepsilon^+_s\right)^2 - \frac{v_\perp^2}{k_{D_J}^{2J-2}} k_-^J k_+^J} = \frac{1}{\mathcal{N}}\sum_{s\mathbf{k}} \frac{|v|^2\varepsilon^+}{(\varepsilon^+)^2 - \frac{v_\perp^2}{k_{D_J}^{2J-2}} k_-^J k_+^J}$.
Logo,

$$\left(\varepsilon^+ - \varepsilon_{d\sigma} - U\right)\tilde{\mathcal{G}}_{d_\sigma n_{d\bar{\sigma}} d_{\sigma'}}(\varepsilon) = \langle n_{d\bar{\sigma}}\rangle + \Sigma^s_{k\sigma z}\tilde{\mathcal{G}}_{d_\sigma n_{d\bar{\sigma}} d_{\sigma'}}(\varepsilon). \tag{3.105}$$

Então,

$$\tilde{\mathcal{G}}_{d_\sigma n_{d\bar{\sigma}} d_{\sigma'}}(\varepsilon) = \frac{\langle n_{d\bar{\sigma}}\rangle}{\varepsilon^+ - \varepsilon_{d\sigma} - U - \Sigma^s_{k\sigma z}}. \tag{3.106}$$

Aplicando a Eq.(3.106) na equação que segue.

$$\left(\varepsilon - \varepsilon_{d\sigma} - \Sigma^s_{k\sigma z}\right)\tilde{\mathcal{G}}_{d_\sigma d_\sigma}(\varepsilon) = 1 + U\tilde{\mathcal{G}}_{d_\sigma n_{d\bar{\sigma}} d_{\sigma'}}(\varepsilon), \tag{3.107}$$

então,

$$\begin{aligned}\left(\varepsilon - \varepsilon_{d\sigma} - \Sigma^s_{k\sigma z}\right)\tilde{\mathcal{G}}_{d_\sigma d_\sigma}(\varepsilon) &= 1 + U\tilde{\mathcal{G}}_{d_\sigma n_{d\bar{\sigma}} d_{\sigma'}}(\varepsilon) \\ &= 1 + \frac{U\langle n_{d\bar{\sigma}}\rangle}{\varepsilon - \varepsilon_{d\sigma} - U - \Sigma^s_{k\sigma z}}\end{aligned} \tag{3.108}$$

Implicando que

$$\begin{aligned}\tilde{\mathcal{G}}_{d_\sigma d_\sigma}(\varepsilon) &= \frac{\varepsilon - \varepsilon_{d\sigma} - U - \Sigma^s_{k\sigma z} + U\langle n_{d\bar{\sigma}}\rangle}{\left(\varepsilon - \varepsilon_{d\sigma} - U - \Sigma^s_{k\sigma z}\right).\left(\varepsilon - \varepsilon_{d\sigma} - \Sigma^s_{k\sigma z}\right)} \\ &= \frac{1 - \langle n_{d\bar{\sigma}}\rangle}{\varepsilon - \varepsilon_{d\sigma} - \Sigma^s_{k\sigma z}} + \frac{\langle n_{d\bar{\sigma}}\rangle}{\varepsilon - \varepsilon_{d\sigma} - U - \Sigma^s_{k\sigma z}} \\ &= \frac{1 - \langle n_{d\bar{\sigma}}\rangle}{\varepsilon - \tilde{\varepsilon}_{d\sigma} + i\Gamma_\sigma} + \frac{\langle n_{d\bar{\sigma}}\rangle}{\varepsilon - \tilde{\varepsilon}_{d\sigma} - U + i\Gamma_\sigma}\end{aligned} \tag{3.109}$$

com , $\Gamma_\sigma = -\Sigma^s_{k\sigma z}$

Capítulo 4

A DOS da impureza e LDOS do hospedeiro

A partir da transformada de Fourier $\tilde{\mathcal{G}}_{\text{Ada.}\sigma}$ da função de Green retardada da impureza (GF) [39] $\mathcal{G}_{\text{Ada.}\sigma} = -i\theta(t)\left\langle\left\{d_\sigma(t), d_\sigma^\dagger(0)\right\}\right\rangle_{\mathcal{H}}$,, definimos a DOS da impureza.

$$\text{DOS} = -\frac{1}{\pi}\text{Im}\tilde{\mathcal{G}}_{\text{Ada.}\sigma}. \tag{4.1}$$

Consideramos o regime de bloqueio de Coloumb [39], em que a correlação U na $\tilde{\mathcal{G}}_{\text{Imp.}\sigma}$ é tratada na aproximação de Hubbard-I [39], que leva a GF do átomo:

$$\tilde{\mathcal{G}}_{\text{Ada.}\sigma} = \frac{1}{(-\text{Im}\Sigma)}\left(\frac{w_x}{x+i} + \frac{w_{\bar{x}}}{\bar{x}+i}\right). \tag{4.2}$$

Essa expressão, então introduz na Eq.(4.1), as bandas de Hubbard centradas em torno das bordas do *gap*, $\varepsilon_{d\sigma}$ e $\varepsilon_{d\sigma}+U$, cada qual com o alargamento de quasipartícula $-\text{Im}\Sigma = -v^2\text{Im}\widetilde{\mathcal{G}}_\sigma^0$ [39], em que $w_x = 1 - \langle n_{d\bar{\sigma}}\rangle$ e $w_{\bar{x}} = 1 - w_x$ os pesos espectrais das bandas, respectivamente. Adicionalmente, $\langle n_{d\sigma}\rangle = \int_{-D}^{0}\text{DOS}d\varepsilon$ é a ocupação eletrônica do átomo e

$$\tilde{\mathcal{G}}_\sigma^0 = \frac{1}{\mathcal{N}}\sum_{\mathbf{k}s}\frac{\varepsilon + i0^+}{(\varepsilon+i0^+)^2 + (\varepsilon_{\mathbf{k}s}^+)^2} \tag{4.3}$$

é a GF do hospedeiro puro para o multi-grafeno ABC, em que definimos os parâmetros adimensionais

$$x = \frac{\varepsilon - \varepsilon_{d\sigma} - \mathrm{Re}\Sigma}{(-\mathrm{Im}\Sigma)} \tag{4.4}$$

e

$$\bar{x} = \frac{\varepsilon - \varepsilon_{d\sigma} - U - \mathrm{Re}\Sigma}{(-\mathrm{Im}\Sigma)}, \tag{4.5}$$

em que $\mathrm{Re}\Sigma$ é a transformada de Kramers-Kronig de $-\mathrm{Im}\Sigma$. Particularmente para $J \geq 3$, demonstraremos que o parâmetro de assimetria entre as partes $\mathrm{Re}\Sigma$ e $-\mathrm{Im}\Sigma$, chamado de q_J (também denominado de parâmetro de Fano [42]), torna-se regido pelo ângulo $(360°/2J)$, ou seja, o ângulo de rotação do grupo de simetria C_{2J}. Para esse fim, temos que aplicar a transformada de Kramers-Kronig para $-\mathrm{Im}\Sigma$, dada por

$$\begin{aligned}
\mathrm{Re}\Sigma &= \frac{1}{\pi}\int_{-D}^{+D} \frac{(-\mathrm{Im}\Sigma)}{\varepsilon - y} dy \\
&= \frac{1}{\pi}\mathrm{sgn}(\varepsilon)(-\mathrm{Im}\Sigma)\int_{-D/\varepsilon}^{+D/\varepsilon} \frac{|u|^{2/J-1}}{1-u} du \\
&= q_J(-\mathrm{Im}\Sigma),
\end{aligned} \tag{4.6}$$

em que $y = u\varepsilon$ e $-\mathrm{Im}\Sigma$ é o alargamento de quasipartícula modulado pelo parâmetro de assimetria

$$q_J = \frac{1}{\pi}\mathrm{sgn}(\varepsilon)\mathrm{P.V.}\int_{-D/\varepsilon}^{+D/\varepsilon} \frac{|u|^{2/J-1}}{1-u} du, \tag{4.7}$$

sendo que P.V. indica o valor principal de Cauchy. Essa quantidade está profundamente conectada com a emergência de estados ligados virtuais na impureza. Antes disso, primeiramente determinamos o alargamento de quasipartícula como segue,

$$-\mathrm{Im}\Sigma = v^2 \frac{\pi\,|\varepsilon|^{2/J-1}}{JD^{2/J}}, \tag{4.8}$$

a qual escala com a lei de potência $|\varepsilon|^{2/J-1}$ exibindo uma singularidade de van Hove no nível de Fermi, $\varepsilon = 0$ para $J \geq 3$. Não discutiremos o caso em que $J = 2$, uma vez que ele corresponde a sistemas metálicos sem divergência. A expressão Eq.(4.8) é obtida a partir Eq.(4.3) seguindo a metodologia: (i) aplicando a substituição $\mathcal{N} = \sum_{\mathbf{k}s} \to \frac{\mathcal{A}}{(2\pi)^2}\int d^2\mathbf{k} = \frac{\Omega}{2\pi}k_D^2$, com $\mathcal{A}$ como elemento de área no espaço real, (ii) a transformação hiper-polar é dada por: $k_x =$

$k_D\left(\frac{\varepsilon^+_{\mathbf{k}s}}{D}\right)^{\frac{1}{J}}\cos\theta$ e $k_y = k_D\left(\frac{\varepsilon^+_{\mathbf{k}s}}{D}\right)^{\frac{1}{J}}\sin\theta$ $(0 \leq \theta \leq 2\pi)$, com Jacobiano $\mathcal{J}(\varepsilon^+_{\mathbf{k}s},\theta) = \frac{k_D^2}{J}\frac{(\varepsilon^+_{\mathbf{k}s})^{2/J-1}}{D^{2/J}}$ e propriedade $\int \tilde{\mathcal{G}}^0_\sigma d^2\mathbf{k} = \int \tilde{\mathcal{G}}^0_\sigma \mathcal{J}(\varepsilon^+_{\mathbf{k}s},\theta)d\varepsilon^+_{\mathbf{k}s}d\theta$.

Mais adiante, observamos que para a situação $q_J = 1$ (monocamada de grafeno), a função na Eq. (4.7) que depende de u não evanesce nos limites $u \to \pm\infty$. Essa característica impõe um desafio matemático para o cálculo integral e para tratá-lo adequadamente, basta seguir a Ref. [38] para a monocamada de grafeno. Resolvemos primeiro a integral analiticamente mantendo ε/D finito e o limite $\varepsilon/D \ll 1$ só é assumido nas avaliações numéricas de ReΣ.

$$\mathrm{Re}\Sigma(J=1) = v^2\frac{\varepsilon}{D^2}\ln\frac{|\varepsilon^2|}{|\varepsilon^2 - D^2|} \tag{4.9}$$

emerge como dependente de energia para $\varepsilon/D \ll 1$.

No entanto, o evanescimento desejado em q_J como uma função de u existe para $q_{J\geq 3}$ e como consequência, a integral na Eq.(4.7) comporta-se de forma finita para $\varepsilon/D \to \infty$. Isso produz um resultado forte, ou seja, um parâmetro de assimetria discretizado no número de camadas do sistema J,

$$q_{J\geq 3} = \mathrm{sgn}(\varepsilon)\cot(C_{2J}), \tag{4.10}$$

sendo definido $C_{2J} \equiv (360^\circ/2J)$ como ângulo para o grupo de simetria rotacional correspondente. Além disso, para compreender também o surgimento de estados ligados virtuais na LDOS do hospedeiro acoplado à impureza e sua interação com a singularidade de van Hove, devemos considerar a seguinte função de Green

$$\mathcal{G}_\sigma = -i\theta(t)\left\langle\left\{\frac{1}{\sqrt{\mathcal{N}}}\sum_{\mathbf{k}s} c_{\mathbf{k}s\sigma}(t), \frac{1}{\sqrt{\mathcal{N}}}\sum_{\mathbf{k}s} c^\dagger_{\mathbf{k}s\sigma}(0)\right\}\right\rangle_{\mathcal{H}}, \tag{4.11}$$

que gera

$$\mathrm{LDOS} = -\frac{1}{\pi}\mathrm{Im}\tilde{\mathcal{G}}_\sigma = \frac{(-\mathrm{Im}\Sigma)}{\pi v^2}\sum_{p=x,\bar{x}} w_p\frac{(p+q_J)^2}{p^2+1} \tag{4.12}$$

em termos da fórmula de Fano [42], sendo $\tilde{\mathcal{G}}_\sigma$ a transformada temporal de Fourier de $\mathcal{G}_\sigma$. Para concluir, se subtrairmos $(-\mathrm{Im}\Sigma)/\pi v^2$ da Eq.(4.12), ou seja, obtemos a LDOS induzida pelo átomo,

$$\Delta\mathrm{LDOS} = \mathrm{LDOS} - \frac{(-\mathrm{Im}\Sigma)}{\pi v^2}. \tag{4.13}$$

Capítulo 5

Resultados e discussões

Apresentamos aqui o análogo do colapso atômico na Física Atômica Relativística. Por meio da Ref. [40] para o regime paramagnético e sendo $J \geq 6$, a singularidade de van Hove torna-se um pico estreito e ligeiramente assimétrico nas proximidades da energia de Fermi na medida em que as correlações de Coulomb são levadas em consideração por meio da teoria do funcional densidade. Além de γ_0 e γ_1 [Fig.1.1 (a)], quando assumidos γ_2, γ_3 e γ_4 finitos, o efeito de deformação trigonal da superfície de Fermi [41] é suave, caracterizado por uma banda quase plana nas vizinhanças da energia de Fermi [40]. Por questão de simplicidade, levamos em consideração o regime de simetria partícula-buraco (PHS) do modelo. Nessa situação, $\varepsilon_{d\sigma} = \varepsilon_d = -\frac{U}{2}$ e $w_x = w_{\bar{x}} = 1/2$ ($\langle n_{d\bar{\sigma}} \rangle = 1/2$, devido a um cálculo autoconsistente, com $U = v = 0.14D$. Ao considerar a Eq. (4.1), nas Figs.5.1 (a) e (c), contrastamos a análise espectral descrita pela DOS da impureza para monocamada de grafeno ($J = 1$) e vários sistemas multi-grafeno ABC ($J \geq 3$), respectivamente. Na Fig.5.1(a), notamos claramente as bandas de Hubbard em torno de $\varepsilon \approx -\frac{U}{2}$ (P1 ou borda inferior do *gap*) e $\varepsilon \approx +\frac{U}{2}$ (P2 ou borda superior), juntamente com um *pseudogap* na energia de Fermi, com alargamento de quasipartícula, conforme representado na inserção a)-II. As posições precisas das bordas deste *gap* isolante podem ser encontradas determinando os pólos da Eq.(4.2). Isso é feito impondo $x = 0$ e $\bar{x} = 0$ nas Eqs.(4.4) e (4.5), respectivamente, das quais extraímos a igualdade $\varepsilon \pm \frac{U}{2} = \mathrm{Re}\Sigma$. Essa última equação aparece resolvida graficamente na Fig.5.1(b), onde obtemos dois pontos de cruzamento entre as curvas preta e vinho[Eq.(4.9)]. Além disso, ReΣ também mostra um *pseudogap* e, o mais importante, ReΣ segue a mesma dependência do sinal de energia de $-\mathrm{Im}\Sigma$. O cenário muda drasticamente ao considerar o multigrafeno ABC com $J \geq 3$ conforme mostrado na Fig.5.1 (c), devido ao parâmetro de assimetria $q_{J\geq 3}$ da Eq (4.10). Nessa análise, verificamos os pontos esperados P1

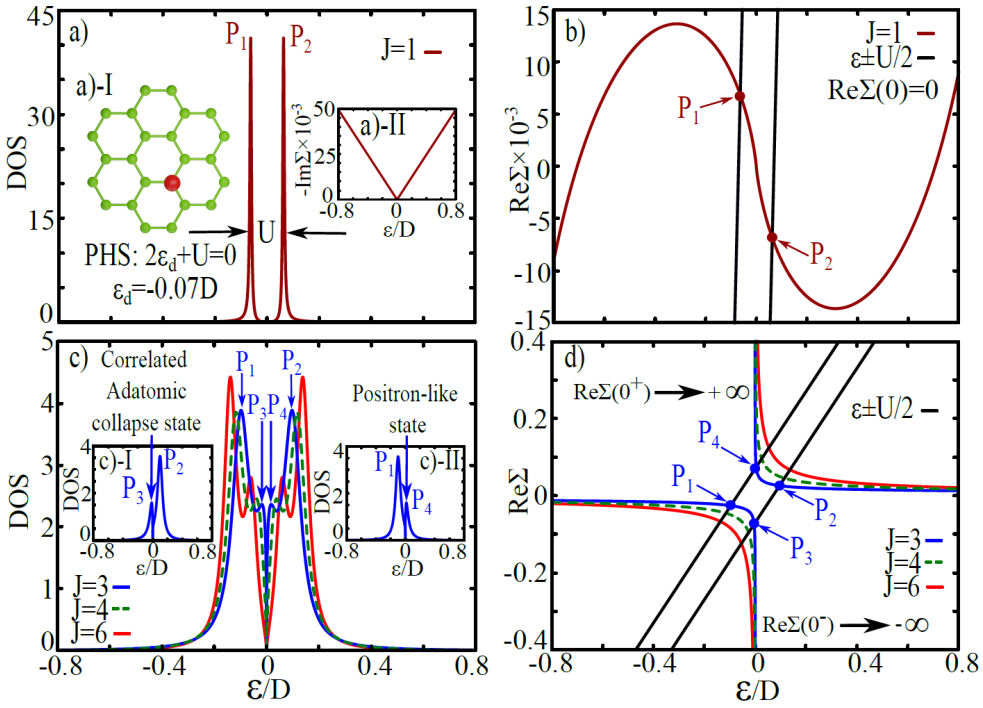


Figura 5.1: A simetria partícula-buraco (PHS) é considerada. (a) Grafeno único com uma impureza [a)-I], alargamento de quasipartícula linear na energia com um *pseudogap* no nível de Fermi [a)-II] e *gap* de Coulomb típico na DOS da impureza. (b) As bordas do *gap* aparecem como P1 e P2 na transformação de Kramers-Kronig de $-\mathrm{Im}\Sigma$, isto é, $\mathrm{Re}\Sigma$. (c) Para $J = 3, 4$ e 6 a DOS da impureza exibe estados ligados virtuais internos ao *gap*, marcados por P3 e P4 apenas para $J = 3$. (d) Para o empilhamento ABC, $\mathrm{Re}\Sigma$ diverge na energia de Fermi e as bordas inferior do *gap* de Coulomb P1 e P2 superior levam aos estados ligados virtuais P4 e P3, respectivamente. O pico ressonante P3 é devido à correlação U e emula o colapso atômico, uma vez que um estado eletronico se localiza-se em $\varepsilon < 0$. Em contraste, P4 é o simétrico partícula-buraco de P3 em $\varepsilon > 0$, analogamente a um estado de pósitron.

e P2, ou seja, as bordas do *gap* de Coulomb e, contraintuitivamente, dois estados ressonantes internos ao *gap* representados por P3 e P4. Tais pontos descrevem estados ligados virtuais emergentes, atribuídos ao multi-grafeno ABC sem a característica de sistemas de Moiré. A característica acima mencionada surge do estado sem dispersão fixado no nível de Fermi de acordo com as estruturas de bandas nos painéis inseridos (b)-(d) da Fig.1.1, que podem ser obtidos da Eq.(2.2). Isso significa que tal banda manifesta-se como uma divergência de van Hove no alargamento de quasipartícula na energia de Fermi [como pode ser visualizado nos painéis inseridos (b)-(d) da Fig.1.1 e na Eq. (4.8)], bem como sua transformação de Kramers-Kronig [Eq.(4.6)]. Porém, a forma como tal singularidade apresenta-se nessa última quantidade é bastante curiosa. Diferentemente de $-\mathrm{Im}\Sigma(0) \to \infty$ do alargamento de quasipartícula[Eq.(4.8)], temos $\mathrm{Re}\Sigma(0^-) \to -\infty$ e $\mathrm{Re}\Sigma(0^+) \to +\infty$, exclusivamente porque existe o fator de assimetria de energia $\mathrm{sgn}(\varepsilon)$ no parâmetro $q_{J\geq 3}$ da Eq.(4.10). Isso inverte o sinal de energia de $-\mathrm{Im}\Sigma$ quando trocamos a banda valência pela de condução. Isso pode ser visualizado na Figura 5.1 (d), na qual são registrados dois pontos de cruzamento extras, ou seja, P3 e P4. Digno de nota, percebemos que tais novos pólos estão correlacionados às bordas do *gap* de Coulomb: a linha preta acima da singularidade de van Hove contém P1 (borda inferior) e P4, enquanto a linha correspondente abaixo tem P2 (borda superior) e P3. Equivalentemente, a existência do estado ligado virtual P3 está correlacionada com a borda do *gap* de Coulomb P2. Como o pico P3 descreve uma localização eletrônica abaixo do nível de Fermi, mais adiante demonstraremos que sua formação emula o análogo do fenômeno do colapso atômico encontrado na Física Atômica Relativística. Particularmente, P3 surge da correlação U, uma vez que tal estado ressonante é derivado da solução de $\bar{x} = 0$ [Eq. (4.5)], que fornece a borda superior do *gap*. Para perceber essa característica no painel inserido c)-I da Fig.5.1, é apresentada a parte correspondente à DOS da impureza dada pela Eq. (4.2) com peso espectral $w_{\bar{x}}$. Nessa inserção, podemos ver explicitamente a localização eletrônica abaixo da energia de Fermi induzida pela correlação U. Adicionalmente, o estado P4 é o buraco, o simétrico da partícula P3 obtido a partir da condição $x = 0$ na Eq. (4.4) e desempenha o papel de um estado de pósitron, uma vez que sua localização ocorre acima da energia de Fermi. Essa característica pode ser encontrada no painel inserido c)-II da Fig.5.1, mas com a parte da DOS correspondente carregando o peso espectral w_x.

Com isso em mente, na Fig.5.2, revelamos o mecanismo subjacente responsável pelo efeito acima mencionado no multigrafeno ABC. A Fig.5.2 (a) mostra a análise da DOS da impureza para vários valores de ε_d para $J = 3$, onde podemos perceber claramente que ao enterrar o nível

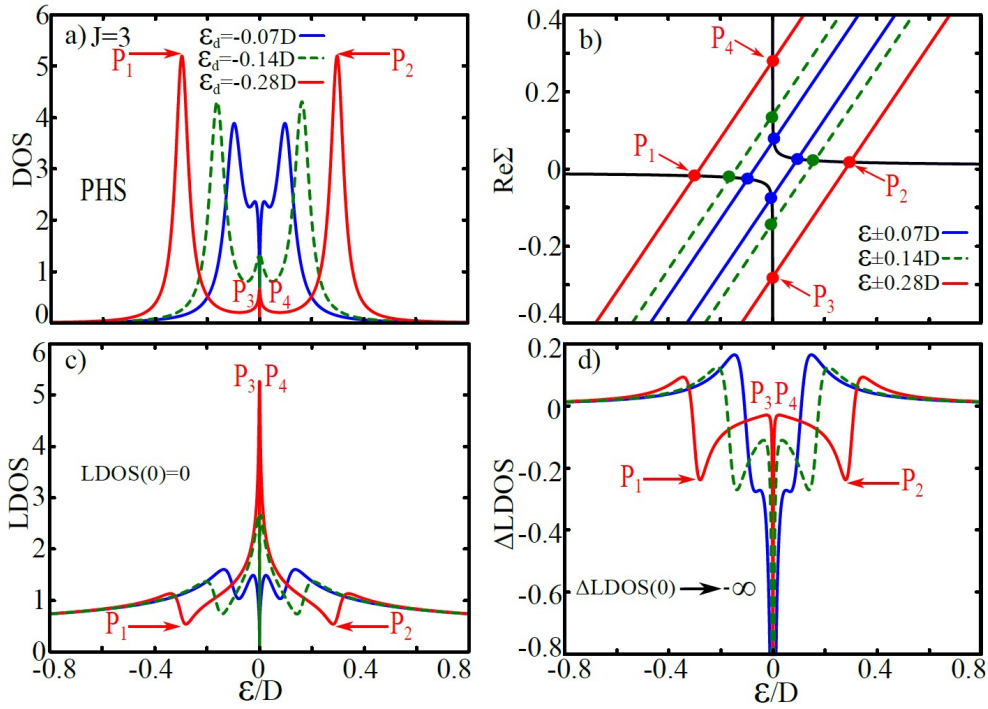


Figura 5.2: Mecanismo do colapso atômico no empilhamento ABC: (a) DOS da impureza do regime PHS para várias energias ε_d onde a extinção dos estados de ligação virtual ocorre ao enterrar a energia da impureza dentro do mar de Fermi do multigrafeno tipo ABC. (b) ReΣ revela quanto mais profundo é ε_d mais os estados virtuais caem na singularidade de van Hove e se desacoplam do átomo. (c) Esses estados aparecem na LDOS do sistema, onde a singularidade está ausente. (d) Esaa falta é devida à ΔLDOS induzida, em que uma singularidade de van Hove negativa cancela a positiva em $-\mathrm{Im}/\pi v^2$.

da impureza no mar de Fermi do hospedeiro, os picos P3 e P4 são suprimidos com suas posições deslocadas em direção à energia de Fermi, onde reside a singularidade de van Hove. Por outro lado, as bordas do *gap* de Coulomb P1 e P2 exibem amplitudes aumentadas com posições de pico deslocadas para longe da singularidade. Assim, para entender o novo comportamento acima mencionado, apresentamos a dependência energética de ReΣ na Fig.5.2 (b). Curiosamente, esse painel revela que os pólos P3 e P4 mergulham na singularidade de van Hove ao diminuir ε_d. Isso significa que quando tais pólos são finalmente capturados pela singularidade, seus estados correspondentes desacoplam-se da impureza e inevitavelmente caem na banda hospedeira [ver P3, P4 no LDOS dado pela Eq. (4.12) e representado no painel (c)]. De forma equivalente, a Fig.5.2 (b) elucida que existe uma região nítida no domínio de energia, que está suficientemente próxima do nível de Fermi para ligar um elétron como um estado no contínuo de energia do hospedeiro [painel (c)], bem como prender um elétron dentro do sítio atômico como um estado de ligação virtual com energia abaixo do nível de Fermi. Além disso, tal aprisionamento leva a um estado ressonante acima da energia de Fermi, que emula um estado de pósitron em analogia sua versão relativística do problema na física atômica.

Quando essa situação se estabelece, percebemos o colapso atômico por nós introduzido. Surpreendentemente, a singularidade de van Hove no alargamento de quasipartícula [painéis (c) - (d) da Fig.1.1] é cancelado na LDOS da Fig.5.2 (c) pela LDOS induzida da Eq. (4.13) mostrada na Fig.5.2(d), uma vez que a LDOS(0) = 0.

Capítulo 6

Conclusões

Neste trabalho, encontramos estados ligados virtuais dentro do *gap* isolante de Coulomb de uma impureza acoplada a um sistema multi-grafeno com empilhamento ABC. Demonstramos que um dos estados virtuais emula o fenômeno do colapso atômico conhecido na Física Atômica Relativística [1, 2]. Curiosamente, o segundo estado virtual relatado corresponde ao simétrico partícula-buraco do último, desempenhando assim o papel do estado de pósitron. Dessa forma, introduzimos nosso colapso atômico, que surge de um sistema do tipo Anderson composto por uma impureza e um hospedeiro multi-grafeno sem a característica de Moiré. Portanto, nossas descobertas deixam explícito que o sistema multi-grafeno ABC é uma estrutura rica para fenômenos fortemente correlacionados e emulação da Física Relativística.

Capítulo 7

Artigo publicado Phys. Rev. B 108, 205407 (2023)

arXiv:2304.02680v2 [cond-mat.str-el] 11 Dec 2023

Analogue of atomic collapse for adatoms on rhombohedral multilayer graphene

W.C. Silva,[1,*] J.E. Sanches,[1] A.M. Freitas,[1] L.T. Lustosa,[1] M. de Souza,[2] and A.C. Seridonio[1,†]

[1] *São Paulo State University (Unesp), School of Engineering, Department of Physics and Chemistry, 15385-000, Ilha Solteira-SP, Brazil*

[2] *São Paulo State University (Unesp), IGCE, Department of Physics, 13506-970, Rio Claro-SP, Brazil*

We propose that a multi-graphene of ABC-type stacking yields virtual bound states lying within the Coulomb insulating gap of an Anderson-like adatom. Wondrously, a virtual state constitutes the counterpart of the atomic collapse phenomenon proposed in relativistic atomic Physics, while the second emerges as its particle-hole symmetric, analogous to a positron state. Thus, we introduce the effect as the adatomic collapse, which occurs due to a flat band with a dispersionless state and a divergent density of states $\sim |\varepsilon - \varepsilon_F|^{2/J-1}$ near the Fermi energy ε_F for $J \geq 3$, where $J\pi$ is the Berry phase. We conclude this scenario based on the Kramers-Kronig transformation of the quasiparticle broadening, from where we observe that the aforementioned van Hove singularity induces virtual bound states. Counterintuitively, near the singularity, we find these states above and below the Fermi energy correlated to the existence of the bottom and top edges of the Coulomb insulating region, respectively. As such a behavior rises without a twist, the system is known as Moiréless and the phenomenon emerges also assisted by the adatom Coulomb correlations. Similarly to Science 340, 734 (2013) we find the effective critical atomic number $\mathcal{Z}_c \sim 0.96$ in contrast to an ultra–heavy nucleus. Thus, we point out that multi-graphene is a proper playground for testing a predicted phenomenon of the relativistic atomic Physics in the domain of the condensed matter Physics.

I. INTRODUCTION

The atomic collapse[1, 2] is an effect predicted by the relativistic atomic Physics, which consists of a phenomenon wherein the charge of a nucleus overpasses its threshold and becomes capable of catching an electron followed by a positron emission. To observe this phenomenon ultra-heavy nuclei are required, but they do not exist in nature spontaneously. Unfortunately, despite the efforts in fabricating the right conditions to emulate these atoms in the experimental native framework of this research field, the observation of the atomic collapse remains elusive[3, 4].

However, some condensed matter platforms rise as successful emulators for this effect wherein the graphene-based systems assume highly the status to this end. In such materials, the aforementioned features are due to the well-established low supercriticality, which can be manufactured artificially[5–8]. As examples we cite calcium ions[5, 6], charged vacancies and electrostatic potentials[7, 8], which once added to graphene monolayer samples play the role of effective supercritical atoms. As aftermath, these atoms within this supercritical regime exhibit a localized virtual bound state appearing in the local density of states (LDOS) as a resonant state below the Fermi level[5] and counterpart of the atomic collapse state.

Alternatively to graphene monolayer, which was already proved reliable for mimicking the atomic collapse, we are free to ask if contemporaneous van der Waals heterostructures could be also candidates for such, once they are characterized by flat bands[10, 11], i.e., the so-called van Hove singularities. However, for the entire accomplishment of these characteristics a fine tuning of the "twist magic angle" and Moiré potential conditions are demanded. Twisted bilayer, double-bilayer and trilayer graphene[10–27], ABC trilayer graphene on aligned hexagonal boron nitride[28–30] and transition-metal dichalcogenides[31–36] compose a set of the most common examples in this research field.

In order to overcome such a technical challenge, one way is to take into account the multilayer rhombohedral (ABC) graphene[9, 37], which naturally shows a low energy flat band without its birth in the Moiré superlattice induced by a twist. Interestingly enough, this is attributed to its divergent density of states (DOS) at the Fermi level[9], where a dispersionless state resides. Thus,

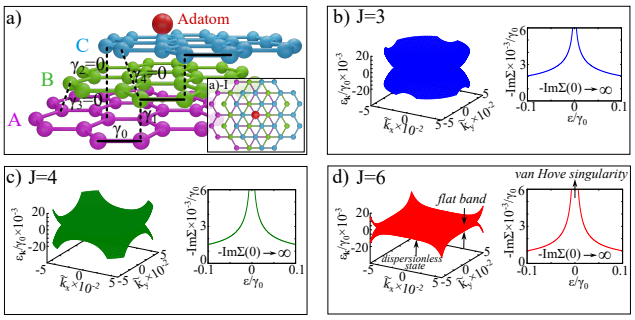


Figure 1. (Color online) (a) Lateral view of multi-graphene following the ABC-type stacking and an adatom on its top [panel a)-I]. (b)-(d) Several cases $J = 3, 4$ and 6, where the band-structure [Eq.(2)] and quasiparticle broadening [Eq.12] versus energy show a dispersionless state and a van Hove singularity at Fermi energy, respectively. Upon increasing the Berry phase $J\pi$, the flat band extension in reciprocal space enlarges too. Besides, J represents the total of monolayers[9].

* corresponding author:willian.carvalho@unesp.br
† corresponding author:antonio.seridonio@unesp.br

the system is known as Moiréless-type.

Consequently, based on this useful experimental aspect we benefit from it within a theoretical perspective by proposing our adatomic collapse effect. Here, we find that the multi-graphene of ABC-type stacking[9, 37] turns out into a novel platform for realizing the analogous effect of the atomic collapse. Distinctly from earlier results[5, 7, 8], the behavior here reported is the net effect of the interplay between Coulomb correlations and the van Hove singularity at the Fermi energy. Interestingly enough, this singularity enters into the power law of the host DOS, which follows $|\varepsilon-\varepsilon_F|^{2/J-1}$, where the Fermi energy is ε_F and leads to a divergence for $J\geq 3$, with the Berry phase $J\pi$.

Physically speaking, an Anderson-like adatom[38] on top of the ABC multi-graphene system, as depicted in Fig.1(a), fulfills entirely the previous constraints. Simultaneously, such an interaction imposes a gap in the adatom DOS, where we find virtual bound states. One of them stays below the Fermi energy due to the correlation and characterizes a trapped electron inside the valence band, while the other corresponds to its particle-hole symmetric (PHS) within the conduction band, thus emulating a positron-like state. For the quantification of this nearby van Hove singularity effect, as we shall see below, the Kramers-Kronig transformation of the quasiparticle broadening is adopted, from where the emergence of virtual bound states becomes clearly evident at the host.

II. THE MODEL

The low-energy Hamiltonian mimicking our system[Fig.1(a)] reads $\mathcal{H}=\mathcal{H}_{\text{ch.-ABC}}+\mathcal{H}_{\text{Ada.}}+\mathcal{H}_{\text{Hyb.}}$, where

$$\mathcal{H}_{\text{ch.-ABC}}=\sum_{\mathbf{k}s}\psi^{\dagger}_{\mathbf{k}s}s[D_J(\tilde{k}^J_{-}\sigma_{+}+\tilde{k}^J_{+}\sigma_{-})]\psi_{\mathbf{k}s} \quad (1)$$

describes the chiral (ch.) ABC multi-graphene by a set of $J\geq 3$ independent monolayers as *pseudospin* doublets[9], where $J\pi$ is the Berry phase, $\psi^{\dagger}_{\mathbf{k}s}=(c^{\dagger}_{\mathbf{k}s\uparrow}c^{\dagger}_{\mathbf{k}s\downarrow})$ represents the spinor, $c^{\dagger}_{\mathbf{k}s\sigma}$ ($c_{\mathbf{k}s\sigma}$) stands for the creation (annihilation) of an electron carrying momentum $\mathbf{k}$, spin $\sigma=\uparrow,\downarrow$ and valley index $s=\pm 1$ in a single *pseudospin* doublet[9]. The part $\tilde{k}_{\pm}=(k_x\pm ik_y)/k_{D_J}$ is of non-relativistic type, $k_{D_J}=D_J/v_F$ ($D_{J\geq 3}\approx\gamma_1=0.1\gamma_0$, with $\gamma_0=3$eV[Fig.1(a),[9]]) gives the *Debye-like* momentum (energy) cutoff in terms of the Slonczewski-Weiss-McClure parametrization[37, 39], with v_F the Fermi velocity and $\sigma_{\pm}=\frac{1}{2}(\sigma_x\pm i\sigma_y)$ the Pauli matrices. The band-structure of Eq.(1) is given straightforwardly by the dispersion relation

$$\varepsilon^{\pm}_{\mathbf{k}s}=\pm sv_F|\tilde{k}_{+}|^J k_{D_J}, \quad (2)$$

wherein the frontal sign $+(-)$ corresponds to the conduction (valence) band. Further, it is worth citing that for $J=1$ we recover one single graphene layer[40] with well-defined Dirac cones in momentum space with $D_{J=1}\approx\gamma_0$, while for $J\geq 3$ we have the chiral multi-graphene, which is characterized by a highly flat band with a van Hove singularity due to a dispersionless state at Fermi energy.

Additionally, a single Anderson-adatom[38] can be described by the Hamiltonian

$$\mathcal{H}_{\text{Ada.}}=-\frac{U}{2}+\sum_{\sigma}(\varepsilon_{d\sigma}+\frac{U}{2})n_{d\sigma}+\frac{U}{2}(\sum_{\sigma}n_{d\sigma}-1)^2, \quad (3)$$

where the adatom levels are $\varepsilon_{d\sigma}$ and $\varepsilon_{d\sigma}+U$, also recognized as the bottom and top edges of the Coulomb insulating gap, respectively and present in the adatom DOS for the Coulomb blockade regime[41]. The U term, actually, represents the Coulomb repulsion between two electrons with opposite spins ($\bar{\sigma}=-\sigma$), as well as the gap size and $n_{d\sigma}=(n_{d\sigma})^2=d^{\dagger}_{\sigma}d_{\sigma}$ stands for the number operator, with $d^{\dagger}_{\sigma}$ (d_{σ}) the corresponding creation (annihilation) operator.

According to Ref.[42], in the paramagnetic regime the van Hove singularity for $J\geq 6$ turns into a narrow peak slightly asymmetric around the Fermi energy when Coulomb correlations are taken into account by an interacting DFT approach. In such a case, despite γ_2,γ_3 and γ_4 finite[Fig.1(a)] the trigonal warping effect of the Fermi surface[39] is smooth characterized by a quasi-flat state nearby the Fermi energy[42]. This scenario is qualitatively captured by Eq.(1) as we shall see below.

The hybridization term stands for an adatom for the top site-type geometry, i.e., right on a carbon atom such as Au and Sn prefer[43]. This leads to

$$\mathcal{H}_{\text{Hyb.}}=v(\frac{1}{\sqrt{\mathcal{N}}}\sum_{\mathbf{k}s\sigma}c^{\dagger}_{\mathbf{k}s\sigma}d_{\sigma}+\text{H.c.}), \quad (4)$$

with v as the host-adatom hopping term and $\mathcal{N}$ is the number of states delimited by the Debye radius k_{D_J}. However, the hollow (center of the hexagon ring) and bridge site-types (middle of C-C bond) are other possibilities for adsorption[43] to be explored elsewhere.

In our Anderson-like Hamiltonian $\mathcal{H}$[38] for $J\geq 3$ we introduce atomic collapse regimes similarly to Ref.[44]: (i) $v\equiv 0$ is enough to define the subcritical limit without host resonant states; (ii) charge criticality is the starting point of $\mathcal{H}$ wherein $v\neq 0$ naturally and $\varepsilon_{d\sigma}=U=0$ stands for the PHS regime without correlation. As $f_{0\sigma}\equiv\frac{1}{\sqrt{\mathcal{N}}}\sum_{\mathbf{k}s}c_{\mathbf{k}s\sigma}$ in Eq.(4) acts as a host localized dispersionless state at Fermi energy coupled to d_{σ}, the so-called bonding (adatomic collapse) and antibonding (positron-like) molecular states symmetrically below and above such an energy emerge, respectively; (iii) in the interacting PHS regime, the super criticality emerges by burying $\varepsilon_{d\sigma}=-\frac{U}{2}\neq 0$ into the Fermi sea. It enhances the effective charge of the adatom in analogy to calcium ions gradually deposited on graphene monolayer up to electronic localization[5, 6]. Consequently, we observe two extra PHS localizations emerging within the Coulomb insulating gap at energies $-|\varepsilon_{d\sigma}|<\varepsilon<0$

and $0 < \varepsilon < |\varepsilon_{d\sigma}|$ as the novel adatomic collapse and positron-like states, respectively.

Simultaneously in (ii) and (iii) *Friedel-like* oscillations exhibit the same spatial dependence as the long-range Coulomb interaction ([45] and out of the present scope). We show that the relativistic linear dispersion of single graphene is needless and that the van Hove singularity is pivotal for the effect.

A. The Adatom DOS and LDOS

From the time Fourier transform $\tilde{\mathcal{G}}_{\mathrm{Ada}.\sigma}$ of the adatom retarded Green's function (GF)[41] $\mathcal{G}_{\mathrm{Ada}.\sigma} = -i\theta(t)\left\langle\left\{d_\sigma(t), d_\sigma^\dagger(0)\right\}\right\rangle_{\mathcal{H}}$, we define the adatom DOS

$$\mathrm{DOS} = -\frac{1}{\pi}\mathrm{Im}\tilde{\mathcal{G}}_{\mathrm{Ada}.\sigma}. \tag{5}$$

We consider the Coulomb blockade regime[41], in which the correlation U in $\tilde{\mathcal{G}}_{\mathrm{Ada}.\sigma}$ is accounted for within the framework of the Hubbard-I approximation[41], which leads to the well-known adatom GF[46]:

$$\tilde{\mathcal{G}}_{\mathrm{Ada}.\sigma} = \frac{1}{(-\mathrm{Im}\Sigma)}\left(\frac{w_x}{x+i} + \frac{w_{\bar{x}}}{\bar{x}+i}\right). \tag{6}$$

This expression introduces in Eq.(5) the Hubbard bands centered around the gap edges $\varepsilon_{d\sigma}$ and $\varepsilon_{d\sigma} + U$, with quasiparticle broadening $-\mathrm{Im}\Sigma = -v^2\mathrm{Im}\tilde{\mathcal{G}}_\sigma^0$ each[41], wherein $w_x = 1 - \langle n_{d\bar{\sigma}}\rangle$ and $w_{\bar{x}} = 1 - w_x$ represent the spectral weights (peak amplitudes) of the bands, respectively.

Additionally, $\langle n_{d\sigma}\rangle = \int_{-D}^{0}\mathrm{DOS}d\varepsilon$ is the electronic occupation of the adatom and

$$\tilde{\mathcal{G}}_\sigma^0 = \frac{1}{\mathcal{N}}\sum_{\mathbf{k}s}\frac{\varepsilon + i0^+}{(\varepsilon+i0^+)^2 - (\varepsilon_{\mathbf{k}s}^+)^2} \tag{7}$$

is the pristine host GF for the ABC multi-graphene, which allows to define the natural Fano coordinates[46]

$$x = \frac{\varepsilon - \varepsilon_{d\sigma} - \mathrm{Re}\Sigma}{(-\mathrm{Im}\Sigma)} \tag{8}$$

and

$$\bar{x} = \frac{\varepsilon - \varepsilon_{d\sigma} - U - \mathrm{Re}\Sigma}{(-\mathrm{Im}\Sigma)}, \tag{9}$$

where $\mathrm{Re}\Sigma$ is the Kramers-Kronig transformation of $-\mathrm{Im}\Sigma$. By applying such a transformation to $-\mathrm{Im}\Sigma$, we obtain

$$\begin{aligned}\mathrm{Re}\Sigma &= \frac{1}{\pi}\int_{-D_J}^{+D_J}\frac{(-\mathrm{Im}\Sigma)}{\varepsilon - y}dy \\ &= q_J(-\mathrm{Im}\Sigma),\end{aligned} \tag{10}$$

wherein $y = u\varepsilon$ and $-\mathrm{Im}\Sigma$ is the quasiparticle broadening modulated by the asymmetry parameter (also called as Fano parameter[47])

$$q_J = \frac{1}{\pi}\mathrm{sgn}(\varepsilon)\mathrm{P.V.}\int_{-D_J/\varepsilon}^{+D_J/\varepsilon}\frac{|u|^{2/J-1}}{1-u}du, \tag{11}$$

where P.V. stands for the Cauchy principal value. This object, as we will see later on, is profoundly connected to the emergence of the virtual bound states at the host.

After applying to Eq.(7) the following methodology: (i) the standard substitution $\mathcal{N} = \sum_{\mathbf{k}s} \to \frac{\mathcal{A}}{(2\pi)^2}\int d^2\mathbf{k} = \frac{\mathcal{A}}{2\pi}k_{D_J}^2$, with $\mathcal{A}$ as the area element in real space; (ii) the hyper-polar transformation given by $k_x = k_{D_J}\left(\frac{\varepsilon_{\mathbf{k}s}^+}{D_J}\right)^{\frac{1}{J}}\cos\theta$ and $k_y = k_{D_J}\left(\frac{\varepsilon_{\mathbf{k}s}^+}{D_J}\right)^{\frac{1}{J}}\sin\theta$ ($0 \le \theta \le 2\pi$), with Jacobian $\mathcal{J}(\varepsilon_{\mathbf{k}s}^+, \theta) = \frac{k_{D_J}^2}{J}\frac{(\varepsilon_{\mathbf{k}s}^+)^{2/J-1}}{D_J^{2/J}}$ and property $\int\tilde{\mathcal{G}}_\sigma^0 d^2\mathbf{k} = \int\tilde{\mathcal{G}}_\sigma^0\mathcal{J}(\varepsilon_{\mathbf{k}s}^+,\theta)d\varepsilon_{\mathbf{k}s}^+ d\theta$, we can determine the quasiparticle broadening as follows

$$-\mathrm{Im}\Sigma = v^2\frac{\pi\,|\varepsilon|^{2/J-1}}{JD_J^{2/J}}, \tag{12}$$

with scaling-law $|\varepsilon|^{2/J-1}$ exhibiting a van Hove singularity at Fermi level $\varepsilon = 0$ for $J \ge 3$. We do not discuss $J = 2$, since it corresponds to metals without divergence.

We remark that for the situation $q_{J=1}$ (single graphene), the function in Eq.(11) that depends on u does not vanish in the boundaries $u \to \pm\infty$. This feature imposes a mathematical challenge for the integral calculation and to handle it accordingly, we just follow Ref.[40] for single graphene, but with the cutoff $D_{J=1} \approx \gamma_0$ instead. We solve first the integral analytically by keeping $D_{J=1}/\varepsilon$ finite and the limit $\varepsilon/D_{J=1} \ll 1$ is only assumed in the numerical evaluations of $\mathrm{Re}\Sigma$. Consequently,

$$\mathrm{Re}\Sigma(J=1) = v^2\frac{\varepsilon}{D_{J=1}^2}\ln\frac{\left|\varepsilon^2\right|}{|\varepsilon^2 - D_{J=1}^2|} \tag{13}$$

emerges as dependent on energy for $\varepsilon/D_{J=1} \ll 1$. Nevertheless, the pursued vanishing characteristic in q_J as a function of u exists for $q_{J\ge3}$ and as aftermath, the integral in Eq.(11) does behave finite for $D_{J\ge3}/\varepsilon \to \infty$. This yields a capital result, i.e., an asymmetry parameter discretized in the number of the system layers J, which reads

$$q_{J\ge3} = \mathrm{sgn}(\varepsilon)\cot(C_{2J}), \tag{14}$$

where we define $C_{2J} \equiv (360°/2J)$ as the angle for the corresponding rotational symmetry group.

Additionally, in order to understand also the emergence of virtual bound states in the host LDOS coupled to the adatom and its interplay with the van Hove singularity, we should consider the following Green's function

$$\mathcal{G}_\sigma = -i\theta(t)\left\langle\left\{\frac{1}{\sqrt{\mathcal{N}}}\sum_{\mathbf{k}s}c_{\mathbf{k}s\sigma}(t), \frac{1}{\sqrt{\mathcal{N}}}\sum_{\mathbf{k}s}c_{\mathbf{k}s\sigma}^\dagger(0)\right\}\right\rangle_{\mathcal{H}}, \tag{15}$$

which yields

$$\mathrm{LDOS} = -\frac{1}{\pi}\mathrm{Im}\tilde{\mathcal{G}}_\sigma = \frac{(-\mathrm{Im}\Sigma)}{\pi v^2}\sum_{p=x,\bar{x}} w_p \frac{(p+q_J)^2}{p^2+1} \quad (16)$$

in terms of the Fano formula[47], where $\tilde{\mathcal{G}}_\sigma$ is the time Fourier transform of $\mathcal{G}_\sigma$. To conclude, if we subtract the background $(-\mathrm{Im}\Sigma)/\pi v^2$ from Eq.(16), i.e., we obtain the adatom induced LDOS, which reads

$$\Delta\mathrm{LDOS} = \mathrm{LDOS} - \frac{(-\mathrm{Im}\Sigma)}{\pi v^2}. \quad (17)$$

III. RESULTS AND DISCUSSION

Here we present the counterpart of the atomic collapse in relativistic atomic Physics, i.e., the adatomic collapse introduced by us. For a sake of simplicity, we take into account the model PHS regime $\varepsilon_{d\sigma} = \varepsilon_d = -\frac{U}{2} = -0.07\gamma_0$ and $w_x = w_{\bar{x}} = 1/2$ for the paramagnetic solution $\langle n_{d\sigma}\rangle = 1/2$ due to a self-consistent calculation and $v/D_J = 0.14$.

By considering Eq.(5) in Figs.2(a) and (c) we contrast the spectral analysis of the adatom DOS for single graphene ($J = 1$) and several ABC multi-graphene systems ($J \geq 6$), respectively. In Fig.2(a) we clearly notice the Hubbard bands around $\varepsilon \approx -|\varepsilon_d|$ (P1 or bottom edge of the gap) and $\varepsilon \approx +|\varepsilon_d|$ (P2 or top edge) together with a pseudogap at Fermi energy in the quasiparticle broadening, as depicted in the inset a)-II. By imposing $x = 0$ and $\bar{x} = 0$ in Eqs.(8) and (9) we obtain $\varepsilon + |\varepsilon_d| = \mathrm{Re}\Sigma$ and $\varepsilon - |\varepsilon_d| = \mathrm{Re}\Sigma$, respectively.

As a result, we are able to determine the poles of Eq.(6) thus providing the precise positions of the insulating gap edges. The latter appear graphically in Fig.2(b), where we see two crossing points between the black and wine[Eq.(13)] curves, once $\mathrm{Re}\Sigma$ just has van Hove singularities far away the Fermi energy and located at energy cutoffs $\pm\gamma_0$[Eq.(13)]. In such a domain interceptions do not occur. Additionally, $\mathrm{Re}\Sigma(0)$ shows a pseudogap too and, most importantly, $\mathrm{Re}\Sigma$ follows the same energy sign dependence of $-\mathrm{Im}\Sigma$.

The scenario changes drastically by considering the ABC multi-graphene with $J \geq 6$ as depicted in Fig.2(c) due to the asymmetry parameter $q_{J\geq 6}$ of Eq(14). In this analysis we verify the expected points P1 and P2, i.e., the Coulomb gap edges. Counterintuitively, two inner resonant states to the gap represented by P3 and P4 appear. Such points describe emerging virtual bound states arising from the Moiréless characteristic of the ABC multi-graphene system.

The aforementioned feature is due to the dispersionless state pinned at the Fermi level according to the band-structures in inset panels (b)-(d) of Fig.1, which can be obtained from Eq.(2). In Fig.1 we relax the condition $J \geq 6$ just for a sake of clearness. It means that such a flat band manifests as a van Hove divergence in the quasiparticle broadening exactly at Fermi energy[Eq.(12) and inset panels (b)-(d) of Fig.1], as well as in its Kramers-Kronig transformation[Eq.(10)]. However, the way that such a singularity presents itself in the latter quantity is quite curious. Differently from $-\mathrm{Im}\Sigma(0) \to \infty$ for the quasiparticle broadening[Eq.(12)] we have $\mathrm{Re}\Sigma(0^-) \to -\infty$ and $\mathrm{Re}\Sigma(0^+) \to +\infty$ instead, exclusively because there is the energy asymmetry factor $\mathrm{sgn}(\varepsilon)$ in the parameter $q_{J\geq 6}$ of Eq.(14). It reverses the energy sign of $-\mathrm{Im}\Sigma$ when we swap the valence by the conduction bands. This can be visualized in Fig.2(d), where two extra crossing points are recorded, i.e., P3 and P4. Noteworthy, we realize that such new poles are correlated to the Coulomb gap edges: the black line above the van Hove singularity contains P1(bottom edge) and P4, while the corresponding below has P2(top edge) and P3. Equivalently, the existence of the virtual bound state P3 is correlated to the Coulomb gap edge P2.

As the peak P3 describes an electronic localization beneath the Fermi level, later on, we will demonstrate that its formation emulates the counterpart of the atomic collapse phenomenon found in relativistic atomic Physics. Particularly, P3 arises from the correlation U, once such a resonant state is derived from the solution of $\bar{x} = 0$[Eq.(9)] and gives the top edge of the gap. To perceive this characteristic at the inset panel c)-I of Fig.2 the corresponding adatom DOS part of Eq.(6) with spectral

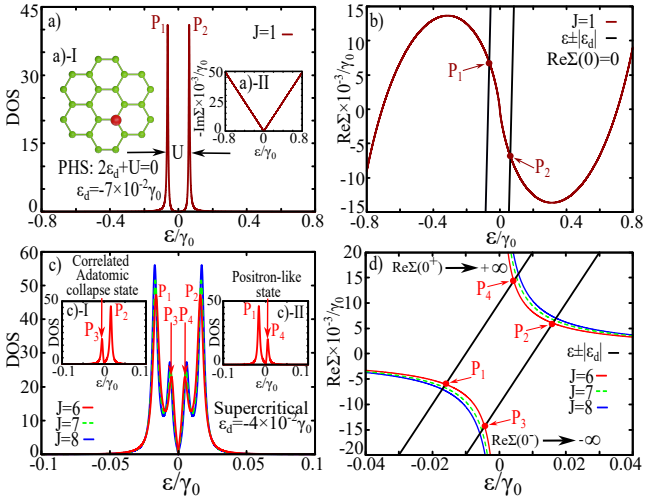


Figure 2. (Color online) Particle-hole symmetry (PHS) is taken into account. (a) Single graphene with an adatom [a)-I], linear quasiparticle broadening on energy with a pseudogap at Fermi level [a)-II] and typical Coulomb gap in the adatom DOS. (b) Gap edges appear as P1 and P2 in the Kramers-Kronig transformation of $-\mathrm{Im}\Sigma$, namely $\mathrm{Re}\Sigma$. (c) Adatom DOS for $J = 6, 7$ and 8 exhibiting inner virtual bound states to the gap marked by P3 and P4 solely for $J = 6$. (d) As for the ABC stacking $\mathrm{Re}\Sigma$ diverges at Fermi energy, the bottom P1 and top P2 Coulomb gap edges lead to virtual bound states P4 and P3, respectively. The resonant peak P3 is due to the correlation U and mimics the atomic collapse, once an electron state localizes at $\varepsilon < 0$. In contrast, P4 is the particle-hole symmetric of P3 at $\varepsilon > 0$, analogously to a positron state.

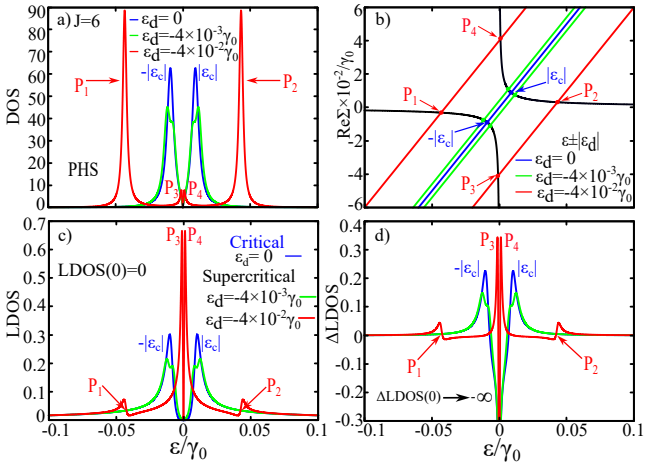


Figure 3. (Color online) Mechanism of the adatomic collapse in the ABC stacking: (a) Adatom DOS in the PHS regime for several energies ε_d, where quenching of virtual bond states occurs upon burying the adatom energy within the Fermi sea of the ABC multi-graphene. (b) ReΣ reveals that more deeper is ε_d, more the states P3 and P4 fall into the van Hove singularity and couple to the host. (c) These states appear in the system LDOS, where the singularity is absent. (d) This lacking is due to the induced ΔLDOS wherein a negative van Hove singularity cancels the one positive in $(-\mathrm{Im}\Sigma)/\pi v^2$. The critical energy is $|\varepsilon_c| \sim 9\times10^{-3}\gamma_0$, where $-(+)$ for the adatomic collapse (positron-like) state and atomic number $\mathcal{Z}_c \sim 0.96$.

weight $w_{\bar{x}}$ is presented. In such an inset, we can see explicitly the electronic localization below the Fermi energy induced by the correlation U.

Additionally, the state P4 is the particle-hole symmetric of P3 obtained from the condition $x = 0$ in Eq.(8) and plays the role of a positron state, since its localization occurs above the Fermi energy. This feature can be found at the inset panel c)-II of Fig.2, but with the corresponding DOS part carrying the spectral weight w_x. With this in mind, in Fig.3 we reveal the underlying mechanism responsible for the aforementioned effect in the ABC multi-graphene.

The critical limit is depicted by the blue curves in Figs.3(a)-(d) with $\varepsilon_d = U = 0$ and energies $\varepsilon = \mp|\varepsilon_c| = \mp[\sqrt{C_{2J}q_J(\varepsilon>0)}(\frac{v}{D_J})]^{\frac{J}{J-1}}D_J$ obtained from $x = \bar{x} = 0$[Eqs.(8) and (9)], where $-(+)$ stands for the adatomic collapse (positron-like) state. Particularly for $J = 6$ we find $|\varepsilon_c| \sim 9\times10^{-3}\gamma_0 = 2.7\times10^{-2}$eV. Here we choose to mimic the adatom as a highly excited effective hydrogen-like atom, which naturally imposes the upper critical atomic number $\mathcal{Z}_c^{\mathrm{upper}} = 1$. In this way, we point out that $n = 22$ provides the very close value $|\varepsilon_c^{\mathrm{upper}}| = \mathcal{Z}_c^{\mathrm{upper}}\frac{13.6\mathrm{eV}}{n^2} \sim 2.8\times10^{-2}$eV for the critical energy $|\varepsilon_c|$. If we maintain $|\varepsilon_c^{\mathrm{upper}}|$ in such a formula, the breakdown of this physics picture is expected to occur for bigger values of n, i.e., $\mathcal{Z}_c^{\mathrm{upper}} \gg 1$. Thus, to match accurately with $|\varepsilon_c|$ and then find an effective critical atomic number $\mathcal{Z}_c < 1$, we keep n instead and perform the evaluation $\mathcal{Z}_c = \frac{n^2|\varepsilon_c|}{13.6\mathrm{eV}} \sim 0.96$, which is certainly not for an ultra-heavy nucleus. Similarly, in Ref.[5] the value is $\mathcal{Z}_c \sim 0.25$.

Fig.3(a) shows the analysis of the adatom DOS for several values of $\varepsilon_d = -\frac{U}{2}$ with $J = 6$, where we can clearly perceive that by burying the adatom level into the Fermi sea of the host, the P3 and P4 peaks become suppressed with their positions shifted towards the Fermi energy, where the van Hove singularity resides. In the other hand, the Coulomb gap edges P1 and P2 exhibit enhanced amplitudes with peak positions displaced far away the singularity. Thus, in order to understand the aforementioned novel behavior, we present the adatom energy dependence of ReΣ in Fig.3(b). Interestingly enough, this panel reveals that the poles P3 and P4 dive into the van Hove singularity upon decreasing ε_d.

Fig.3(b) elucidates that there is a sharp region in energy domain sufficiently close to the Fermi level that bonds an electron as a state in the host energy continuum [panel (c)], as well as traps an electron within the adatom site as a virtual bond state with energy below the Fermi level. Additionally, such a trapping leads to a resonant state above the Fermi energy, which mimics a positron state in analogy to its counterpart in relativistic atomic Physics.

When such a situation is established, we realize the adatomic collapse introduced by us. It means that when such poles are finally captured by the singularity, these states inevitably localize in the host band [see P3, P4 in the LDOS given by Eq.(16) and depicted in panel (c)]. Surprisingly, as we have the negative van Hove singularity in $\Delta\mathrm{LDOS}(0) \to -\infty$ shown in Fig.3(d), which interferes destructively with the corresponding positive in $-\mathrm{Im}\Sigma(0)/\pi v^2 \to \infty$, we find $\mathrm{LDOS}(0) = 0$ in Fig.3(c).

As expected, if we extrapolate the analysis away from the PHS regime $\varepsilon_d \neq -\frac{U}{2}$ in Figs.2 and 3 the states P3 and P4 would exhibit distinct spectral amplitudes without mirror symmetry around the Dirac point. Such a feature is derived straightforwardly from the molecular binding in Eq.(4) with the dispersionless states ε_d and $\varepsilon_d + U$ for the orbital d_σ flanking asymmetrically the observed in $f_{0\sigma} \equiv \frac{1}{\sqrt{\mathcal{N}}}\sum_{\mathbf{k}s} c_{\mathbf{k}s\sigma}$ at the Dirac point. This mimics the Fermi energy off the Dirac point situation and independently, the adatomic collapse would persist. In summary, according to Fig.3(b) in this generalized situation P3 and P4 would emerge from the crossings $\varepsilon - (U - |\varepsilon_d|) = \mathrm{Re}\Sigma$ and $\varepsilon + |\varepsilon_d| = \mathrm{Re}\Sigma$, respectively.

IV. CONCLUSIONS

In this work we find virtual bound states within the Coulomb insulating gap of an adatom coupled to a multi-graphene system obeying the ABC stacking. We demonstrate that one of the virtual states mimics the atomic collapse phenomenon known in relativistic atomic Physics[1, 2]. Interestingly enough, the second virtual state reported corresponds to the particle-hole symmet-

ric of the latter, thus playing the role of the positron state. In this way, we introduce our adatomic collapse, which arises from the interplay between the Moiréless feature of the multi-graphene host and the Coulomb correlations within the Anderson-like adatom. In this manner we estimate the effective critical atomic number $\mathcal{Z}_c \sim 0.96$[5]. Therefore, our findings make explicit that the ABC multi-graphene system is a rich environment for strongly correlated phenomena and emulation of relativistic Physics.

V. ACKNOWLEDGMENTS

We thank the Brazilian funding agencies CNPq (Grants Nr. 302887/2020-2 and 308695/2021-6), Coordenação de Aperfeiçoamento de Pessoal de Nível Superior - Brasil (CAPES) – Finance Code 001 and the São Paulo Research Foundation (FAPESP Grant No. 2018/09413-0). We thank Prof. Edson Vernek for discussions of the adatomic collapse in terms of a molecular binding, which helped us to better explain the effect.

[1] Andrei Shytov, Mark Rudner, Nan Gu, Mikhail Katsnelson, and Leonid Levitov. Atomic collapse, lorentz boosts, klein scattering, and other quantum-relativistic phenomena in graphene. *Solid State Communications*, 149(27):1087–1093, 2009. Recent Progress in Graphene Studies.

[2] J Reinhardt and W Greiner. Quantum electrodynamics of strong fields. *Reports on Progress in Physics*, 40(3):219, mar 1977.

[3] J. Schweppe, A. Gruppe, K. Bethge, H. Bokemeyer, T. Cowan, H. Folger, J. S. Greenberg, H. Grein, S. Ito, R. Schule, D. Schwalm, K. E. Stiebing, N. Trautmann, P. Vincent, and M. Waldschmidt. Observation of a peak structure in positron spectra from u+cm collisions. *Phys. Rev. Lett.*, 51:2261–2264, Dec 1983.

[4] T. Cowan, H. Backe, M. Begemann, K. Bethge, H. Bokemeyer, H. Folger, J. S. Greenberg, H. Grein, A. Gruppe, Y. Kido, M. Klüver, D. Schwalm, J. Schweppe, K. E. Stiebing, N. Trautmann, and P. Vincent. Anomalous positron peaks from supercritical collision systems. *Phys. Rev. Lett.*, 54:1761–1764, Apr 1985.

[5] Yang Wang, Dillon Wong, and Andrey V. et al. Shytov. Observing atomic collapse resonances in artificial nuclei on graphene. *Science (New York, N.Y.)*, 340(6133):734–737, May 2013.

[6] Alireza Saffarzadeh and George Kirczenow. Coulomb bound states and resonances due to groups of ca dimers adsorbed on suspended graphene. *Phys. Rev. B*, 90:155404, Oct 2014.

[7] Jinhai Mao, Yuhang Jiang, and Dean et al. Moldovan. Realization of a tunable artificial atom at a supercritically charged vacancy in graphene. *Nature Physics*, 12:545–549, 2016.

[8] Yuhang Jiang, Jinhai Mao, and Dean et al. Moldovan. Tuning a circular p-n junction in graphene from quantum confinement to optical guiding. *Nature Nanotechnology*, 12:1045–1049, 2017.

[9] Hongki Min and Allan H. MacDonald. Electronic structure of multilayer graphene. *Progress of Theoretical Physics Supplement*, 176:227–252, 06 2008.

[10] Yuan Cao, Valla Fatemi, Ahmet Demir, Shiang Fang, Spencer L. Tomarken, Jason Y. Luo, Javier D. Sanchez-Yamagishi, Kenji Watanabe, Takashi Taniguchi, Efthimios Kaxiras, Ray C. Ashoori, and Pablo Jarillo-Herrero. Correlated insulator behaviour at half-filling in magic-angle graphene superlattices. *Nature*, 556:7699, 2018.

[11] Y. Cao, S. Fatemi, V.and Fang, Kenji Watanabe, Takashi Taniguchi, Efthimios Kaxiras, and Pablo Jarillo-Herrero. Unconventional superconductivity in magic-angle graphene superlattices. *Nature*, 556:7699, Feb 2018.

[12] Cheng Shen, Yanbang Chu, QuanSheng Wu, Na Li, Shuopei Wang, Yanchong Zhao, Jian Tang, Jieying Liu, Jinpeng Tian, Kenji Watanabe, Takashi Taniguchi, Rong Yang, Zi Yang Meng, Dongxia Shi, Oleg V. Yazyev, and Guangyu Zhang. Correlated states in twisted double bilayer graphene. *Nature Physics*, 16:520–525, 2020.

[13] Yuan Cao, Daniel Rodan-Legrain, Oriol Rubies-Bigorda, Jeong Min Park, Kenji Watanabe, Takashi Taniguchi, and Pabl Jarillo-Herrero. Tunable correlated states and spin-polarized phases in twisted bilayer-bilayer graphene. *Nature*, 583:215–220, 2020.

[14] Yuan Cao, Debanjan Chowdhury, Daniel Rodan-Legrain, Oriol Rubies-Bigorda, Kenji Watanabe, Takashi Taniguchi, T. Senthil, and Pablo Jarillo-Herrero. Strange metal in magic-angle graphene with near planckian dissipation. *Phys. Rev. Lett.*, 124:076801, Feb 2020.

[15] Ming Xie and A. H. MacDonald. Weak-field hall resistivity and spin-valley flavor symmetry breaking in magic-angle twisted bilayer graphene. *Phys. Rev. Lett.*, 127:196401, Nov 2021.

[16] Grigory Tarnopolsky, Alex Jura Kruchkov, and Ashvin Vishwanath. Origin of magic angles in twisted bilayer graphene. *Phys. Rev. Lett.*, 122:106405, Mar 2019.

[17] Moon Jip Park, Youngkuk Kim, Gil Young Cho, and SungBin Lee. Higher-order topological insulator in twisted bilayer graphene. *Phys. Rev. Lett.*, 123:216803, Nov 2019.

[18] Hiroki Isobe, Noah F. Q. Yuan, and Liang Fu. Unconventional superconductivity and density waves in twisted bilayer graphene. *Phys. Rev. X*, 8:041041, Dec 2018.

[19] Naoto Nakatsuji and Mikito Koshino. Moiré disorder effect in twisted bilayer graphene. *Phys. Rev. B*, 105:245408, Jun 2022.

[20] Hoi Chun Po, Liujun Zou, Ashvin Vishwanath, and T. Senthil. Origin of mott insulating behavior and superconductivity in twisted bilayer graphene. *Phys. Rev. X*, 8:031089, Sep 2018.

[21] Narasimha Raju Chebrolu, Bheema Lingam Chittari, and Jeil Jung. Flat bands in twisted double bilayer graphene. *Phys. Rev. B*, 99:235417, Jun 2019.

[22] Xia Liang, Zachary A. H. Goodwin, Valerio Vitale, Fabiano Corsetti, Arash A. Mostofi, and Johannes Lischner. Effect of bilayer stacking on the atomic and electronic structure of twisted double bilayer graphene. *Phys. Rev.*

B, 102:155146, Oct 2020.

[23] G. William Burg, Jihang Zhu, Takashi Taniguchi, Kenji Watanabe, Allan H. MacDonald, and Emanuel Tutuc. Correlated insulating states in twisted double bilayer graphene. *Phys. Rev. Lett.*, 123:197702, Nov 2019.

[24] Mikito Koshino. Band structure and topological properties of twisted double bilayer graphene. *Phys. Rev. B*, 99:235406, Jun 2019.

[25] J. A. Crosse, Naoto Nakatsuji, Mikito Koshino, and Pilkyung Moon. Hofstadter butterfly and the quantum hall effect in twisted double bilayer graphene. *Phys. Rev. B*, 102:035421, Jul 2020.

[26] Yi-Xiang Wang, Fuxiang Li, and Zi-Yue Zhang. Phase diagram and orbital chern insulator in twisted double bilayer graphene. *Phys. Rev. B*, 103:115201, Mar 2021.

[27] Yuncheng Mao, Daniele Guerci, and Christophe Mora. Supermoiré low-energy effective theory of twisted trilayer graphene. *Phys. Rev. B*, 107:125423, Mar 2023.

[28] M. J. Calderón, A. Camjayi, and E. Bascones. Mott correlations in abc graphene trilayer aligned with hbn. *Phys. Rev. B*, 106:L081123, Aug 2022.

[29] Guorui Chen, Aaron L Sharpe, Patrick Gallagher, Ilan T Rosen, Eli J Fox, Lili Jiang, Bosai Lyu, Hongyuan Li, Kenji Watanabe, Takashi Taniguchi, Jeil Jung, Zhiwen Shi, David Goldhaber-Gordon, Yuanbo Zhang, and Feng Wang. Signatures of tunable superconductivity in a trilayer graphene moire superlattice. *Nature*, 572(7768):215–219, August 2019.

[30] Guorui Chen, Lili Jiang, Shuang Wu, Bosai Lyu, Hongyuan Li, Bheema Lingam Chittari, Kenji Watanabe, Takashi Taniguchi, Zhiwen Shi, Jeil Jung, Yuanbo Zhang, and Feng Wang. Evidence of a gate-tunable mott insulator in a trilayer graphene moire superlattice. *Nature Physics*, 15:237–241, 2019.

[31] Lei Wang, En-Min Shih, Augusto Ghiotto, Lede Xian, Daniel A. Rhodes, Cheng Tan, Martin Claassen, Dante M. Kennes, Yusong Bai, Bumho Kim, Kenji Watanabe, Takashi Taniguchi, Xiaoyang Zhu, James Hone, Angel Rubio, Abhay N. Pasupathy, and Cory R. Dean. Correlated electronic phases in twisted bilayer transition metal dichalcogenides. *Nature Materials*, 19:861–866, 2020.

[32] Mathieu Bélanger, Jérôme Fournier, and David Sénéchal. Superconductivity in the twisted bilayer transition metal dichalcogenide wse_2: A quantum cluster study. *Phys. Rev. B*, 106:235135, Dec 2022.

[33] Xueheng Kuang, Zhen Zhan, and Shengjun Yuan. Flat-band plasmons in twisted bilayer transition metal dichalcogenides. *Phys. Rev. B*, 105:245415, Jun 2022.

[34] Mit H. Naik and Manish Jain. Ultraflatbands and shear solitons in moiré patterns of twisted bilayer transition metal dichalcogenides. *Phys. Rev. Lett.*, 121:266401, Dec 2018.

[35] Yi-Ming Wu, Zhengzhi Wu, and Hong Yao. Pair-density-wave and chiral superconductivity in twisted bilayer transition metal dichalcogenides. *Phys. Rev. Lett.*, 130:126001, Mar 2023.

[36] Jiawei Zang, Jie Wang, Jennifer Cano, and Andrew J. Millis. Hartree-fock study of the moiré hubbard model for twisted bilayer transition metal dichalcogenides. *Phys. Rev. B*, 104:075150, Aug 2021.

[37] Fan Zhang, Bhagawan Sahu, Hongki Min, and A. H. MacDonald. Band structure of *abc*-stacked graphene trilayers. *Phys. Rev. B*, 82:035409, Jul 2010.

[38] P. W. Anderson. Localized magnetic states in metals. *Phys. Rev.*, 124:41–53, Oct 1961.

[39] Mikito Koshino and Edward McCann. Trigonal warping and berry's phase $n\pi$ in abc-stacked multilayer graphene. *Phys. Rev. B*, 80:165409, Oct 2009.

[40] Bruno Uchoa, Valeri N. Kotov, N. M. R. Peres, and A. H. Castro Neto. Localized magnetic states in graphene. *Phys. Rev. Lett.*, 101(2):026805, Jul 2008.

[41] H. Bruus and K. Flensberg. Many-body quantum theory in condensed matter physics, an introduction. *(Oxford: Oxford University Press)*, 2012.

[42] Betül Pamuk, Jacopo Baima, Francesco Mauri, and Matteo Calandra. Magnetic gap opening in rhombohedral-stacked multilayer graphene from first principles. *Phys. Rev. B*, 95:075422, Feb 2017.

[43] Kevin T. Chan, J. B. Neaton, and Marvin L. Cohen. First-principles study of metal adatom adsorption on graphene. *Phys. Rev. B*, 77:235430, Jun 2008.

[44] R Van Pottelberge, D Moldovan, S P MilovanoviA, and F M Peeters. Molecular collapse in monolayer graphene. *2D Materials*, 6(4):045047, sep 2019.

[45] C. Dutreix and M. I. Katsnelson. Friedel oscillations at the surfaces of rhombohedral n-layer graphene. *Phys. Rev. B*, 93:035413, Jan 2016.

[46] W. C. Silva, W. N. Mizobata, J. E. Sanches, L. S. Ricco, I. A. Shelykh, M. de Souza, M. S. Figueira, E. Vernek, and A. C. Seridonio. Topological charge fano effect in multi-weyl semimetals. *Phys. Rev. B*, 105:235135, Jun 2022.

[47] Andrey E. Miroshnichenko, Sergej Flach, and Yuri S. Kivshar. Fano resonances in nanoscale structures. *Rev. Mod. Phys.*, 82:2257–2298, Aug 2010.

Referências Bibliográficas

[1] SHYTOV, A. et al. Atomic collapse, lorentz boosts, klein scattering, and other quantum-relativistic phenomena in graphene. *Solid State Communications*, v. 149, n. 27, p. 1087–1093, 2009. ISSN 0038-1098. Recent Progress in Graphene Studies. Disponível em: <https://www.sciencedirect.com/science/article/pii/S0038109809001434>.

[2] REINHARDT, J.; GREINER, W. Quantum electrodynamics of strong fields. *Reports on Progress in Physics*, v. 40, n. 3, p. 219, mar 1977. Disponível em: <https://dx.doi.org/10.1088/0034-4885/40/3/001>.

[3] SCHWEPPE, J. et al. Observation of a peak structure in positron spectra from u+cm collisions. *Phys. Rev. Lett.*, American Physical Society, v. 51, p. 2261–2264, Dec 1983. Disponível em: <https://link.aps.org/doi/10.1103/PhysRevLett.51.2261>.

[4] COWAN, T. et al. Anomalous positron peaks from supercritical collision systems. *Phys. Rev. Lett.*, American Physical Society, v. 54, p. 1761–1764, Apr 1985. Disponível em: <https://link.aps.org/doi/10.1103/PhysRevLett.54.1761>.

[5] WANG, Y.; WONG, D.; SHYTOV, A. V. e. a. Observing atomic collapse resonances in artificial nuclei on graphene. *Science (New York, N.Y.)*, v. 340, n. 6133, p. 734–737, May 2013. ISSN 0036-8075. Disponível em: <https://doi.org/10.1126/science.1234320>.

[6] MAO, J.; JIANG, Y.; MOLDOVAN, D. e. a. Realization of a tunable artificial atom at a supercritically charged vacancy in graphene. *Nature Physics*, Nature, v. 12, p. 545–549, 2016. Disponível em: <https://doi.org/10.1038/nphys3665>.

[7] JIANG, Y.; MAO, J.; MOLDOVAN, D. e. a. Tuning a circular p-n junction in graphene from quantum confinement to optical guiding. *Nature Nanotechnology*, Nature, v. 12, p. 1045–1049, 2017. Disponível em: <https://doi.org/10.1038/nnano.2017.181>.

[8] CAO, Y. et al. Correlated insulator behaviour at half-filling in magic-angle graphene superlattices. *Nature*, Nature, v. 556, p. 7699, 2018. Disponível em: <https://doi.org/10.1038/nature26154>.

[9] CAO, Y. et al. Unconventional superconductivity in magic-angle graphene superlattices. *Nature*, Nature, v. 556, p. 7699, Feb 2018. Disponível em: <https://doi.org/10.1038/nature26160>.

[10] SHEN, C. et al. Correlated states in twisted double bilayer graphene. *Nature Physics*, NATURE PUBLISHING GROUP, London, v. 16, p. 520–525, 2020. Disponível em: <http://infoscience.epfl.ch/record/276992>.

[11] CAO, Y. et al. Tunable correlated states and spin-polarized phases in twisted bilayer-bilayer graphene. *Nature*, v. 583, p. 215–220, 2020. Disponível em: <https://doi.org/10.1038/s41586-020-2260-6>.

[12] CAO, Y. et al. Strange metal in magic-angle graphene with near planckian dissipation. *Phys. Rev. Lett.*, American Physical Society, v. 124, p. 076801, Feb 2020. Disponível em: <https://link.aps.org/doi/10.1103/PhysRevLett.124.076801>.

[13] XIE, M.; MACDONALD, A. H. Weak-field hall resistivity and spin-valley flavor symmetry breaking in magic-angle twisted bilayer graphene. *Phys. Rev. Lett.*, American Physical Society, v. 127, p. 196401, Nov 2021. Disponível em: <https://link.aps.org/doi/10.1103/PhysRevLett.127.196401>.

[14] TARNOPOLSKY, G.; KRUCHKOV, A. J.; VISHWANATH, A. Origin of magic angles in twisted bilayer graphene. *Phys. Rev. Lett.*, American Physical Society, v. 122, p. 106405, Mar 2019. Disponível em: <https://link.aps.org/doi/10.1103/PhysRevLett.122.106405>.

[15] PARK, M. J. et al. Higher-order topological insulator in twisted bilayer graphene. *Phys. Rev. Lett.*, American Physical Society, v. 123, p. 216803, Nov 2019. Disponível em: <https://link.aps.org/doi/10.1103/PhysRevLett.123.216803>.

[16] ISOBE, H.; YUAN, N. F. Q.; FU, L. Unconventional superconductivity and density waves in twisted bilayer graphene. *Phys. Rev. X*, American Physical Society, v. 8, p. 041041, Dec 2018. Disponível em: <https://link.aps.org/doi/10.1103/PhysRevX.8.041041>.

[17] NAKATSUJI, N.; KOSHINO, M. Moiré disorder effect in twisted bilayer graphene. *Phys. Rev. B*, American Physical Society, v. 105, p. 245408, Jun 2022. Disponível em: <https://link.aps.org/doi/10.1103/PhysRevB.105.245408>.

[18] PO, H. C. et al. Origin of mott insulating behavior and superconductivity in twisted bilayer graphene. *Phys. Rev. X*, American Physical Society, v. 8, p. 031089, Sep 2018. Disponível em: <https://link.aps.org/doi/10.1103/PhysRevX.8.031089>.

[19] CHEBROLU, N. R.; CHITTARI, B. L.; JUNG, J. Flat bands in twisted double bilayer graphene. *Phys. Rev. B*, American Physical Society, v. 99, p. 235417, Jun 2019. Disponível em: <https://link.aps.org/doi/10.1103/PhysRevB.99.235417>.

[20] LIANG, X. et al. Effect of bilayer stacking on the atomic and electronic structure of twisted double bilayer graphene. *Phys. Rev. B*, American Physical Society, v. 102, p. 155146, Oct 2020. Disponível em: <https://link.aps.org/doi/10.1103/PhysRevB.102.155146>.

[21] BURG, G. W. et al. Correlated insulating states in twisted double bilayer graphene. *Phys. Rev. Lett.*, American Physical Society, v. 123, p. 197702, Nov 2019. Disponível em: <https://link.aps.org/doi/10.1103/PhysRevLett.123.197702>.

[22] KOSHINO, M. Band structure and topological properties of twisted double bilayer graphene. *Phys. Rev. B*, American Physical Society, v. 99, p. 235406, Jun 2019. Disponível em: <https://link.aps.org/doi/10.1103/PhysRevB.99.235406>.

[23] CROSSE, J. A. et al. Hofstadter butterfly and the quantum hall effect in twisted double bilayer graphene. *Phys. Rev. B*, American Physical Society, v. 102, p. 035421, Jul 2020. Disponível em: <https://link.aps.org/doi/10.1103/PhysRevB.102.035421>.

[24] WANG, Y.-X.; LI, F.; ZHANG, Z.-Y. Phase diagram and orbital chern insulator in twisted double bilayer graphene. *Phys. Rev. B*, American Physical Society, v. 103, p. 115201, Mar 2021. Disponível em: <https://link.aps.org/doi/10.1103/PhysRevB.103.115201>.

[25] MAO, Y.; GUERCI, D.; MORA, C. Supermoiré low-energy effective theory of twisted trilayer graphene. *Phys. Rev. B*, American Physical Society, v. 107, p. 125423, Mar 2023. Disponível em: <https://link.aps.org/doi/10.1103/PhysRevB.107.125423>.

[26] CALDERÓN, M. J.; CAMJAYI, A.; BASCONES, E. Mott correlations in abc graphene trilayer aligned with hbn. *Phys. Rev. B*, American Physical Society, v. 106, p. L081123, Aug 2022. Disponível em: <https://link.aps.org/doi/10.1103/PhysRevB.106.L081123>.

[27] CHEN, G. et al. Signatures of tunable superconductivity in a trilayer graphene moire superlattice. *Nature*, v. 572, n. 7768, p. 215–219, August 2019. ISSN 0028-0836. Disponível em: <https://doi.org/10.1038/s41586-019-1393-y>.

[28] CHEN, G. et al. Evidence of a gate-tunable mott insulator in a trilayer graphene moire superlattice. *Nature Physics*, Nature, v. 15, p. 237–241, 2019. Disponível em: <https://doi.org/10.1038/s41567-018-0387-2>.

[29] WANG, L. et al. Correlated electronic phases in twisted bilayer transition metal dichalcogenides. *Nature Materials*, Nature, v. 19, p. 861–866, 2020. Disponível em: <https://doi.org/10.1038/s41563-020-0708-6>.

[30] BÉLANGER, M.; FOURNIER, J.; SÉNÉCHAL, D. Superconductivity in the twisted bilayer transition metal dichalcogenide wse_2: A quantum cluster study. *Phys. Rev. B*, American Physical Society, v. 106, p. 235135, Dec 2022. Disponível em: <https://link.aps.org/doi/10.1103/PhysRevB.106.235135>.

[31] KUANG, X.; ZHAN, Z.; YUAN, S. Flat-band plasmons in twisted bilayer transition metal dichalcogenides. *Phys. Rev. B*, American Physical Society, v. 105, p. 245415, Jun 2022. Disponível em: <https://link.aps.org/doi/10.1103/PhysRevB.105.245415>.

[32] NAIK, M. H.; JAIN, M. Ultraflatbands and shear solitons in moiré patterns of twisted bilayer transition metal dichalcogenides. *Phys. Rev. Lett.*, American Physical Society, v. 121, p. 266401, Dec 2018. Disponível em: <https://link.aps.org/doi/10.1103/PhysRevLett.121.266401>.

[33] WU, Y.-M.; WU, Z.; YAO, H. Pair-density-wave and chiral superconductivity in twisted bilayer transition metal dichalcogenides. *Phys. Rev. Lett.*, American Physical Society, v. 130, p. 126001, Mar 2023. Disponível em: <https://link.aps.org/doi/10.1103/PhysRevLett.130.126001>.

[34] ZANG, J. et al. Hartree-fock study of the moiré hubbard model for twisted bilayer transition metal dichalcogenides. *Phys. Rev. B*, American Physical Society, v. 104, p. 075150, Aug 2021. Disponível em: <https://link.aps.org/doi/10.1103/PhysRevB.104.075150>.

[35] MIN, H.; MACDONALD, A. H. Electronic structure of multilayer graphene. *Progress of Theoretical Physics Supplement*, v. 176, p. 227–252, 06 2008. ISSN 0375-9687. Disponível em: <https://doi.org/10.1143/PTPS.176.227>.

[36] ZHANG, F. et al. Band structure of *abc*-stacked graphene trilayers. *Phys. Rev. B*, American Physical Society, v. 82, p. 035409, Jul 2010. Disponível em: <https://link.aps.org/doi/10.1103/PhysRevB.82.035409>.

[37] ANDERSON, P. W. Localized magnetic states in metals. *Phys. Rev.*, American Physical Society, v. 124, p. 41–53, Oct 1961. Disponível em: <https://link.aps.org/doi/10.1103/PhysRev.124.41>.

[38] UCHOA, B. et al. Localized magnetic states in graphene. *Phys. Rev. Lett.*, American Physical Society (APS), v. 101, n. 2, p. 026805, Jul 2008. ISSN 1079-7114. Disponível em: <http://dx.doi.org/10.1103/PhysRevLett.101.026805>.

[39] BRUUS, H.; FLENSBERG, K. Many-body quantum theory in condensed matter physics, an introduction. *(Oxford: Oxford University Press)*, 2012.

[40] PAMUK, B. et al. Magnetic gap opening in rhombohedral-stacked multilayer graphene from first principles. *Phys. Rev. B*, American Physical Society, v. 95, p. 075422, Feb 2017. Disponível em: <https://link.aps.org/doi/10.1103/PhysRevB.95.075422>.

[41] KOSHINO, M.; MCCANN, E. Trigonal warping and berry's phase $n\pi$ in abc-stacked multilayer graphene. *Phys. Rev. B*, American Physical Society, v. 80, p. 165409, Oct 2009. Disponível em: <https://link.aps.org/doi/10.1103/PhysRevB.80.165409>.

[42] MIROSHNICHENKO, A. E.; FLACH, S.; KIVSHAR, Y. S. Fano resonances in nanoscale structures. *Rev. Mod. Phys.*, American Physical Society, v. 82, p. 2257–2298, Aug 2010. Disponível em: <https://link.aps.org/doi/10.1103/RevModPhys.82.2257>.